9-3-2014

The Role of Dcdc2 in Spike Timing and Glutamatergic Synaptic Transmission in Mouse Neocortex

Alicia Yue Che
University of Connecticut - Storrs, chealicia@gmail.com

The Role of Dcdc2 in Spike Timing and Glutamatergic Synaptic Transmission in Mouse Neocortex

Alicia Yue Che, Ph.D.

University of Connecticut 2014

Dyslexia is a phenotypically complex developmental disorder that involves significant impairment in reading fluency and/or accuracy, despite adequate intelligence and educational background. Variants in dyslexia-associated genes, including *DCDC2*, have been linked to altered neocortical activation, suggesting that they may play as of yet unspecified roles in neuronal physiology. In this study we explored changes in electrophysiological properties of excitatory neurons in a Dcdc2 mutant mouse model. We found elevated intrinsic excitability as a result of depolarized resting membrane potential in mutant neurons. Next, we measured decreased trial-to-trial temporal precision in spike trains elicited by either step currents or noise stimuli simulating synaptic inputs, independent from the change in excitability. NMDAR blockade was found effective in returning the heightened variability in spike timing back to wildtype levels, and we confirmed the presence of elevated NMDAR-mediated current, both tonic and phasic. We concluded that the decreased spike-time precision was a result of elevated NMDAR-mediated synaptic noise. These results are discussed in chapter 2.

To identify the cause of increased NMDAR-mediated activities, we further tested a number of possible synaptic changes in Dcdc2 mutant layer 4 somatosensory cortex. We found that elevated presynaptic release probability, but not increase in postsynaptic

glutamate receptor numbers or ambient glutamate levels, is responsible for excess postsynaptic excitatory activities. By blocking postsynaptic NMDARs first with hyperpolarization and MK-801, we showed that in the mutant enhanced presynaptic NMDAR function leads to higher release probability from presynaptic terminals. We further demonstrated that the increased preNMDAR function is present at layer 4-layer 4 connections, but not thalamus-layer 4 connections, at least for the evoked response-mediated preNMDAR activation. These findings are discussed in chapter 3.

In summary, we demonstrated a preNMDAR-mediated increase in glutamate release in Dcdc2 mutant neurons, which then results in elevated synaptic noise and degraded spike-time precision in regular spiking neurons. These results demonstrate the first synaptic role of a dyslexia-associated gene, and reveal that *Dcdc2* plays a role in restricting NMDAR, in particular preNMDAR function, within neocortical circuits.

The Role of Dcdc2 in Spike Timing and Glutamatergic Synaptic Transmission in Mouse Neocortex

Alicia Yue Che

B.S. Pacific Lutheran University 2009

A Dissertation

Submitted in Partial Fulfillment of the

Requirements for the Degree of

Doctor of Philosophy

At the

University of Connecticut

2014

APPROVAL PAGE

Doctor of Philosophy Dissertation

The Role of Dcdc2 in Spike Timing and Glutamatergic Synaptic Transmission in Mouse Neocortex

Presented by

Alicia Yue Che, B.S.

Major Advisor:_____
Joseph J. LoTurco, Ph.D.

Associate Advisor:_____
Anastasios V Tzingounis, Ph.D.

Associate Advisor:_____
Andrew Moiseff, Ph.D.

Associate Advisor:_____
Heather Read, Ph.D.

University of Connecticut, 2014

This dissertation is dedicated to my husband, Matthew James Girgenti,

whose boundless love and compassion,

finally,

give true meaning to my passion.

Acknowledgements

I wish to thank:

My major advisor, Dr. Joseph LoTurco,

for his guidance and support.

My committee, especially Dr. Anastasios Tzingounis,

for their invaluable suggestions and advice,

on my projects and career.

Past and present lab colleagues,

For their constant help, expertise and encouragement.

Aarti Tarkar, for all her help and love.

My parents, Che Qiang and Yang Shaoying,

and my grandmother Zhang shuhuai,

for their unconditional trust and support in everything I choose to do in life,

and for all their sacrifices.

My father and mother-in-law Jack and Eileen Girgenti,

for their whole-hearted acceptance and kindness.

Matt Girgenti, my husband and love, my partner in everything.

Curriculum Vitae

Education

7/2009- 8/2014	Ph.D. in Physiology and Neurobiology, University of Connecticut, Storrs, CT 06269
6/2011	Completion of Ion Channel Physiology course, Cold Spring Harbor Laboratory, Cold spring harbor, NY 11724
9/2005-5/2009	B.S. in Biology, Physical Chemistry and General Physics (Summa Cum Laude), Pacific Lutheran University, Tacoma, WA 98447

Research experience

7/2009-present	Graduate Research Assistant, Department of Physiology and Neurobiology, University of Connecticut
2/2008-5/2009	Research Student, Department of Chemistry, Pacific Lutheran University
5/2008-8/2008	SURF Research Student, Department of Molecular Neurobiology, Mayo Clinic Graduate School
1/2006-12/2009	Research Student, Department of Biology, Pacific Lutheran University

Teaching experience

6/2014	Teaching Assistant for Ion Channel Physiology course, Cold Spring Harbor Laboratory, Cold spring harbor, NY 11724
7/2011	Teaching Assistant for *in utero* Electroporation Module, Advanced Molecular Techniques Course, Cold Spring Harbor Laboratory
Fall 2012, 2013	Lab Teaching Assistant, Investigations in Neurobiology, Department of Physiology and Neurobiology, University of Connecticut
9/2007-5/2009	Science Tutor, Academic Assistance Center, Pacific Lutheran University

9/2006-12/2009	Lab Teaching Assistant, Department of Biology, Pacific Lutheran University

Technique skills

Electrophysiology:	whole-cell patch clamping, electrical and optical stimulation, paired recording, in slice and in cultured cells
Microscopy:	two-photon laser microscopy and *in vivo* calcium imaging, epifluorescence and confocal microscopy, atomic force microscopy
Animal surgeries:	*in utero* electroporation, craniotomy, microinjection, ovariectomy
Immuno- Methods:	Immunohistochemistry; Western transfer and immunoblotting
Molecular biology:	PCR amplification, gene cloning and subcloning, plasmid manipulations, mutagenesis
Gene Expression:	qRT-PCR, RNA amplification and *in vitro* transcription.
Behavioral tests:	rotarod, open field, elevated plus maze, novel object recognition test

Honors

Outstanding Scholar Award, University of Connecticut Graduate School, 2009-2012

Presentation of the Year Award, PNB department, University of Connecticut, 2011-2012

Pacific Lutheran University Areté Honor Society since 2008

Pacific Lutheran University Chemistry Student of the Year Award 2007-2008

Dean's List, Pacific Lutheran University, 2005-2009

Interdisciplinary Contest in Modeling (ICM), Honorable Mention, 2007

Membership in scientific society

Member of the Society for Neuroscience since 2009

Publications

Truong DT, **Che A**, Rendall AR, Szalkowski CE, LoTurco JJ, Galaburda AM, Fitch RH. Mutation of Dcdc2 in mice leads to impairments in auditory processing and memory ability. Genes, Brain and behavior. 2014 (in press)

Che A and LoTurco JJ, Presynaptic NMDA receptor function in neocortex is restricted by the dyslexia-associated gene Dcdc2. (In preparation)

Che A, Girgenti MJ and LoTurco J, The dyslexia-associated gene Dcdc2 is required for spike-timing precision in mouse neocortex. *Biological Psychiatry.* 2014 Sep 1; 76(5):387-96.

Gabel LA, Marin I, LoTurco JJ, **Che A**, Murphy C, Manglani M, Kass S, Mutation of the dyslexia-associated gene Dcdc2 impairs LTM and visuo-spatial learning and memory. *Genes, Brain, and Behavior.* 2011 Nov;10(8):868-75.

Book chapter

LoTurco JJ, Tarkar A and **Che AY**, Loss if the dyslexia susceptibility gene Dcdc2 increases synaptic connectivity in the mouse neocortex. *Developmental Dyslexia: Early Precursors, Neurobehavioral Markers, and Biological Substrates*, edited by April A. Benasich and R. Holly Fitch. Brookes Publishing. 2012

Presentations and abstracts

2014: Neuronal Circuits Meeting at CSHL: Synaptic function in neocortex is regulated by the dyslexia-associated gene Dcdc2 through preNMDAR-mediated mechanisms. **Che A** and LoTurco JJ.

2012: Society for Neuroscience Poster: Loss of the dyslexia-associated gene Dcdc2 increases presynaptic NMDA receptor function in neocortical circuits. **Che AY** and LoTurco JJ.

2011: Society for Neuroscience Poster: Increased activation of NMDA receptors alters spike timing in knockout mouse for candidate dyslexia susceptibility gene Dcdc2. **Che AY** and LoTurco JJ.

2010: Society for Neuroscience Poster: Loss of the dyslexia susceptibility gene Dcdc2 increases synaptic activity and alters in spike timing in mouse neocortex. **Che Y**, Yin X, Wang Y, Maher BJ and LoTurco JJ.

2007: Society for Neuroscience Faculty for Undergraduate Research Social Poster: Neuropeptie Y-containing neurons in the rat intergeniculate leaflet are direct targets of substance P. **Che Y** and Smith MJ.

2006: Murdock Undergraduate Reseach Conference Poster

Table of Contents

List of Tables and Figures

I. Introduction

II. Dcdc2 is Essential for Spike-Time Precision in Mouse Neocortex

III. *Dcdc2* Regulates Presynaptic Glutamate Release between Layer 4 Neurons of Neocortex

I. Introduction

Dyslexia and candidate dyslexia susceptibility genes

Dyslexia or reading disability (RD) is a phenotypically complex developmental disorder that involves significant impairment in reading fluency and/or accuracy, despite adequate intelligence and educational background. RD is the most common learning disability, affecting 5-12% of school-aged children (Shaywitz and Shaywitz 2005; Schumacher et al. 2007). While the biological causes remain poorly understood, it is clear that the manifestation of dyslexia is the result of multiple interacting factors, many of which have a genetic origin. Genetic linkage disequilibrium analyses have now led to the identification of nine chromosomal loci across the human genome that significantly associate with risk of RD: DYX1-DYX9 (Caylak 2007; Petryshen and Pauls 2009; Gabel et al. 2010). Among those loci, six dyslexia candidate genes have been identified to date – *DYX1C1* in the DYX1 locus on chromosome 15q21 (Taipale et al. 2003; Wigg et al. 2004, but also see Cope et al. 2004; Scerri et al. 2004; Bellini et al. 2005; Marino et al. 2005; Meng et al. 2005a); *DCDC2* and *KIAA0319* in the DYX2 locus on chromosome 6p21 (Grigorenko et al. 1997; Fisher et al. 1999; Grigorenko et al. 2000; Ahn et al. 2001; Petryshen et al. 2001; Kaplan et al. 2002; Willcutt et al. 2002; MacPhie et al. 2004; Cope et al. 2005; Meng et al. 2005b; Paracchini 2006; Schumacher et al. 2006; Scerri et al. 2011; Marino et al. 2012; Zou et al. 2012; Zhong et al. 2013); *C2Orf3* and *MRPL19* in the DYX3 locus on chromosome 2p16–p15 (Anthoni et al. 2007); and *ROBO1* in the DYX5 locus on chromosome 3p12–q12 (Hannula-Jouppi et al. 2005; Peterson and Pennington

2012; Tran et al. 2014). Of these genes, *DYX1C1*, *DCDC2*, *KIAA0319*, and *ROBO1* play roles in neuronal development, migration and axon guidance (Kidd et al. 1998; Brose et al. 1999; Simpson et al. 2000; Whitford et al. 2002; Meng et al. 2005b; Wang et al. 2006; Gabel et al. 2010). Their identification presents a unique opportunity to test hypotheses with respect to potential cellular causes of RD, which subsequently lead to functional impairments in neocortical circuits.

Evidence for altered neuro-cognitive functions and cortical networks in RD

A battery of functional and physiological approaches has been used to understand the neurobiology of RD over the past three decades. Traditionally, case studies on consequences of focal brain lesions in skilled adult readers (McKenna and Warrington 1980; de Lacy Costello and Warrington 1989) and postmortem brain specimens (Galaburda et al. 1985; Cohen et al. 1989) were used in examining the neurobiological underpinnings of dyslexia. Findings of these studies focus on anatomical anomalies in patients with RD, including reorganization of the brain after early lesions, cerebral asymmetries and developmental ectopias or dysplasias. Since then, brain morphometry and functional neuroimaging such as PET, MRI/fMRI and MEG, have been widely used to investigate functional neuroanatomy relevant to reading skills (review see Sun et al. 2010; Peterson and Pennington 2012). The most consistent findings include abnormalities in white matter tracts as measured by fractional anisotropy, and reduced gray matter volume in regions implicated in reading skills (Peterson and Pennington 2012). Functional studies, on the other hand, indicate under-activation, changes in connectivity, and oscillation anomalies in key areas such

as superior temporal, inferior temporal-occipital, and temporo-parietal cortices, as well as subcortical areas (Gaab et al. 2007; Shaywitz and Shaywitz 2008; Singer 2009; Sun et al. 2010; Goswami 2011; Lehongre et al. 2011; Díaz et al. 2012; Peterson and Pennington 2012; Eicher and Gruen 2013; Finn et al. 2013; Richlan et al. 2013; Fan et al. 2014). In addition, increasing numbers of studies have linked structural and functional data to RD risk gene variants (Eicher and Gruen 2013), establishing a framework for investigating the neurobiological causality of RD and the resultant alterations in physiological pathways. Based on these brain-imaging phenotypes, in this study we aim to explore functional changes on a cellular physiology level as a direct result of mutation in the dyslexia-associated gene, *DCDC2*.

DCDC2 and reading disability

DCDC2 (Doublecortin domain containing 2) and *KIAA0319* were both identified within the DYX2 locus on 6p22, one of the most replicated dyslexia susceptibility loci to date (Carrion-Castillo et al. 2013). Association of the gene *DCDC2* to RD was first established by Meng et al. in a set of US families (Colorado sample), where single nucleotide polymorphisms (SNPs) and a 2.4 kb deletion in intron 2 that contained a short tandem repeat (STR, GenBank ID BV677278), were identified within the DCDC2 locus (Meng et al. 2005b). Several subsequent studies have verified the association between this STR marker with RD (Schumacher et al. 2006; Ludwig et al. 2008; Marino et al. 2012), and BV677278 has been shown to bind to the transcription factor ETV6 in human brain (Meng et al. 2010; Powers et al. 2014). Five alleles of BV677278 were

found to display a range of *DCDC2*-specific enhancer activities (Meng et al. 2010). Other SNPs within *DCDC2* have also been identified to associate with RD (Schumacher et al. 2006; Wilcke et al. 2009; Newbury et al. 2011; Zhong et al. 2013), and together these studies provide strong evidence for establishing the role of *DCDC2* in RD genetics.

Imaging-genetic studies have started to show correlations between gray and white matter volume and variants of *DCDC2* in brains regions implicated in reading, including superior prefrontal, temporal and occipital networks (Meda et al. 2007; Darki et al. 2012; Eicher and Gruen 2013; Jamadar et al. 2013). In addition, *DCDC2* variants was linked to activation and connections in a number of language and reading centers (Cope et al. 2012; Jamadar et al. 2013), suggesting its function in regulating structural and functional neural networks.

Functions of *DCDC2*

Biochemically, DCDC2 is one of an eleven-member family of proteins characterized by the presence of DCX or doublecortin domain that is critical for binding to and stabilizing microtubules, and is regulated by phosphorylation via cJun-N-terminal kinase (JNK) and dephosphotylation via protein phosphates 1 (PP1) (Gleeson et al. 1999; Coquelle et al. 2006). DCDC2 itself contains two DCX domains, and was found to stimulate microtubule assembly in vitro and interacts with JNK/MAP-kinase pathway(Coquelle et al. 2006). Functionally, DCDC2 has been implicated in migration and neuronal morphology. In prostate cancer cells, DCDC2 colocalizes with microtubules and promotes cell migration, making them resistant to the microtubule-targeting drug taxol (Longoni et al.

2012). DCDC2 was also found to localize to primary cilium in rat primary hippocampal neurons, in close proximity with the kinesin-2 subunit Kif3a, and is involved in ciliary signaling (Massinen et al. 2011). Over-expression of DCDC2 alters morphologies of hippocampal cultured neurons as well as ciliated neurons in *C. elegans in vivo* (Massinen et al. 2011).

DCDC2 is most highly expressed in the entorhinal cortex, inferior temporal cortex, medial temporal cortex, hypothalamus, amygdala, and hippocampus in human brain (Meng et al. 2005b). RNAi studies in rat neocortex and hippocampus show that DCDC2 knockdown leads to interruptions in neuronal migration, scattered heterotopias, and a population of neurons to over-migrate to ectopic positions in neocortex (Meng et al. 2005b; Burbridge et al. 2008). Conversely, a *Dcdc2* mutant mouse loss-of-function model developed in our lab displays normal neurogenesis, migration and morphology unless DCX is also down-regulated by RNAi (Wang et al. 2011), suggesting *in vivo* DCDC2 and DCX share functional redundancy in neuronal migration and dendritic growth. Nevertheless, *Dcdc2* mutant mice performed worse in behavioral tests involving long-term and visuo-spacial memory, indicating neuronal migration is neither an essential nor the sole function of DCDC2 in the cortex. Together with human imaging-genetic studies showing connections between *DCDC2* variants and neural network activation, these results suggest effects of *DCDC2* go beyond maintaining normal neuronal migration, and may connect its function to cellular neurophysiology.

NMDAR functions and neurodevelopmental disorders

NMDARs are cation channels activated by the neurotransmitter glutamate, and their functions are central in synaptic transmission, development, and many forms of synaptic plasticity (Aamodt and Constantine-Paton 1998; Hardingham and Bading 2010). The diverse functions of NMDARs are mediated by their unique properties, including voltage-dependent extracellular Mg^{2+} block, high Ca^{2+} permeability, and slow activation/inaction kinetics (Paoletti et al. 2013).

Several distinct NMDAR subunits have been identified in central neurons – the ubiquitously expressed NR1 subunit, NR2 subunits (A to D), and two NR3 subunits. The functional attributes of an NMDAR are defined by its constituent subunits, each with distinct biophysical properties. A number of isoforms resulting from alternative splicing have also been identified for each subunit, although their functional relevance is less clear (Paoletti et al. 2013). Typical NMDARs are heterodimers comprised of multiple obligatory NR1 subunits in combination with at least one NR2 subunit; NR3 subunits can form functional NMDARs with NR1/NR2 complexes but not on their own (Pérez-Otaño et al. 2001). Subunit compositions of NMDARs are determined by their locations subcellularly, cell types, as well as regions of the brain. On the single cell level, growing evidence indicates that extrasynaptic NMDARs can differ from synaptic NMDARs in their subunit composition, and certain compositions can distribute only on a selected subset of synapses depending on specific connections (Ito et al. 1997). Dynamics of NMDAR function are further complicated by the developmental regulation of subunit composition. For example, one of the most

well studied developmental subunit transition is the replacement or supplementation of NR2B by NR2A subunits postnatally, and the resultant faster decay time of NMDAR-mediated synaptic responses are thought to be critical for experience-dependent synaptic plasticity, particularly in visual cortex (Constantine-Paton and Cline 1998; Quinlan et al. 1999). Although the current knowledge of NMDAR subunit is still far from complete, it is evident that the expression, composition, and location of NMDARs are tightly regulated both spatially and temporally.

Due to the important role of NMDARs in neural circuits and intricate regulation required for their proper function, inappropriate activation of NMDARs have been implicated in several disease states. Excess activation, in particular, leads to increased intracellular Ca^{2+} concentration, over-activation, and eventually cell injury and death (Lipton 2006). Growing evidence suggests that disorders such as Parkinson's disease, Alzheimer's disease, multiple sclerosis and neuropathic pain may share a common final pathway to neuronal injury and degeneration as a result of NMDAR overstimulation, despite their different initial causes (Epstein et al. 1994). In addition, acute disorders including stroke, seizure and CNS trauma also manifest NMDAR-mediated excitotoxicity, and NMDAR blockade has neuroprotective effects in animal models of both stroke and seizure (Lee et al. 1999; Lipton 2006). As heightened cell excitation by NMDAR activation is associated with neural pathology, smaller changes NMDAR function within the range of homeostatic regulation is less studied, particularly

given the fact that NMDARs not only critically affect overall neural activity, but also ensure normal synaptic transmission, plasticity and development.

Presynaptic NMDAR function and synaptic transmission

Classically, NMDARs are thought to be involved in postsynaptic depolarization and calcium influx. Over the past two decades, there has been growing evidence supporting that functional NMDARs also exist on presynaptic locations and may be involved in regulating synaptic transmission and activity-dependent plasticity (review see Corlew et al. 2008). The subunit composition of preNMDARs in various brain regions and developmental stages have yet to be investigated to the extend of postsynaptic NMDARs, but they have been found to comprise of mostly of NR1/NR2B subunits in the cortex and hippocampus after early postnatal stages (Woodhall et al. 2001; Corlew et al. 2007; Brasier and Feldman 2008; Kunz et al. 2013), NR1/NR2B/NR3A subunits in juvenile visual cortex, and NR1/NR2A subunits in cerebellar molecular layer interneurons (Bidoret et al. 2009; Rossi et al. 2012; Rossi and Collin 2013). Anatomically, the presence of preNMDARs have been observed using immunoperoxidase and immunogold electron microscopy (EM), though at a limited number of terminals (Aoki et al. 1994; Fujisawa and Aoki 2003; Pickel et al. 2006; Corlew et al. 2007; Larsen et al. 2011). The relatively limited identification of preNMDARs have been attributed to factors such as low prevalence compared to postsynaptic NMDARs, and age- or region-specific expression of preNMDARs. These limitations also present challenges to study preNMDAR using biochemical or molecular approaches.

The more commonly used approach to study preNMDAR function has been the electrophysiological approach of measuring the effect of pharmacological preNMDAR blockade on transmitter release and synaptic transmission. Since most preNMDAR blockers also block postsynaptic NMDARs, this method requires postsynaptic NMDAR to be selectively blocked first, thus the subsequent effect of antagonists can only be attributed to non-postsynaptic, presumably presynaptic NMDARs (Corlew et al. 2008). This effort is aided by the discovery that in addition to hyperpolarization, inclusion of the open channel NMDAR blocker MK-801 in the in the internal solution selectively block postsynaptic NMDARs, making the functions of preNMDARs more tractable (Figure 1-1, Wong et al. 1986; Berretta and Jones 1996; Woodhall et al. 2001).

Using the aforementioned electrophysiological approaches, preNMDARs have been shown functionally to increase transmitter release probability (Berretta and Jones 1996; Woodhall et al. 2001; Yang 2006; Corlew et al. 2007; Brasier and Feldman 2008; Pinheiro 2008; Larsen et al. 2011; Kunz et al. 2013), participate in synaptic plasticity (Sjöström and Turrigiano 2003; Corlew et al. 2007; Rodríguez-Moreno and Paulsen 2008; Larsen et al. 2011; Rodríguez-Moreno et al. 2013), and more recently, regulate direction of synaptic transmission in local circuits by being selectively present on specific inhibitory inputs (Brasier and Feldman 2008; Buchanan et al. 2012; De-May and Ali 2012; Zhou et al. 2013). Given their subunit composition, preNMDAR activation during evoked release requires depolarization and promotes Ca^{2+} entry at the axonal

terminal to facilitate vesicular release (Woodhall et al. 2001; Sjöström and Turrigiano 2003; Brasier and Feldman 2008), however a recent study shows that tonic preNMDAR activation for enhancing spontaneous transmitter release require no extracellular or intracellular free Ca^{2+}, but affected by extracellular Na^{+} levels, and acts in part through protein kinase C signaling pathway (Kunz et al. 2013).

Controversy over presence and location of preNMDARs

Although there has been a great number of studies establishing the function of presynaptic NMDARs, their locations, or even their existence still remain a contentious issue fiercely debated over the past decade, mainly due to the relative lack of compelling proof for their presynaptic locus of expression, and in studies where their physical localization is identified at the presynaptic terminals, the lack of direct connection between the activation of these particular preNMDARs and the enhanced synaptic efficacy presumably attributed to them. This has led to considerable debate over whether they are truly presynaptic, or whether the observed physiological effects from NMDAR blockade, in particular, in fact act through other mechanisms, for example dendritic receptors influencing synaptic release from afar (Christie and Jahr, 2008).

The controversy over the presence of preNMDARs and their location in part stems from the common experimental manipulations designed to block preNMDARs, which also block somatodendritically located NMDARs. As somatodendritic depolarization can also lead to change in release probabilities in axonal terminals with a space constant of several hundred microns, the non-

specificity of NMDAR blockade can become significant in accessing these experimental results (Glitsch and Marty 1999; Duguid 2013). In molecular layer interneurons and Purkinje cells of the cerebellum, bath application of NMDA significantly increases the frequencies of miniature inhibitory postsynaptic currents (mIPSCs), and although NMDAR significantly depolarizes the postsynaptic cell somatodendritically, the electrotonic spread of depolarization along the axon was shown to be insufficient to account for the large increase in mIPSC rate, suggesting that presynaptic NMDARs are present at inhibitory axonal terminals (Glitsch and Marty 1999). However, this view has been directly challenged by results showing that targeted-activation of dendritic NMDARs by 2-photon microscopy was able to cause electrotonic spread of depolarization to activate voltage-gated calcium channels in the axons to increase release probability. Direct activation of axonal NMDARs, on the other hand, were not detected using similar methods including 2-photon activation, axonal iontophoresis and calcium imaging (Christie and Jahr 2008). These results suggest that activation of dendritic NMDARs can influence release probabilities, but do not agree with results from other studies where NMDAR-type currents were directly measured in axons of molecular layer interneurons (Fiszman et al 2005; Duguid et al 2007; Duguid 2013).

The presence of preNMDARs is also debated in the cortex. Functionally, preNMDARs have been found to regulate synaptic release and participate in synaptic plasticity, in particular tLTD, at layer 4 to layer 2/3 synapses, inputs to layer 4 and layer 5, and layer 5 to layer 5 synapses in visual cortex (Sjöström

and Turrigiano 2003; Corlew et al. 2007; Larsen et al. 2011; Buchanan et al. 2012); inputs to layer 2 and layer 4 in entorhinal cortex (Berretta and Jones 1996; Woodhall et al. 2001; Yang 2006), and layer 4 to layer 2/3 (but not layer 4 to layer 4) synapses in somatosensory cortex (Bender et al. 2006; Brasier and Feldman 2008; Rodríguez-Moreno and Paulsen 2008; Rodríguez-Moreno et al. 2013). Interestingly, the induction of tLTD appears to go through a pre- to postsynaptic NMDAR-dependent mechanism switch in visual cortex, indicating that preNMDARs may be important in establishing cortical networks before the onset of critical period (Corlew et al. 2007). This is consistent with the finding that preNMDAR expression is also developmentally regulated – NR3A to NR2B subunit switch has been shown during critical period in visual cortex (Larsen et al. 2011). Taken together, these results provide strong evidence supporting the presence of preNMDARs and their role in synaptic transmission and long-term plasticity in cortical circuits. However, this view is again challenged by failure to directly visualize NMDARs at pyramidal neuron axonal terminals, and focal iontophoretic stimulation with a NMDAR agonist failed to depolarize the axon or evoke NMDAR-mediated calcium entry, pointing to the absence of functional preNMDARs that regulate axonal release (Christie and Jahr 2009).

One possible explanation for the conflicting data is that preNMDARs are sparse, and their expression are tightly regulated spatially and temporally based on cellular specialization and developmental processes (Duguid 2013). However genes other than those encoding NMDAR subunits themselves, which serve to regulate and restrict functional preNMDARs, remain unidentified. We explore the

connection of the gene *Dcdc2* and preNMDAR function in chapter 3. It is worth noting, however, that our study remains an electrophysiological assessment of functional changes associated with presumed presynaptic NMDAR activation, as the most parsimonious explanation. Changes in somatodendritic NMDAR activation, or changes in other cellular mechanisms, may manifest into increased synaptic release sensitive to NMDAR blockade, or coexist with changes in preNMDAR function in the Dcdc2 mutant mouse model – this possibility is further discussed in chapter 3 and 4.

References

Aamodt SM, Constantine-Paton M. The role of neural activity in synaptic development and its implications for adult brain function. Advances in neurology. 1999 79:133-144.

Ahn J, Won T-W, Zia A, Reutter H, Kaplan DE, Sparks R, et al. Peaks of Linkage Are Localized by a BAC/PAC Contig of the 6p Reading Disability Locus. Genomics. 2001 Nov;78(1-2):19–29.

Anthoni H, Zucchelli M, Matsson H. A locus on 2p12 containing the co-regulated MRPL19 and C2ORF3 genes is associated to dyslexia. Human molecular genetics. 2007 Feb;16(6):667-677.

Aoki C, Venkatesan C, Go CG, Mong JA, Dawson TM. Cellular and subcellular localization of NMDA-R1 subunit immunoreactivity in the visual cortex of adult and neonatal rats. J Neurosci. 1994 Sep;14(9):5202–22.

Bellini G, Bravaccio C, Calamoneri F. No evidence for association between dyslexia and DYX1C1 functional variants in a group of children and adolescents from Southern Italy. J molecular Neurosci.2005 Nov;27(3):311-314.

Bender KJ, Allen CB, Bender VA, Feldman DE. Synaptic basis for whisker deprivation-induced synaptic depression in rat somatosensory cortex. J Neurosci. 2006 Apr 19;26(16):4155–65.

Berretta N, Jones RS. Tonic facilitation of glutamate release by presynaptic N-methyl-D-aspartate autoreceptors in the entorhinal cortex. Neuroscience. 1996 Nov;75(2):339–44.

Bidoret C, Ayon A, Barbour B, Casado M. Presynaptic NR2A-containing NMDA receptors implement a high-pass filter synaptic plasticity rule. Proc Natl Acad Sci USA. 2009;106(33):14126–31.

Brasier D, Feldman DE. Synapse-Specific Expression of Functional Presynaptic NMDA Receptors in Rat Somatosensory Cortex. J Neurosci. 2008 Feb 27;28(9):2199-2211.

Brose K, Bland KS, Wang KH, Arnott D, Henzel W, Goodman CS, et al. Slit proteins bind Robo receptors and have an evolutionarily conserved role in repulsive axon guidance. Cell. 1999 Mar 19;96(6):795–806.

Buchanan KA, Blackman AV, Moreau AW, Elgar D, Costa RP, Lalanne T, et al. Target-Specific Expressionof Presynaptic NMDA Receptors in Neocortical Microcircuits. Neuron. 2012 Aug 9;75(3):451–66.

Burbridge TJ, Wang Y, Volz AJ, Peschansky VJ, Lisann L, Galaburda AM, et al.

Postnatal analysis of the effect of embryonic knockdown and overexpression of candidate dyslexia susceptibility gene homolog Dcdc2 in the rat. Neuroscience. 2008 Mar 27;152(3):723–33.

Carrion-Castillo A, Franke B, Fisher SE. Molecular Genetics of Dyslexia: An Overview. van der Leij A, Maassen B, editors. Dyslexia. 2013 Oct 17;19(4):214–40.

Caylak E. A review of association and linkage studies for genetical analyses of learning disorders. American Journal of Medical Genetics. 2007 Oct;144B(7):923-943.

Christie JM, Jahr CE. Dendritic NMDA receptors activate axonal calcium channels. Neuron. 2008;60:298–307.

Christie JM, Jahr CE. Selective expression of ligand-gated ion channels in L5 pyramidal cell axons. J Neurosci. 2009;29:11441-50.

Cohen M, Campbell R, Yaghmai F. Neuropathological abnormalities in developmental dysphasia. Ann Neurol. 1989 Jun;25(6):567–70.

Constantine-Paton M, Cline HT. LTP and activity-dependent synaptogenesis: the more alike they are, the more different they become. Current Opinion in Neurobiology. 1998 Feb;8(1):139-148.

Cope N, Eicher JD, Meng H, Gibson CJ, Hager K, Lacadie C, et al. Variants in the DYX2 locus are associated with altered brain activation in reading-related brain regions in subjects with reading disability. NeuroImage. 2012 Oct;63(1):148–56.

Cope N, Harold D, Hill G, Moskvina V. Strong evidence that KIAA0319 on chromosome 6p is a susceptibility gene for developmental dyslexia. Am J Hum Genet. 2005 Apr;76(4):581-591.

Cope NA, Hill G, Van Den Bree M, Harold D. No support for association between dyslexia susceptibility 1 candidate 1 and developmental dyslexia. Molecular Psychiatry 2004;10:237-238.

Coquelle FM, Levy T, Bergmann S, Wolf SG, Bar-El D, Sapir T, et al. Common and divergent roles for members of the mouse DCX superfamily. Cell cycle 2006 May 1;5(9):976–83.

Corlew R, Brasier DJ, Feldman DE, Philpot BD. Presynaptic NMDA Receptors: Newly Appreciated Roles in Cortical Synaptic Function and Plasticity. The Neuroscientist. 2008 Dec 1;14(6):609–25.

Corlew R, Wang Y, Ghermazien H, Erisir A, Philpot BD. Developmental Switch in the Contribution of Presynaptic and Postsynaptic NMDA Receptors to Long-

Term Depression. J Neurosci. 2007 Sep 12;27(37):9835–45.

Darki F, Peyrard-Janvid M, Matsson H, Kere J, Klingberg T. Three Dyslexia Susceptibility Genes, DYX1C1, DCDC2, and KIAA0319, Affect Temporo-Parietal White Matter Structure. Biological Psychiatry. 2012 Jun 8;1–6.

de Lacy Costello A, Warrington EK. Dynamic Aphasia: The Selective Impairment of Verbal Planning. Cortex. 1989 Mar;25(1):103–14.

De-May CL, Ali AB. Involvement of pre- and postsynaptic NMDA receptors at local circuit interneuron connections in rat neocortex. Neuroscience. 2012 Oct 15;:1–34.

Díaz B, Hintz F, Kiebel SJ, Kriegstein von K. Dysfunction of the auditory thalamus in developmental dyslexia. Proc Natl Acad Sci USA. 2012 Aug 21;109(34):13841–6.

Duguid IC, Pankratov Y, Moss GW, Smart TG. Somatodendritic release of glutamate regulates synaptic inhibition in cerebellar Purkinje cells via autocrine mGluR1 activation. J Neurosci. 2007;27:12464-74.

Duguid IC. Presynaptic NMDA receptors: are they dendritic receptors in disguise? Brain Res Bul. 2013;93:4-9.

Eicher JD, Gruen JR. Imaging-genetics in dyslexia: Connecting risk genetic variants to brain neuroimaging and ultimately to reading impairments. Molecular Genetics and Metabolism. 2013 Nov 1;110(3):201–12.

Epstein FH, Lipton SA, Rosenberg PA. Excitatory amino acids as a final common pathway for neurologic disorders. New England Journal of Medicine. 1994;330(9):613–22.

Fan Q, Davis N, Anderson AW, Cutting LE. Thalamo-Cortical Connectivity: What Can Diffusion Tractography Tell Us about Reading Difficulties in Children? Brain Connectivity. 2014 Jun 25.

Finn ES, Shen X, Holahan JM, Scheinost D, Lacadie C, Papademetris X, et al. Disruption of Functional Networks in Dyslexia_ A Whole-Brain, Data-Driven Analysis of Connectivity. Biological psychiatry. 2013 Oct 11;1–8.

Fisher SE, Marlow AJ, Lamb J, Maestrini E. A quantitative-trait locus on chromosome 6p influences different aspects of developmental dyslexia. Am J Hum Genet.1999 Jan;64(1):146-156.

Fiszman ML, Barberis A, Lu C, Fu Z, Erdélyi F, Szabó G, Vicini S. NMDA receptors increase the size of GABAergic terminals and enhance GABA release. J Neurosci 2005a;25:2024–2031.

Fujisawa S, Aoki C. In vivo blockade of N-methyl-D-aspartate receptors induces rapid trafficking of NR2B subunits away from synapses and out of spines and terminals in adult cortex. Neuroscience. 2003;121(1):51–63.

Gaab N, Gabrieli JDE, Deutsch GK, Tallal P, Temple E. Neural correlates of rapid auditory processing are disrupted in children with developmental dyslexia and ameliorated with training: an fMRI study. Restor Neurol Neurosci. 2007;25(3-4):295–310.

Gabel LA, Gibson CJ, Gruen JR, LoTurco JJ. Progress towards a cellular neurobiology of reading disability. Neurobiology of Disease. 2010 May 1;38(2):173–80.

Galaburda AM, Sherman GF, Rosen GD, Aboitiz F, Geschwind N. Developmental dyslexia: four consecutive patients with cortical anomalies. Ann Neurol. 1985 Aug;18(2):222–33.

Gleeson JG, Lin PT, Flanagan LA, Walsh CA. Doublecortin is a microtubule-associated protein and is expressed widely by migrating neurons. Neuron. 1999 Jun;23(2):257–71.

Glitsch M, Marty A. Presynaptic effects of NMDA in cerebellar purkinje cells and interneurons. J Neurosci. 1999;19(511-519)

Goswami U. A temporal sampling framework for developmental dyslexia. Trends in Cognitive Sciences. 2011 Jan;15(1):3–10.

Grigorenko EL, Wood FB, Meyer MS. Chromosome 6p influences on different dyslexia-related cognitive processes: further confirmation. Am J Hum Genet. 2000 Feb;66(2):715-723.

Grigorenko EL, Wood FB, Meyer MS, Hart LA, Speed WC, Shuster A, et al. Susceptibility loci for distinct components of developmental dyslexia on chromosomes 6 and 15. Am J Hum Genet. 1997 Jan;60(1):27–39.

Hannula-Jouppi K, Kaminen-Ahola N, Taipale M. The axon guidance receptor gene ROBO1 is a candidate gene for developmental dyslexia. PLoS Genetics. 2005.

Hardingham GE, Bading H. Synaptic versus extrasynaptic NMDA receptor signalling: implications for neurodegenerative disorders. Nat Rev Neurosci. Nature Publishing Group; 2010 Sep 15;11(10):682–96.

Ito I, Futai K, Katagiri H, Watanabe M. Synapse-selective impairment of NMDA receptor functions in mice lacking NMDA receptor epsilon 1 or epsilon 2 subunit. J Phys 1997 Apr 15;500:401-408.

Jamadar S, Powers NR, Meda SA, Calhoun VD, Gelernter J, Gruen JR, et al.

Genetic influences of resting state fMRI activity in language-related brain regions in healthy controls and schizophrenia patients: a pilot study. Brain Imaging and Behavior. 2013 Mar;7(1):15–27.

Kaplan DE, Gayan J, Ahn J, Won TW, Pauls D. Evidence for linkage and association with reading disability, on 6p21. 3-22. Am J Hum Genet. 2002 May;70(5):1287-1298.

Kidd T, Brose K, Mitchell KJ, Fetter RD. Roundabout controls axon crossing of the CNS midline and defines a novel subfamily of evolutionarily conserved guidance receptors. Cell. 1998 Jan 23;92(2):205-215.

Kunz PA, Roberts AC, Philpot BD. Presynaptic NMDA Receptor Mechanisms for Enhancing Spontaneous Neurotransmitter Release. J Neurosci. 2013 May 1;33(18):7762–9.

Larsen RS, Corlew RJ, Henson MA, Roberts AC, Mishina M, Watanabe M, et al. NR3A-containing NMDARs promote neurotransmitter release and spike timing–dependent plasticity. Nat Neurosci.; 2011 Feb 6;14(3):338–44.

Lee JM, Zipfel GJ, Choi DW. The changing landscape of ischaemic brain injury mechanisms. Nature. 1999 Jun 24;399(6738 Suppl):A7–14.

Lehongre K, Ramus F, Villiermet N, Schwartz D, Giraud A-L. Altered low-γ sampling in auditory cortex accounts for the three main facets of dyslexia. Neuron. 2011 Dec 22;72(6):1080–90.

Lipton SA. Paradigm shift in neuroprotection by NMDA receptor blockade: Memantine and beyond. Nat Rev Drug Discov. 2006 Jan 20;5(2):160–70.

Longoni N, Kunderfranco P, Pellini S, Albino D, Mello-Grand M, Pinton S, et al. Aberrant expression of the neuronal-specific protein DCDC2 promotes malignant phenotypes and is associated with prostate cancer progression. Oncogene. 2012 Jun 25;1–10.

Ludwig KU, Schumacher J, Schulte-Körne G, König IR, Warnke A, Plume E, et al. Investigation of the DCDC2 intron 2 deletion/compound short tandem repeat polymorphism in a large German dyslexia sample. Psychiatr Genet. 2008 Dec;18(6):310–2.

MacPhie IL, Walter J, Pennington BF, Fisher SE. A 77-kilobase region of chromosome 6p22. 2 is associated with dyslexia in families from the United Kingdom and from the United States. Am J Hum Genet. 2004 Dec 75(6): 1046-1058.

Marino C, Giorda R, Lorusso ML, Vanzin L. A family-based association study does not support DYX1C1 on 15q21. 3 as a candidate gene in developmental dyslexia. Eur J Hum Genet.2005 Jan;13:491-499.

Marino C, Meng H, Mascheretti S, Rusconi M, Cope N, Giorda R, et al. DCDC2 genetic variants and susceptibility to developmental dyslexia. Psychiatr Genet. 2012 Feb;22(1):25–30.

Massinen S, Hokkanen M-E, Matsson H, Tammimies K, Tapia-Páez I, Dahlström-Heuser V, et al. Increased Expression of the Dyslexia Candidate Gene DCDC2 Affects Length and Signaling of Primary Cilia in Neurons. PLoS ONE. 2011 Jun 16;6(6):e20580.

McKenna P, Warrington EK. Testing for nominal dysphasia. Journal of Neurology, Neurosurgery & Psychiatry. 1980 Sep 1;43(9):781–8.

Meda SA, Gelernter J, Gruen JR, Calhoun VD, Meng H, Cope NA, et al. Polymorphism of DCDC2 Reveals Differences in Cortical Morphology of Healthy Individuals—A Preliminary Voxel Based Morphometry Study. Brain Imaging and Behavior. 2007 Nov 27;2(1):21–6.

Meng H, Hager K, Held M, Page GP, Olson RK. TDT-association analysis of EKN1 and dyslexia in a Colorado twin cohort. Human genetics. 2005 Nov;118(1):87-90.

Meng H, Powers NR, Tang L, Cope NA, Zhang P-X, Fuleihan R, et al. A Dyslexia-Associated Variant in DCDC2 Changes Gene Expression. Behav Genet. 2010 Nov 2;41(1):58–66.

Meng H, Smith SD, Hager K, Held M, Liu J, Olson RK, et al. DCDC2 is associated with reading disability and modulates neuronal development in the brain. Proc Natl Acad Sci USA. 2005 Nov 22;102(47):17053–8.

Newbury DF, Paracchini S, Scerri TS, Winchester L. Investigation of dyslexia and SLI risk variants in reading-and language-impaired subjects. Behav Genet. 2011 Jan;41(1):90-104.

Paoletti P, Bellone C, Zhou Q. NMDA receptor subunit diversity: impact on receptor properties, synaptic plasticity and disease. Nat Rev Neurosci. 2013;14(6):383–400.

Paracchini S. The chromosome 6p22 haplotype associated with dyslexia reduces the expression of KIAA0319, a novel gene involved in neuronal migration. Human Molecular Genetics. 2006 Apr 6;15(10):1659–66.

Peterson RL, Pennington BF. Developmental dyslexia. The Lancet. 2012 May 26;379(9830):1997–2007.

Petryshen TL, Kaplan BJ, Fu Liu M, de French NS, Tobias R, Hughes ML, et al. Evidence for a susceptibility locus on chromosome 6q influencing phonological coding dyslexia. Am J Med Genet. 2001;105(6):507–17.

Petryshen TL, Pauls DL. The genetics of reading disability. Curr Psychiatry Rep. 2009 Apr;11(2):149–55.

Pérez-Otaño I, Schulteis CT, Contractor A. Assembly with the NR1 subunit is required for surface expression of NR3A-containing NMDA receptors. J Neurosci.2001 Feb 15;21(4):1228-37.

Pickel VM, Colago EE, Mania I, Molosh AI, Rainnie DG. Dopamine D1 receptors co-distribute with N-methyl-D-aspartic acid type-1 subunits and modulate synaptically-evoked N-methyl-D-aspartic acid currents in rat basolateral amygdala. Neuroscience. 2006 Oct 27;142(3):671–90.

Pinheiro P. Presynaptic glutamate receptors: physiological functions and mechanisms of action. Nat Rev Neurosci. 2008 Jun;9(6):423-36.

Powers NR, Eicher JD, Butter F, Kong Y, Miller LL, Ring SM, et al. Alleles of a Polymorphic ETV6 Binding Site in DCDC2 Confer Risk of Reading and Language Impairment. Am J Hum Genet. 2014;94(5).

Quinlan EM, Philpot BD, Huganir RL, Bear MF. Rapid, experience-dependent expression of synaptic NMDA receptors in visual cortex in vivo. Nat Neurosci. 1999 Apr;2(4):352-7.

Richlan F, Kronbichler M, Wimmer H. Structural abnormalities in the dyslexic brain: a meta-analysis of voxel-based morphometry studies. Hum Brain Mapp. 2013 Nov;34(11):3055–65.

Rodríguez-Moreno A, González-Rueda A, Banerjee A, Upton AL, Craig MT, Paulsen O. Presynaptic Self-Depressionat Developing Neocortical Synapses. Neuron. 2013 Jan 9;77(1):35–42.

Rodríguez-Moreno A, Paulsen O. Spike timing–dependent long-term depression requires presynaptic NMDA receptors. Nat Neurosci. 2008 May 30;11(7):744–5.

Rossi B, Collin T. Presynaptic NMDA receptors act as local high-gain glutamate detector in developing cerebellar molecular layer interneurons. J Neurochem. 2013 May 15;126(1):47–57.

Rossi B, Ogden D, Llano I, Tan YP, Marty A, Collin T. Current and Calcium Responses to Local Activation of Axonal NMDA Receptors in Developing Cerebellar Molecular Layer Interneurons. PLoS ONE. 2012 Jun 27;7(6):e39983.

Scerri TS, Fisher SE, FRANCKS C, MacPhie IL. Putative functional alleles of DYX1C1 are not associated with dyslexia susceptibility in a large sample of sibling pairs from the UK. J Med Genet. 2004 Nov;41(11):853-7.

Scerri TS, Morris AP, Buckingham LL, Newbury DF, Miller LL, Monaco AP, et al. DCDC2, KIAA0319 and CMIP Are Associated with Reading-Related Traits. Biol Psychiatry. 2011 Aug 1;70(3):237-45.

Schumacher J, Anthoni H, Dahdouh F, König IR, Hillmer AM, Kluck N, et al. Strong Genetic Evidence of DCDC2 as a Susceptibility Gene for Dyslexia. Am J Hum Genet. 2006 Jan;78(1):52-62.

Schumacher J, Hoffmann P, Schmal C, Schulte-Korne G, Nothen MM. Genetics of dyslexia: the evolving landscape. Journal of Medical Genetics. 2007 May 1;44(5):289–97.

Shaywitz SE, Shaywitz BA. Dyslexia (Specific Reading Disability). Biological Psychiatry. 2005 Jun;57(11):1301–9.

Shaywitz SE, Shaywitz BA. Paying attention to reading: the neurobiology of reading and dyslexia. Dev Psychopathol. 2008;20(4):1329–49.

Simpson JH, Bland KS, Fetter RD, Goodman CS. Short-range and long-range guidance by Slit and its Robo receptors: a combinatorial code of Robo receptors controls lateral position. Cell. 2000 Dec 22;103(7):1019-32.

Singer W. Distributed processing and temporal codes in neuronal networks. Cogn Neurodyn. 2009;3(3):189–96.

Sjöström P, Turrigiano G. Neocortical LTD via coincident activation of presynaptic NMDA and cannabinoid receptors. Neuron. 2003 Aug 14;39(4):641-54.

Sun Y-F, Lee J-S, Kirby R. Brain imaging findings in dyslexia. Pediatr Neonatol. 2010 Apr;51(2):89–96.

Taipale M, Kaminen N, Nopola-Hemmi J, Haltia T, Myllyluoma B, Lyytinen H, et al. A candidate gene for developmental dyslexia encodes a nuclear tetratricopeptide repeat domain protein dynamically regulated in brain. Proc Natl Acad Sci USA. 2003 Sep 30;100(20):11553–8.

Tran C, Wigg KG, Zhang K, Cate-Carter TD, Kerr E, Field LL, et al. Association of the ROBO1 gene with reading disabilities in a family-based analysis. Genes, Brain and Behavior. 2014 Apr;13(4):430–8.

Wang Y, Paramasivam M, Thomas A, Bai J. DYX1C1 functions in neuronal migration in developing neocortex. Neuroscience. 2006 Dec 1;143(2):515-22.

Wang Y, Yin X, Rosen G, Gabel L, Guadiana SM, Sarkisian MR, et al. Dcdc2 knockout mice display exacerbated developmental disruptions following knockdown of doublecortin. Neuroscience. 2011 Sep 8;190:398–408.

Whitford KL, Marillat V, Stein E, Goodman CS, Tessier-Lavigne M, Chédotal A, et al. Regulation of cortical dendrite development by Slit-Robo interactions. Neuron. 2002 Jan 3;33(1):47–61.

Wigg KG, Couto JM, Feng Y, Anderson B, Cate-Carter TD, Macciardi F, et al. Support for EKN1 as the susceptibility locus for dyslexia on 15q21. Molecular Psychiatry. 2004 Dec;9(12):1111–21.

Wilcke A, Weissfuss J, Kirsten H, Wolfram G, Boltze J, Ahnert P. The role of gene DCDC2 in German dyslexics. Ann Dyslexia. 2009 Jun;59(1):1–11.

Willcutt EG, Pennington BF, Smith SD, Cardon LR, Gayán J, Knopik VS, et al. Quantitative trait locus for reading disability on chromosome 6p is pleiotropic for attention-deficit/hyperactivity disorder. Am J Med Genet. 2002 Apr 8;114(3):260–8.

Wong EH, Kemp JA, Priestley T. The anticonvulsant MK-801 is a potent N-methyl-D-aspartate antagonist. Proc Natl Acad Sci USA. 1986 Sep;83(18):7104-8.

Woodhall G, Evans DI, Cunningham MO, Jones RSG. NR2B-Containing NMDA Autoreceptors at Synapses on Entorhinal Cortical Neurons. J Neurophysiol. 2001 Oct;86(4):1644-51.

Yang J. Tonic Facilitation of Glutamate Release by Presynaptic NR2B-Containing NMDA Receptors Is Increased in the Entorhinal Cortex of Chronically Epileptic Rats. J Neurosci. 2006 Jan 11;26(2):406–10.

Zhong R, Yang B, Tang H, Zou L, Song R, Zhu L-Q, et al. Meta-analysis of the association between DCDC2 polymorphisms and risk of dyslexia. Mol Neurobiol. 2013 Feb;47(1):435–42.

Zhou N, Rungta RL, Malik A, Han H, Wu DC, MacVicar BA. Regenerative glutamate release by presynaptic NMDA receptors contributes to spreading depression. J Cereb Blood Flow Metab. 2013 Jul 3;33(10):1582–94.

Zou L, Chen W, Shao S, Sun Z, Zhong R. Genetic variant in KIAA0319, but not in DYX1C1, is associated with risk of dyslexia: An integrated meta-analysis. Am J Med Genet B Neuropsychiatr Genet. 2012 Dec;159B(8):970-6.

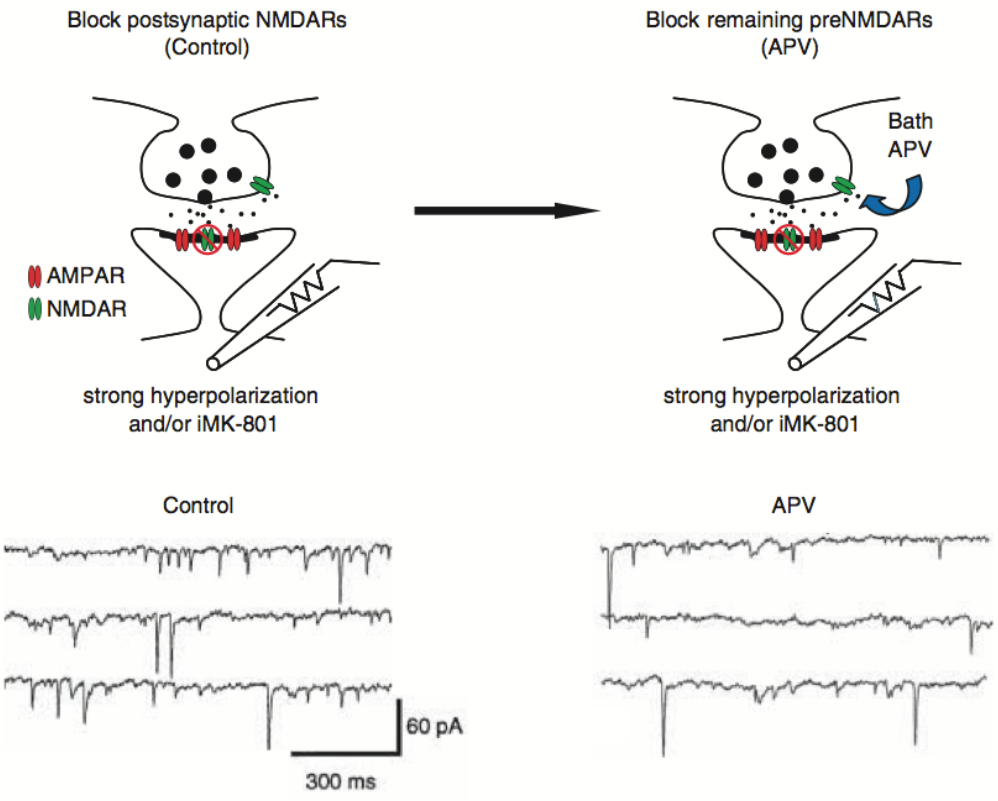

Figure 1-1. Measure the effect of preNMDAR blockade on spontaneous transmitter release. Top, cartoon depicting the typical electrophysiological method used to isolate preNMDAR functions. Postsynaptic NMDARs are blocked by strong hyperpolarization and the open channel NMDAR blocker MK-801 is included introduced in the recording pipette to block postsynaptic NMDARs. With postsynaptic NMDARs blocked, the pan NMDAR antagonist APV can only block non-postsynaptic, presumably presynaptic NMDARs. Bottom, example mEPSC traces for control (before APV) and after APV application demonstrate decreased frequency and release probability due to preNMDAR blockade. Adapted from Corlew et al. 2008.

II. Dcdc2 is Essential for Spike-Time Precision in Mouse Neocortex

Abstract

Variants in dyslexia-associated genes, including Dcdc2, have been linked to altered neocortical activation, suggesting that they may play as of yet unspecified roles in neuronal physiology. Whole-cell patch clamp recordings were used to compare the electrophysiological properties of regular spiking (RS) pyramidal neurons of neocortex in Dcdc2 mutant and wildtype mice. Neurons in the mutants showed increased excitability and decreased temporal precision in action potential (AP) firing. Whole-transcriptome RNA-seq screen revealed that the NMDAR subunit Grin2B was elevated in Dcdc2 mutants, and the electrophysiological assessment confirmed a functional increase in spontaneous NMDAR-mediated activity. The decreased AP temporal precision could be restored in mutants by treatment with either the NMDAR antagonist APV or the NMDAR 2B subunit (NR2B)-specific antagonist Ro 25-6981. These results link the function of Dcdc2 to spike timing through elevated activity of NMDAR.

Introduction

Developmental dyslexia is caused by a still poorly understood interaction between genetic and environmental factors (Rosenberg et al. 2012; Petersen and Crochet 2013). Single gene association studies and subsequent meta-analyses provide relatively strong evidence for association between variants of genes on chromosome 6p21.3, including DCDC2 and KIAA0319, and risk for developmental dyslexia (Meng et al. 2005; Schumacher et al. 2006; Zou et al. 2012). In addition, recent neuroimaging experiments demonstrate that variants of

both DCDC2 and KIAA0319 also associate with alterations in neocortical activation during reading related tasks (Meda et al. 2007; Cope et al. 2012; Darki et al. 2012; Pinel et al. 2012). One hypothesis emerging from these findings is that dyslexia associated genes may play a role in the neurophysiology of neocortical circuits.

Results of previous *in utero* RNAi experiments show that targeting expression of either Kiaa0319 or Dcdc2 in fetal rat somatosensory neocortex causes a displacement of neocortical pyramidal neurons in neocortical circuits by disrupting neuronal migration (Meng et al. 2005; Paracchini 2006). Recent studies now show that neuronal migration is neither an essential nor the sole function of Kiaa0319 or Dcdc2 in the cortex. For example, in Dcdc2 mutant mice there are no apparent disruptions in neuronal migration or displacement of neurons in neocortical circuits (Gabel et al. 2011; Wang et al. 2011). In spite of normal neocortical patterning, Dcdc2 mutants display behavioral deficits in performing novel object recognition tasks, and in learning difficult versions of the Hebb-Williams maze (Gabel et al. 2011). In addition, RNAi targeting Kiaa0319 in developing auditory neocortex does not result in significant displacement of neurons, but nevertheless results in alterations in neurophysiological responses to speech stimuli, and in elevated excitability of neocortical pyramidal neurons (Centanni et al. 2013). Together, these results suggest effects of dyslexia-associated genes that go beyond maintaining normal neuronal migration, and may connect its function to cellular neurophysiology.

In this study we sought to determine whether the genetic loss of Dcdc2 is associated with measureable cellular neurophysiological changes in pyramidal neurons of mouse neocortex. Cognitive processes required for reading involve learning to accurately associate visual stimuli or written words, with rapidly changing auditory stimuli and language sounds (Tallal 1980; Wagner 1986). Reliable and precise spike-timing is a fundamental property of neurons that facilitates processing rapidly changing stimuli (Tchumatchenko et al. 2011), processing visual stimuli (Tiesinga et al. 2008) and for making learned associations. Therefore in the initial characterization we focused on properties of AP rate and AP timing, and found consistently heightened excitability and altered spike-time precision in pyramidal neurons in the mutants. High throughput RNA-sequencing of the wildtypes and mutants revealed up-regulation of the 2B subunit of NMDAR, Grin2B, and blocking NMDARs restored measures of temporal precision in mutant neurons to wildtype levels. Our results indicate that Dcdc2 functions in maintaining temporal coding in neocortical neurons by regulating the expression and function of NMDARs in neocortical pyramidal neurons.

Materials and methods

Slice Preparation

P18-P28 wildtype and Dcdc2 mutant mice were deeply anesthetized with isoflurane and then decapitated. All experiments were performed under the approval of the University of Connecticut Animal Care and Use Committee. Brains were rapidly removed and immersed in ice-cold oxygenated (95% O_2 and

5% CO_2) dissection buffer containing (in mM): 83 NaCl, 2.5 KCl, 1 NaH_2PO_4, 26.2 $NaHCO_3$, 22 glucose, 72 sucrose, 0.5 $CaCl_2$, and 3.3 $MgCl_2$. Coronal slices (400 μm) were cut using a vibratome (VT1200S, Leica), incubated in dissection buffer for 40 min at 34°C, and then stored at room temperature for reminder of the recording day. All slice recordings were performed at 34°C. Slices were visualized using IR differential interference microscopy (DIC) (E600FN, Nikon) and a CCD camera (QICAM, QImaging). Individual neurons were visualized with a 40x Nikon Fluor water immersion (0.8 NA) objective.

Electrophysiology

For all experiments, extracellular recording buffer was oxygenated (95% O_2 and 5% CO_2) and contained (in mM): 125 NaCl, 25 $NaHCO_3$, 1.25 NaH_2PO_4, 3 KCl, 25 dextrose, 1 $MgCl_2$, and 2 $CaCl_2$. Patch pipettes were fabricated from borosilicate glass (N51A, King Precision Glass, Inc.) to a resistance of 2-5 MΩ. The resultant errors were minimized with bridge balance and capacitance compensation. For current-clamp experiments and slope current measurement, pipettes were filled with an internal solution containing (in mM): 125 potassium gluconate, 10 HEPES, 4 Mg-ATP, 0.3 Na-GTP, 0.1 EGTA, 10 2-Tris-phosphocreatine, 0.05% biocytin, adjusted to pH 7.3 with KOH and to 278 mOsm with double-distilled H_2O. Signals were amplified with a Multiclamp 700A amplifier (Molecular Devices), digitized (ITC-18, HEKA Instruments Inc.) and filtered at 2 kHz. Data were monitored, acquired and in some cases analyzed using Axograph X software. Series resistance was monitored throughout the experiments by applying a small test voltage step and measuring the capacitive

current. Series resistance was 5~25 MΩ and only cells with <20% change in series resistance and holding current were included in the analysis. Reported membrane potentials and holding potentials were not corrected for liquid junction potential unless otherwise specified.

For excitability measurements, 500 ms current steps were applied at 50 pA increments from -300 pA to 500 pA. Numbers of APs per 500 ms were only quantified for steps 250 pA and above to ensure all wildtype and mutant cells were above firing threshold. For all spike-timing experiments, GABAa receptors were blocked with SR-95531 (Gabazine, 5μM, Ascent Scientific), and RMP was adjusted to -75 mV for all cells by injecting a small current. Amplitudes of dc current steps were adjusted for individual cells to obtain 12 spikes in 500 ms. This firing rate was chosen based on input-output relations observed for cells recorded – 12 APs could be reliably achieved in all wildtype and Dcdc2 mutant neurons by applying 200 - 450 pA current. Spike trains were repeatedly generated for 10 to 20 times with 14.5 s between trials for each cell. Noise stimuli were generated in Matlab (Mathworks) according to methods used by Mainen et al., which consisted of a Gaussian white noise with mean (μ_s) = 200 pA and SD (σ_s) = 100 pA, convolved with the function $f(t) = t \exp(-t / \tau_s)$ with time constant τ_s = 3 ms to simulate synaptic integration (Mainen and Sejnowski 1995). The step duration in these experiments was 1 s. In specified experiments, DL-2-amino-5-phosphopentanoic acid (DL-AP5, 100 μM, Ascent Scientific) was used to block NMDARs, Ro25-6981 (0.5 μM, Ascent Scientific) to block specifically

NMDAR 2B subunits (NR2Bs), and 2,3,dioxo-6-nitro-1,2,3,4,tetrahydrobenzo-quinoxaline-7-sulfonamide (NBQX, 10 μM, Ascent Scientific) to block AMPARs.

For spontaneous NMDA activity measurements, internal solution used contained (in mM): 110 $CsMeSO_4$, 10 CsCl, 10 HEPES, 10 Cs_4-BAPTA, 5 QX-314•Br, 0.1 spermine, 4 Mg-ATP, 0.4 Na-ATP, 10 2-Tris-phosphocreatine, 0.05% biocytin, adjusted to pH 7.3 with KOH to 278 mOsm with double-distilled H_2O. Recordings began at least 10 min after initial whole cell recording to allow dialysis of Cs^+ internal solution. Cells were voltage-clamped at +40 mV in the presence of NBQX (10 μM) and tetrodotoxin (TTX, 1 μM, Ascent Scientific). GABAa receptors were blocked with SR-95531 (Gabazine, 5μM, Ascent Scientific). DL-APV (100 μM) washes were 8 – 10 minutes in duration, and 180 s recordings before and after (while DL-APV application continued) were used for spontaneous phasic event analysis.

Data Analysis and Statistics

APs were detected using either Axograph X built-in data analysis package or IGOR Pro software (Wavemetrics) on a Macintosh computer. AP shape analyses were performed according to previously established criteria (Bean 2007). Since the focus of this study was spike trains, for AP shape measurement, the third AP in a 12-spike, 500 ms spike train was used for analysis to avoid bursting APs. Peak amplitude was measured as the voltage relative to 0 mV. Rise time as measured as the duration between 10-90% of spike height, defined as the distance between AP threshold and AP peak, and spike width was measured as the width at half-maximum of spike height. To

calculate AP maximum rate of rise, phase-plane plots were constructed by plotting the time derivative of membrane voltage (dV/dt) versus membrane voltage (V). Threshold was determined at where dV/dt exceeds 50 mV/ms, and the maximum rate of rise was measured as the highest dV/dt value.

For membrane property measurements, voltage responses to 1s current steps from -300 pA to 300 pA at 20 pA increments were recorded and current-voltage relations (I-Vs) were constructed by measuring the average amplitude of the last 20 ms of the steady-state sub-threshold responses. Resting membrane potentials (RMPs) were measured within first 20 s of break-in with no holding current. Slope current and conductance was accessed in voltage-clamp configuration, by applying a slow voltage ramp at the rate of 30 mV/s from -110 mV to +10 mV, and current response was measured between -110 to -55 mV.

Current-voltage relations (I-Vs) were constructed by measuring the average amplitude of the last 20 ms of the steady-state response of 1 s sub-threshold current steps. Polynomials with 3 degrees of freedom were used for curve fitting. Input resistance of each cell was measured as the slope at x = 0 pA. In voltage clamp experiments, the slope conductance (G_{slope}) was determined by measuring the slope of linear regression to the passive region (-110 to -80 mV) of the slope current. Liquid junction potential was not corrected in experiments.

In spike-timing experiments, rastergrams were generated using Igor Pro software. Inter-spike interval (ISI) was calculated by subtracting the time when the AP peak occurs by that of the previous AP for each spike train.

Instantaneous firing rate was calculated as the inverse of ISI and plotted against the peak time of the first spike in the pair. ISI histogram was generated by sorting peak time of spikes from all spike trains, and plotting ISI between two subsequent spikes. Each spike in a train, or spike alignment across all trials, was classified as an event. Jitter of an event was quantified as the standard deviation (SD) of times at which AP peaks occur from all trials at that particular event. Temporal jitter and jitter histograms represented the average jitter of all cells at the n^{th} event:

$$\text{Jitter}_{nth} = \frac{\text{Cell 1 jitter}_{nth} + \text{Cell 2 jitter}_{nth} + \ldots + \text{Cell N jitter}_{nth}}{N}$$

where N is the number of cells recorded.

Coefficient of variance (CV) of the n_{th} inter-stimulus-interval (ISI) was quantified by dividing the standard deviation (SD) of ISIs between two events by their mean across all trials. Similar methods histograms as described for jitter quantification were used to construct CV.

To detect phasic spontaneous NMDAR-mediated events, a variable amplitude template was slid through 180 s chart recordings (Clements 1997). The parameters of the template, including amplitude, 10-90% rise time, and decay time, were determined based on an average of real events as well as previously reported values. The detection threshold is 4 to 9 times of the noise standard deviation. Events detected were in some cases verified manually. Tonic current is measured by subtracting the mean current response recorded before and after the application of DL-APV. Statistics were performed using Excel (Microsoft) and

Prism 6 software (Graphpad), and graphs were generated in IGOR Pro software (Wavemetrics). Statistical significance was determined using either two-tailed Student's t-Test (indicated on figures with asterisks) or repeated measures ANOVA. Significance was based on *P* values < 0.05. Means and standard errors were reported for all results unless otherwise specified.

RNA-seq Analysis

Forebrain dissection was performed on one WT (3 technical replicates) and two Dcdc2 mutant (3 technical replicates for one, 1 for the other) P21 animals. All forebrains were immediately frozen in liquid nitrogen and stored at -80°C before RNA extraction. Approximately 200mg of forebrain tissue from either wildtype or mutant was subjected to RNA extraction by Trizol©, yielding approximately 19-23ug of total RNA. Samples were treated with DNAse1 to remove contamination. Three technical replicates for both wildtype and mutant of 8ug of total RNA were purified for mRNA and cDNA library construction for sequencing using the Illumina/Solexa technology.

The GERALD pipeline was used to map all 32-bp length reads to specific chromosomal locations. The mouse genome sequence assembly was downloaded from UCSC genome informatics portal (http://genome.ucsc.edu/). All reads were mapped to their chromosomal locations and tallied for wildtype and mutant by customized computer scripts. In subsequent analyses only the uniquely mapped reads were used and all multi-reads were eliminated. Transcripts with insufficient number of reads (<10) were also eliminated. Total reads for each gene were normalized by dividing them by the total number of

reads in each run, then averaged from three technical replicates and one biological replicate in the case of Dcdc2 mutant. Three technical replicates and one biological replicate in the mutants (KO5,6,7,8), and three technical replicates in wildtype (WT2,3,4) were used to determine the normalized expression ratios. Expression ratio for each gene was calculated by dividing the average normalized Dcdc2 mutant reads by normalized wildtype reads.

For secondary validation of RNA-sequencing, 1ug of total mRNA from mouse forebrain was reverse-transcribed into cDNA using oligo-dT primers and reverse transcriptase. RNA was then hydrolyzed, cDNA precipitated and resuspended in nuclease-free water. Gene specific primers were designed and tested for efficiency and specificity by serial dilutions and melt curve analysis. Sybr Green mix (ABI, Life Technologies) was used to amplify cDNA.

Results

Increased spike rate and decreased spike-time precision in Dcdc2 mutants

Neuronal spike rates and temporal patterns together encode stimulus features and stimulus change (Panzeri et al. 2001; Butts et al. 2007; Tiesinga et al. 2008; Kayser et al. 2010). We therefore assessed both spike rate and spike-time precision in neocortical pyramidal neurons in wildtype and Dcdc2 mutant mice. The rates of APs generated by a range of supra-threshold current steps were significantly increased in mutant neurons compared to wildtype neurons (repeated measures ANOVA, main effect of genotype: $F_{1, 36} = 9.34$, $P < 0.005$; $Dcdc2^{wt/wt}$, n = 16; $Dcdc2^{del2/del2}$, n = 22, Figure 2-1A,B). In addition, mutant neurons had more depolarized RMPs ($t_{44} = 3.61$, $p < 0.001$), and elevated input

resistances relative to WT (t_{44} = 2.34, p < 0.05), but were not significantly different from wildtypes in AP voltage threshold (t_{20} = 0.87, NS), amplitude (t_{20} = 0.16, NS) or width (t_{20} = 1.08, NS, Table 2-1).

In order to assess whether spike temporal precision was altered in Dcdc2 mutant neurons, we repeatedly presented supra-threshold depolarizing current steps to neurons with pre-stimulus RMPs adjusted to -75 mV. Spike rastergrams from 10 to 20 repeated stimulus trials were then used to calculate the temporal jitter in the timing of each AP. As an additional related measure of temporal precision, CV for each ISI was also calculated (Tiesinga et al. 2008). Dcdc2 mutants (n=10) showed far less AP temporal precision than wildtypes (n = 10, Figure 2-1C-F, right). Temporal jitter was significantly elevated in the mutants (repeated measures ANOVA, interaction: $F_{11, 198}$ = 8.38, p < 0.0001, Figure 2-1G; main effect of genotype: $F_{1,18}$ = 12.14, p < 0.005, Figure 2-1H). Similarly, CVs of ISIs were significantly elevated in mutants relative to wildtypes throughout the duration of stimulation (repeated measures ANOVA followed by Holm-Sidak's test, Figure 2-1I; main effects of genotype: $F_{1,18}$ = 22.76, P < 0.001, Figure 2-1J). The results indicate that mutant neurons exhibit increased spike rates and decreased spike-time temporal precision.

Increased spike rate, but not decreased temporal precision, is due to elevated RMP

Our comparison identified three changes in electrophysiological parameters in the mutant relative to wildtype neurons: elevated membrane potential, increased spike rate, and decreased temporal precision. In order to determine whether the elevation in RMP was responsible for elevated spike rate,

we performed an additional set of current clamp recordings in mutant neurons (n=14) in which the membrane potential of each mutant neuron was set to the average RMP of wildtype neurons, -75 mV, by injection of a hyperpolarizing rheobase. When repolarized to -75 mV, the firing rates of the mutants were no longer significantly different from the wildtypes (repeated measures ANOVA, main effect of genotype: $F_{1,28} = 0.029$, NS, Figure 2-1B). In contrast to the effect on spike rate, adjustment of RMPs in mutant neurons to wildtype levels did not reduce the average CV of spike timing nor did it reduce temporal jitter in the mutants to wildtype levels (Figure 2-2). Consistent with this dissociation, the average temporal jitter (repeated measures ANOVA followed by Holm-Sidak's test, main effect of genotype: $F_{1,16} = 16.14$, $P < 0.001$) and CV collapsed from all ISIs in mutants were consistently higher relative to the wildtypes at every spike rate tested (repeated measures ANOVA followed by Holm-Sidak's test, main effect of genotype: $F_{1,16} = 9.62$, $P < 0.01$; Dcdc2$^{wt/wt}$, n = 9; Dcdc2$^{del2/del2}$, n = 9, Figure 2-2A,B). Furthermore, RMP did not significantly correlate with average temporal jitter in either wildtype or mutant neurons (linear regression of Dcdc2$^{wt/wt}$ at 300 pA: $R^2 = 0.00085$, at 500 pA: $R^2 = 0.015$; Dcdc2$^{del2/del2}$ at 300 pA: $R^2 = 0.29$, at 500 pA: $R^2 = 0.014$; Dcdc2$^{wt/wt}$, n = 9; Dcdc2$^{del2/del2}$, n = 9; Figure 2-2C,D). These results together indicate that changes in spike rate and membrane depolarization observed in the mutants were not responsible for changes in AP temporal precision.

Grin2B expression is elevated in Dcdc2 mutants and NR2B blockade restores spike-time precision

In an effort to identify changes in ion channels or receptors that may be responsible for the underlying electrophysiological changes that could degrade spike-time precision in Dcdc2 mutants, we performed a whole-transcriptome RNA-seq comparison of wildtype and mutant neocortex at P21 (Figure 2-3A). A total of 155 transcripts were found to be up-regulated by 2-fold or more, and 113 transcripts were found to be down-regulated by 2-fold or more in mutants relative to wildtype neocortex. We searched the lists for ion channels that could be implicated in spike-time precision (i.e. voltage gated potassium channels or neurotransmitter receptors) and found that the most up-regulated transcript that encoded an ion channel or receptor was Grin2B, the 2B subunit of NMDAR (Figure 2-3A). The up-regulation of Grin2B was confirmed in a follow-up qRT-PCR experiment (n=6, Figure 2-3B). The possibility that elevated NMDAR-mediated currents could be involved in degrading temporal precision was shown previously in dynamic clamp experiments in which injected NMDAR-like conductances decreased temporal precision in neocortical pyramidal neurons(Harsch and Robinson 2000). To test whether elevated Grin2B contributed to spike timing changes, we examined the effect of bath applying the NR2B-specific blocker Ro 25-6981 (0.5 μM) to mutant neurons (n = 7). We found that Ro 25-6981, similar to the pan NMDAR blocker DL-APV (see below), significantly increased measures of temporal precision in mutant neurons (repeated measures ANOVA, main effect of treatment: $F_{1,6} = 9.40$, $p < 0.01$], and

resulted in CVs of ISIs not significantly differ from wildtype neurons (repeated measures ANOVA, main effect of genotype: $F_{1,15} = 4.06$, NS, Figure 2-3C,D).

Tonic and phasic NMDAR activity is elevated in Dcdc2 mutants

We next tested for increases in NMDAR activity by directly measuring spontaneous NMDAR activity in voltage clamp. There are two types of spontaneous NMDAR currents in cortical neurons, a phasic current that reflects the discrete synaptic release of glutamate, and a tonic current that reflects activation of NMDARs by ambient glutamate (Sah et al. 1989; Mody et al. 1990). To determine whether these spontaneous NMDAR conductances were elevated in Dcdc2 mutant neurons, we isolated spontaneous NMDAR-mediated currents pharmacologically (SR-95531 and NBQX) and relieved voltage-dependent magnesium block by holding the membrane potential at +40 mV in physiological extracellular magnesium concentrations. We found a significant increase in the frequency (1.46 ± 0.24 Hz in Dcdc2$^{del2/del2}$ vs. 0.65 ± 0.12 in Dcdc2$^{wt/wt}$; $t_{22} = 2.46$, $p < 0.05$, Figure 2-4A-C), but not amplitude (10.69 ± 0.86 pA in Dcdc2$^{del2/del2}$ vs. 8.76 ± 0.75 pA in Dcdc2$^{wt/wt}$; $t_{22} = 1.54$, NS, Figure 2-4D), rise time (4.19 ± 0.15 ms in Dcdc2$^{del2/del2}$ vs. 4.16 ± 0.29 in Dcdc2$^{wt/wt}$; $t_{22} = 0.13$, NS, Figure 2-4E) or decay time (38.79 ± 1.18 ms in Dcdc2$^{del2/del2}$ vs. 39.45 ± 1.09 in Dcdc2$^{wt/wt}$; $t_{22} = 0.38$, NS, Figure 2-4F) of phasic NMDAR-mediated currents in the mutants relative to wildtypes (Dcdc2$^{wt/wt}$, n = 9; Dcdc2$^{del2/del2}$, n = 15). The tonic NMDAR current, measured by the change in steady-state current amplitude after APV application, was also increased in mutants relative to wildtype neurons (47.2 ±

6.2 pA in Dcdc2$^{del2/del2}$, n =8; 23.3 ± 4.1 in Dcdc2$^{wt/wt}$, n = 8; t_{14} = 3.23, p < 0.01. Figure 2-4G,H).

Blockade of NMDARs but not AMPARs restores spike-time precision

We next tested whether the effect on AP temporal precision in the mutants was specific to blockade of the NMDA class of glutamate receptors. We compared the effects of the pan-NMDAR antagonist APV with effects of the non-NMDA glutamate receptor antagonist NBQX in both mutant and wildtype neurons. In Dcdc2 mutants blocking NMDARs with DL-APV (100 μM) was, similar to the effects of the NR2B specific antagonist, effective at reducing CVs (repeated measures ANOVA, main effect of treatment: $F_{1,9}$ = 40.26, p < 0.005) and returning AP timing precision to wildtype levels (repeated measures ANOVA, main effect of genotype: $F_{1,18}$ = 0.67, NS, n = 10, Figure 2-5A,C). In contrast, blockade of the non-NMDA glutamate receptors (AMPARs) by NBQX (10 μM) had no significant effect on the temporal precision of AP timing in Dcdc2 mutants (repeated measures ANOVA, main effects of treatment: $F_{1,9}$ = 0.16, NS, n = 10, Figure 2-5B,D). Thus, the rescue of AP temporal precision in the mutants is specific to the NMDA class of glutamate receptors.

Blockade of NMDARs restores spike-time precision in response to stationary noisy stimuli

Neurons *in vivo* typically receive stimulation from relatively noisy barrages of synaptic currents. We therefore assessed whether the temporal precision changes in the mutants were apparent to noisy stimuli typical of *in vivo* synaptic inputs. The stimulus applied was a filtered Gaussian distribution designed

previously to approximate the rapid fluctuation of membrane potentials resulting from the integration of many synaptic events (Mainen and Sejnowski 1995; Cecchi et al. 2000). Similar to previous reports, fluctuating noise stimuli elicited spike trains with higher temporal precision than did square wave current stimulation (Figure 2-6A). Even with these noisy stimuli that produce more temporally precise patterns of APs, mutant neurons showed significantly less precise spike timing than wildtype neurons (Figure 6B). Moreover, similar to the changed response to square wave stimuli, APV significantly reduced both measures of temporal precision, jitter (repeated measures ANOVA followed by Sidak's test, interaction: genotype x treatment interaction: $F_{1,14} = 9.40$, $p < 0.01$) and CV (repeated measures ANOVA followed by Sidak's test, genotype x treatment interaction: $F_{1,14} = 13.34$, $p < 0.005$) in mutant neurons to wildtype levels (Figure 2-6C-F).

Discussion

Several electrophysiological properties influence the temporal precision of APs in central neurons, including nonlinearity of membrane conductances at threshold (Schoppa and Westbrook 1999; Azouz and Gray 2000; Cudmore et al. 2010) and synaptic noise (Chance et al. 2002; Tiesinga and Sejnowski 2004). Spontaneous synaptic noise can either enhance or reduce the temporal precision of spike trains depending on their features (review see Ermentrout et al. 2008). In cortical RS neurons specifically, the type of background synaptic conductance added can affect the gain and variability in the timing of APs elicited by depolarizing inputs (Harsch and Robinson 2000; Chance et al. 2002; Fellous et

al. 2003; Zsiros and Hestrin 2005). We show that in Dcdc2 mutant mice, cortical RS neurons have higher trial-to-trial spike-time variability, elevated NMDA conductances, and spike timing can be returned to wildtype levels by blocking NMDARs. Our results show that change in endogenous NMDAR activity, which can occur in many physiological (Grosshans et al. 2001; Ngo-Anh et al. 2005; Yuen et al. 2005) and pathological states (Epstein et al. 1994; Lau and Zukin 2007), can result in altered spike-time temporal precision.

In addition to impaired spike-time precision, our findings show that deletion of Dcdc2 results in heightened excitability associated with depolarized RMP. In recent years, changes in intrinsic excitability of neurons as a type of non-synaptic plasticity have been shown to link to learning, and can be both synaptically driven or independent of synaptic stimulation (review see Mozzachiodi and Byrne 2010). Heightened cell excitability is often associated with more extreme pathology (Patricio O'Donnell MD 2008; Mozzachiodi and Byrne 2010; Badawy et al. 2012), but smaller changes in excitability could be related to degradation in sensory processing. For example, *in utero* RNAi of Kiaa0319 in rat neocortex has been recently shown to cause elevated excitability of neocortical pyramidal neurons (Centanni et al. 2013). This elevation in excitability caused by Kiaa0319 RNAi is also associated with less precise neural encoding of auditory stimuli (Centanni et al. 2013). Regulation of neuronal excitability may be a common function of Dcdc2 and Kiaa0319.

Dcdc2 is one of the 11-member doublecortin (DCX) gene family, whose molecular functions are mostly inferred from the DCX domain and its ability to

bind microtubules (Taylor et al. 2000). Although Dcdc2 biochemically interacts with tubulin and JIP 1/2 (Coquelle et al. 2006), its molecular role remains elusive. Members of DCX families have been shown to be involved in neuronal migration, intracellular transport, and cell signaling through protein-protein interaction (Dijkmans et al. 2010). Given the specific increase in NMDAR-mediated activity and Grin2B expression in Dcdc2 KO mice, it is possible that Dcdc2 is involved in homeostatic Grin2B transcript up-regulation. The mRNA up-regulation of Grin2B in the mutants also suggests the possibility that Dcdc2 acts as a co-repressor or RNA binding protein that destabilizes Grin2B, regulating Grin2B transcript levels directly. In fact, some members of the DCX-family can localize to the nucleus and Dcdc2 itself has a domain consistent with possible nuclear localization. Future studies will test these hypotheses by investigating interactions between Dcdc2 and known proteins involved in the transport of NR2B protein or Grin2B transcript, cellular localization of Dcdc2, and potential link between Dcdc2 and regulatory regions on Grin2B.

It is interesting to note that short-term memory for words in individuals with RD has been found to link to variants in GRIN2B (Ludwig et al. 2009). NMDAR activation is well known for its positive role in synaptic plasticity and learning. Intriguingly, increased NMDAR activity would be predicted to enhance plasticity at synapses by Hebbian mechanisms, but at the same time decreased spike-timing precision would tend to decrease Hebbian plasticity in a network. This balance may be a homeostatic change to counter spurious spike-timing dependent plasticity in networks that could result from elevated NMDAR activity.

Alternatively, a network with greater synaptic plasticity but with increased spike-time variability may be more dynamic in terms of new patterns that can be stored.

Although dyslexia is primarily a language-specific learning disorder, there is evidence that the underlying neurological changes may be dissociable from language, and associated with more generalized changes in temporal and sensory processing (McAnally and Stein 1996; Ramus 2003; Lehongre et al. 2011). Several cognitive changes that do not directly involve reading have been linked to dyslexia, including alterations in event-related potentials (Czamara et al. 2010) and fMRI responses to non-word stimuli (Gaab et al. 2007), as well as in general sensory stimulus sampling (Vandermosten et al. 2010; Goswami 2011; Lehongre et al. 2011). It has been theorized that temporal processing deficits are associated with abnormal cortical firing (Ahissar et al. 2000; Engineer et al. 2008), and precise spike timing may contribute to high-speed population coding and synchronization (Tchumatchenko et al. 2011) as well as enhance discrimination of stimuli (Tiesinga and Toups 2005). Our study indicates the possible link between a dyslexia-associated gene, Dcdc2, and a cellular physiological dysfunction in spike-time precision that could be the basis for changes in temporal processing on a system level.

This study demonstrates that genetic manipulation of Dcdc2 leads to increases in NMDAR activity. Several possibilities may account for this elevated activity: 1) an increased number of postsynaptic NMDARs; 2) an increased number of synapses; 3) increased ambient glutamate concentration; 4) an increased number of presynaptic NMDARs (comprised of mostly NR1/NR2B in

the cortex after early postnatal stages (Corlew et al. 2007; Brasier and Feldman 2008; Kunz et al. 2013)), which leads to higher transmitter release probability from the presynaptic terminals. Elevated Grin2B mRNA expression level and potential functional changes associated with this increase (such as altered NMDAR subunit composition, change in receptor distribution, or change in developmental switch) does not directly provide evidence favoring one of the above listed possibilities. The following chapter, Chapter 3, tests these possible changes using electrophysiology to identify the cause for increased NMDAR activity in the Dcdc2 mutants.

References

Ahissar M, Protopapas A, Reid M, Merzenich MM. Auditory processing parallels reading abilities in adults. Proc Natl Acad Sci USA. 2000 Jun 6;97(12):6832–7.

Azouz R, Gray CM. Dynamic spike threshold reveals a mechanism for synaptic coincidence detection in cortical neurons in vivo. Proc Natl Acad Sci USA. 2000 Jul 5;97(14):8110–5.

Badawy RAB, Freestone DR, Lai A, Cook MJ. Epilepsy: Ever-changing states of cortical excitability. Neuroscience. 2012 Oct 11;222:89–99.

Bean BP: The action potential in mammalian central neurons. Nat Rev Neurosci 2007;8: 451–465.

Brasier D, Feldman DE. Synapse-Specific Expression of Functional Presynaptic NMDA Receptors in Rat Somatosensory Cortex. J Neurosci. 2008 Feb 27;28(9):2199-211.

Butts DA, Weng C, Jin J, Yeh C-I, Lesica NA, Alonso J-M, et al. Temporal precision in the neural code and the timescales of natural vision. Nature. 2007 Sep 6;449(7158):92–5.

Cecchi GA, Sigman M, Alonso J-M, Martinez L, Chialvo DR, Magnasco MO. Noise in Neurons Is Message Dependent. Proc Natl Acad Sci USA. 2000 May 9;97(10):5557–61.

Centanni TM, Booker AB, Sloan AM, Chen F, Maher BJ, Carraway RS, et al. Knockdown of the Dyslexia-Associated Gene Kiaa0319 Impairs Temporal Responses to Speech Stimuli in Rat Primary Auditory Cortex. Cerebral Cortex. Cereb Cortex. 2014 Jul;24(7):1753-66.

Chance FS, Abbott LF, Reyes AD. Gain modulation from background synaptic input. Neuron. 2002 Aug 15;35(4):773–82.

Clements J: Detection of spontaneous synaptic events with an optimally scaled template. Biophysical Journal.1997;73: 220-229

Cope N, Eicher JD, Meng H, Gibson CJ, Hager K, Lacadie C, et al. Variants in the DYX2 locus are associated with altered brain activation in reading-related brain regions in subjects with reading disability. NeuroImage. 2012 Oct;63(1):148–56.

Coquelle FM, Levy T, Bergmann S, Wolf SG, Bar-El D, Sapir T, et al. Common and divergent roles for members of the mouse DCX superfamily. Cell cycle (Georgetown, Tex) [Internet]. 2006 May 1;5(9):976–83.

Corlew R, Wang Y, Ghermazien H, Erisir A, Philpot BD. Developmental Switch in the Contribution of Presynaptic and Postsynaptic NMDA Receptors to Long-Term Depression. Journal of Neuroscience. 2007 Sep 12;27(37):9835–45.

Cudmore RH, Fronzaroli-Molinieres L, Giraud P, Debanne D. Spike-Time Precision and Network Synchrony Are Controlled by the Homeostatic Regulation of the D-Type Potassium Current. Journal of Neuroscience. 2010 Sep 22;30(38):12885–95.

Czamara D, Bruder J, Becker J, Bartling J, Hoffmann P, Ludwig KU, et al. Association of a Rare Variant with Mismatch Negativity in a Region Between KIAA0319 and DCDC2 in Dyslexia. Behav Genet. 2010 Nov 21;41(1):110–9.

Darki F, Peyrard-Janvid M, Matsson H, Kere J, Klingberg T. Three Dyslexia Susceptibility Genes, DYX1C1, DCDC2, and KIAA0319, Affect Temporo-Parietal White Matter Structure. Biol Psychiatry. 2012 Oct 15;72(8):671-6.

Dijkmans TF, van Hooijdonk A, Wilhelmina L, Fitzsimons CP, Vreugdenhil E. The doublecortin gene family and disorders of neuronal structure. Cent Nerv Syst Agents Med Chem. 2010 Mar;10(1):32-46.

Engineer CT, Perez CA, Chen YH, Carraway RS, Reed AC, Shetake JA, et al. Cortical activity patterns predict speech discrimination ability. Nat Neurosci. 2008 May;11(5):603–8.

Epstein FH, Lipton SA, Rosenberg PA. Excitatory amino acids as a final common pathway for neurologic disorders. New England Journal of Medicine. 1994;330(9):613–22.

Ermentrout GB, Galán RF, Urban NN. Reliability, synchrony and noise. Trends in Neurosciences. 2008 Aug;31(8):428–34.

Fellous JM, Rudolph M, Destexhe A, Sejnowski TJ. Synaptic background noise controls the input/output characteristics of single cells in an in vitro model of in vivo activity. Neuroscience. 2003;122(3):811–29.

Gaab N, Gabrieli JDE, Deutsch GK, Tallal P, Temple E. Neural correlates of rapid auditory processing are disrupted in children with developmental dyslexia and ameliorated with training: an fMRI study. Restor Neurol Neurosci. 2007;25(3-4):295–310.

Gabel LA, Marin I, Loturco JJ, Che A, Murphy C, Manglani M, et al. Mutation of the dyslexia-associated gene Dcdc2 impairs LTM and visuo-spatial performance in mice. Genes, Brain and Behavior. 2011 Oct 19;10(8):868–75.

Goswami U. A temporal sampling framework for developmental dyslexia. Trends in Cognitive Sciences. 2011 Jan;15(1):3–10.

Grosshans DR, Clayton DA, Coultrap SJ, Browning MD. LTP leads to rapid surface expression of NMDA but not AMPA receptors in adult rat CA1. Nat Neurosci. Nature Publishing Group; 2001 Dec 10;5(1):27–33.

Harsch A, Robinson H. Postsynaptic variability of firing in rat cortical neurons: the roles of input synchronization and synaptic NMDA receptor conductance. J Neurosci. 2000;20(16):6181–92.

Kayser C, Logothetis NK, Panzeri S. Millisecond encoding precision of auditory cortex neurons. Proc Natl Acad Sci USA. 2010 Sep 28;107(39):16976–81.

Kunz PA, Roberts AC, Philpot BD. Presynaptic NMDA Receptor Mechanisms for Enhancing Spontaneous Neurotransmitter Release. J Neurosci. 2013 May 1;33(18):7762–9.

Lau CG, Zukin RS. NMDA receptor trafficking in synaptic plasticity and neuropsychiatric disorders. Nat Rev Neurosci. 2007 Jun;8(6):413–26.

Lehongre K, Ramus F, Villiermet N, Schwartz D, Giraud A-L. Altered low-γ sampling in auditory cortex accounts for the three main facets of dyslexia. Neuron. 2011 Dec 22;72(6):1080–90.

Ludwig KU, Roeske D, Herms S, Schumacher J, Warnke A, Plume E, et al. Variation in GRIN2Bcontributes to weak performance in verbal short-term memory in children with dyslexia. Am J Med Genet B Neuropsychiatr Genet. 2010 Mar 5;153B(2):503-11.

Mainen ZF, Sejnowski TJ. Reliability of Spike Timing in Neocortical Neurons. Science. 1995 Jun 9;268(5216):1503–6.

McAnally KI, Stein JF. Auditory temporal coding in dyslexia. Proc Biol Sci. 1996 Aug 22;263(1373):961–5.

Meda SA, Gelernter J, Gruen JR, Calhoun VD, Meng H, Cope NA, et al. Polymorphism of DCDC2 Reveals Differences in Cortical Morphology of Healthy Individuals—A Preliminary Voxel Based Morphometry Study. Brain Imaging and Behavior. 2007 Nov 27;2(1):21–6.

Meng H, Smith SD, Hager K, Held M, Liu J, Olson RK, et al. DCDC2 is associated with reading disability and modulates neuronal development in the brain. Proc Natl Acad Sci USA. 2005 Nov 22;102(47):17053–8.

Mody I, Kriegstein A, LoTurco J. Differential activation of glutamate receptors by spontaneously released transmitter in slices of neocortex. Neuroscience letters. 1990;114:265–71.

Mozzachiodi R, Byrne JH. More than synaptic plasticity: role of nonsynaptic plasticity in learning and memory. Trends in Neurosci. 2010 Jan;33(1):17–26.

Ngo-Anh TJ, Bloodgood BL, Lin M, Sabatini BL, Maylie J, Adelman JP. SK channels and NMDA receptors form a Ca2+-mediated feedback loop in dendritic spines. Nat Neurosci. 2005 May;8(5):642–9.

Panzeri S, Petersen RS, Schultz SR, Lebedev M, Diamond ME. The role of spike timing in the coding of stimulus location in rat somatosensory cortex. Neuron. 2001;29:769–77.

Paracchini S. The chromosome 6p22 haplotype associated with dyslexia reduces the expression of KIAA0319, a novel gene involved in neuronal migration. Human Molecular Genetics. 2006 Apr 6;15(10):1659–66.

Patricio O'Donnell MD P. Increased Cortical Excitability as a Critical Element in Schizophrenia Pathophysiology. Cortical Deficits in Schizophrenia. Springer US; 2008. pp. 219–36.

Petersen CCH, Crochet S. Synaptic Computation and Sensory Processing in Neocortical Layer 2/3. Neuron. 2013 Apr 10;78(1):28–48.

Pinel P, Fauchereau F, Moreno A, Barbot A, Lathrop M, Zelenika D, et al. Genetic Variants of FOXP2 and KIAA0319/TTRAP/THEM2 Locus Are Associated with Altered Brain Activation in Distinct Language-Related Regions. J Neurosci. 2012 Jan 18;32(3):817–25.

Ramus F. Developmental dyslexia: specific phonological deficit or general sensorimotor dysfunction? Current Opinion in Neurobiology. 2003 Apr;13(2):212–8.

Rosenberg J, Pennington BF, Willcutt EG, Olson RK. Gene by environment interactions influencing reading disability and the inattentive symptom dimension of attention deficit/hyperactivity disorder. J Child Psychol Psychiatry. 2012 Mar;53(3):243-51.

Sah P, Hestrin S, Nicoll RA. Tonic Activation of NMDA Receptors by Ambient Glutamate Enhances Excitability of Neurons. Science. 1989 Nov 10;246(4931):815–8.

Schoppa NE, Westbrook GL. Regulation of synaptic timing in the olfactory bulb by an A-type potassium current. Nat Neurosci. 1999 Dec;2(12):1106–13.

Schumacher J, Anthoni H, Dahdouh F, König IR, Hillmer AM, Kluck N, et al. Strong Genetic Evidence of DCDC2 as a Susceptibility Gene for Dyslexia. Am J Hum Genet. 2006 Jan;78(1):52-62.

Tallal P. Auditory temporal perception, phonics, and reading disabilities in children. Brain Lang. 1980 Mar;9(2):182-98.

Taylor KR, Holzer AK, Bazan JF, Walsh CA, Gleeson JG. Patient mutations in

doublecortin define a repeated tubulin-binding domain. J Biol Chem. 2000 Nov 3;275(44):34442–50.

Tchumatchenko T, Malyshev A, Wolf F, Volgushev M. Ultrafast Population Encoding by Cortical Neurons. Journal of Neuroscience. 2011 Aug 24;31(34):12171–9.

Tiesinga P, Fellous JM, Sejnowski TJ. Regulation of spike timing in visual cortical circuits. Nat Rev Neurosci. 2008;9(2):97–107.

Tiesinga P, Sejnowski TJ. Rapid temporal modulation of synchrony by competition in cortical interneuron networks. Neural Comput. 2004;16(2):251–75.

Tiesinga PHE, Toups JV. The possible role of spike patterns in cortical information processing. J Comput Neurosci. 2005 Jun;18(3):275–86.

Vandermosten M, Boets B, Luts H, Poelmans H, Golestani N, Wouters J, et al. Adults with dyslexia are impaired in categorizing speech and nonspeech sounds on the basis of temporal cues. Proc Natl Acad Sci USA. 2010 Jun 8;107(23):10389–94.

Wagner RK. Phonological processing abilities and reading implications for disabled readers. Journal of Learning Disabilities. J Learn Disabil. 1986 Dec;19(10):623-30.

Wang Y, Yin X, Rosen G, Gabel L, Guadiana SM, Sarkisian MR, et al. Dcdc2 knockout mice display exacerbated developmental disruptions following knockdown of doublecortin. Neuroscience. 2011 Sep 8;190:398–408.

Yuen EY, Jiang Q, Chen P, Gu Z, Feng J, Yan Z. Serotonin 5-HT1A Receptors Regulate NMDA Receptor Channels through a Microtubule-Dependent Mechanism. Journal of Neuroscience. 2005 Jun 8;25(23):5488–501.

Zou LL, Chen WW, Shao SS, Sun ZZ, Zhong RR, Shi JJ, et al. Genetic variant in KIAA0319, but not in DYX1C1, is associated with risk of dyslexia: an integrated meta-analysis. Am J Med Genet. 2012 Dec 1;159B(8):970–6.

Zsiros V, Hestrin S. Background Synaptic Conductance and Precision of EPSP-Spike Coupling at Pyramidal Cells. J Neurophysiol. 2005 Jun;93(6):3248-56.

Table 1. Electrophysiological properties of Dcdc2$^{wt/wt}$ and Dcdc2$^{del2/del2}$ RS neurons

Membrane properties	Dcdc2$^{wt/wt}$ cells (n = 21)	Dcdc2$^{del2/del2}$ cells (n = 25)
V_{rmp}* (mV)	-74.50 ± 0.88	-68.94 ± 1.19
R_{input}* (MΩ)	91.72 ± 7.74	125.20 ± 11.35
G_{slope}* (nS)	17.38 ± 0.08	11.13 ± 0.11
Action potential properties	Dcdc2$^{wt/wt}$ cells (n = 11)	Dcdc2$^{del2/del2}$ cells (n = 11)
Rise time (ms)	0.23 ± 0.01	0.21 ± 0.01
Width (ms)	0.93 ± 0.06	0.84 ± 0.05
Threshold (mV)	-37.65 ± 1.02	-38.69 ± 0.63
Peak (mV)	42.17 ± 2.00	42.61 ± 1.84
Max. rate of rise (mV/ms)	218.00 ± 11.63	228.20 ± 7.63

Data are means ± standard error. Asterisks indicate properties that are significantly different between Dcdc2$^{wt/wt}$ and Dcdc2$^{del2/del2}$ neurons.

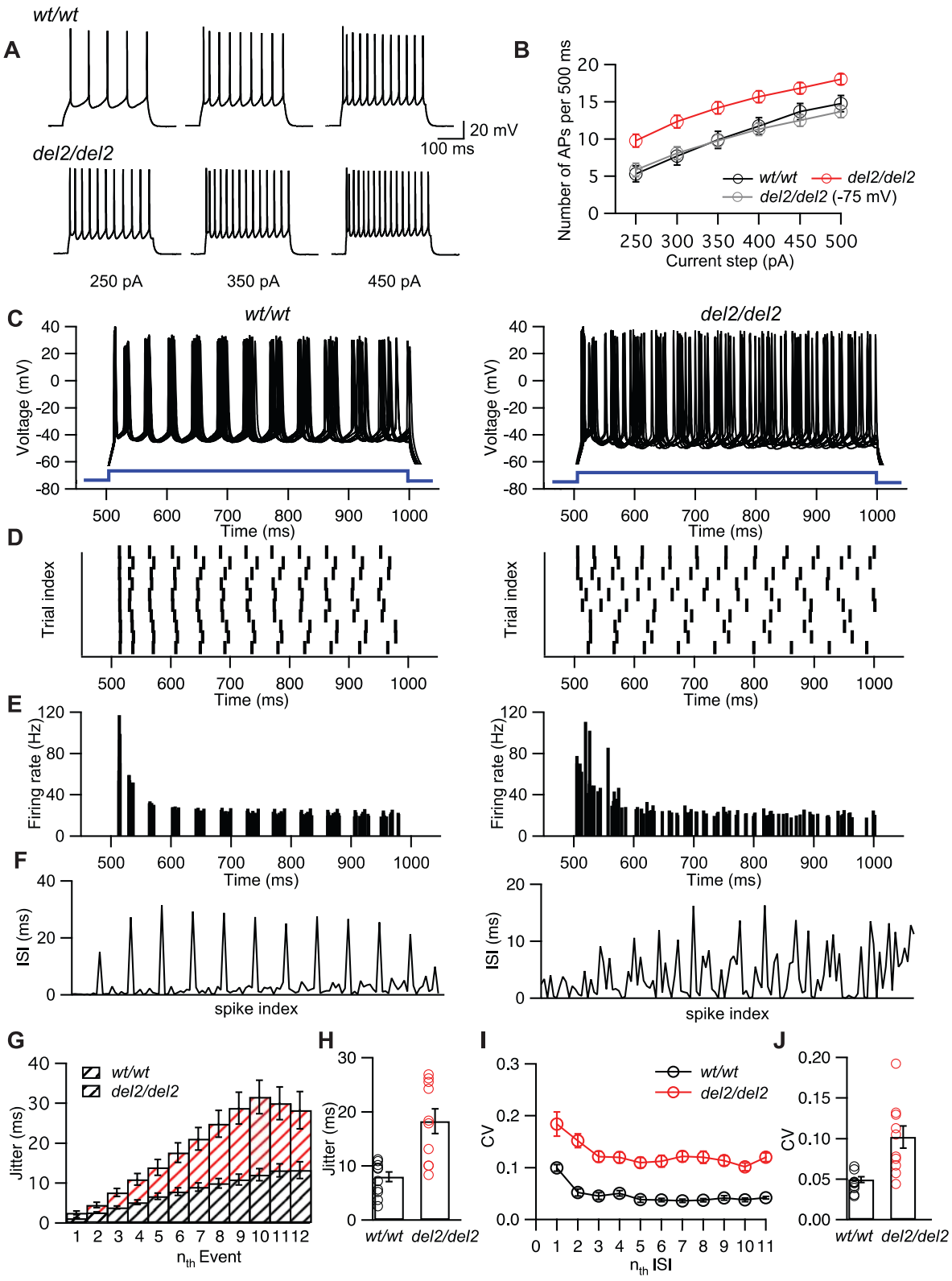

Figure 2-1. Dcdc2 mutant neurons have increased spike rates and spike-time variability. (A) Action potential trains elicited by 250 (left), 350 (middle), and 450 pA

(right) current steps in a Dcdc2$^{wt/wt}$ (top) and a Dcdc2$^{del2/del2}$ neuron (bottom). **(B)** Average number of APs generated by 500 ms current steps from 250 pA to 500 pA at 50 pA increments in Dcdc2$^{wt/wt}$ (black), Dcdc2$^{del2/del2}$ (red), and Dcdc2$^{del2/del2}$ neurons with RMP adjusted to -75 mV with holding current (gray). Repeated measures ANOVA, between variables: condition (Dcdc2$^{wt/wt}$, Dcdc2$^{del2/del2}$, and Dcdc2$^{del2/del2}$ at -75 mV), within variables: current step (250, 300, 350, 400, 450, 500 pA); main effect of condition: $F_{2,49} = 6.30$, $p < 0.005$; followed by Dunnett's test, difference significant between Dcdc2$^{wt/wt}$ and Dcdc2$^{del2/del2}$ for all 6 current steps, no significance between Dcdc2$^{wt/wt}$ and Dcdc2$^{del2/del2}$ (-75 mV) for all 6 current steps. Dcdc2$^{wt/wt}$: n = 16, Dcdc2$^{del2/del2}$: n = 22, Dcdc2$^{del2/del2}$ (-75 mV): n = 14. **(C)** Spike trains were evoked by 500 ms dc current injection and voltage traces from ten trials were overlaid for a Dcdc2$^{wt/wt}$ (left) and a Dcdc2$^{del2/del2}$ (right) neuron. Stimulus waveforms are indicated in blue. RMPs for recorded neurons were adjusted to -75 mV by constant current injection, and 12-spike AP trains for both conditions was achieved by adjusting the amplitude of current step. Correspondent **(D)** rastergrams and **(E)** histograms of instantaneous firing rate for a representative Dcdc2$^{wt/wt}$ (left) and Dcdc2$^{del2/del2}$ (right) neuron. Spikes from all ten trials were ordered according to their peak times, and histograms of ISIs between subsequent peaks were shown in **(F)**. **(G)** Temporal jitter (the standard deviation of spike times for each event) for Dcdc2$^{del2/del2}$ (red) and Dcdc2$^{wt/wt}$ (black) neurons. Repeated measures ANOVA, between variables: genotype (Dcdc2$^{wt/wt}$ and Dcdc2$^{del2/del2}$); within variables: event (1 to 12th event); genotype x event interaction: $F_{11, 198} = 8.38$, $p < 0.0001$. **(H)** the average jitter, or the main effect of genotype on jitter: $F_{1,18} = 12.14$, $p < 0.005$. The significant interaction between genotype and event is likely due to the accumulation of increased jitter towards later spikes. Holm-Sidak's test, no significance between Dcdc2$^{wt/wt}$ and Dcdc2$^{del2/del2}$ jitter: 1st to 6th event; significant different: 7th to 12th event. **(I)** The coefficient of variance (CV) of inter-spike intervals (ISIs) for each event in Dcdc2$^{wt/wt}$ and Dcdc2$^{del2/del2}$ neurons. Repeated measures ANOVA, between variables: genotype (Dcdc2$^{wt/wt}$ and Dcdc2$^{del2/del2}$); within variables: event (1st to 11th ISI), followed by Holm-Sidak's test, difference significant between genotypes for all 11 ISIs. **(J)** the average jitter, or the main effect of genotype: $F_{1,18} = 22.76$, $P < 0.0005$. Circles in **(H)** and **(J)** indicate collapsed averages from individual neurons. Error bars indicate SEM. Dcdc2$^{wt/wt}$: n = 10, Dcdc2$^{del2/del2}$: n = 10.

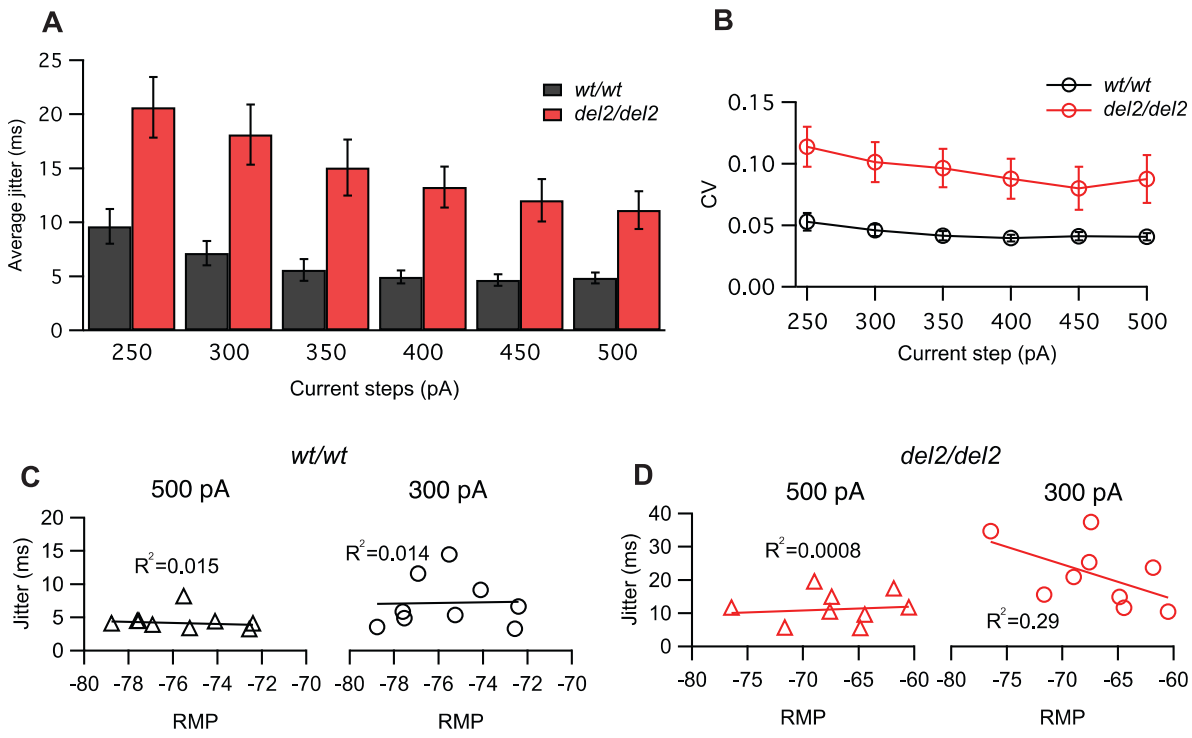

Figure 2-2. Decreased spike-time precision in Dcdc2$^{del2/del2}$ neurons is not a result of altered excitability and RMP. (A) Average jitter for Dcdc2$^{wt/wt}$ (dark grey bars) and Dcdc2$^{del2/del2}$ (red bars) neurons at 250, 300, 350, 400, 450, and 500 pA current injection. Repeated measures ANOVA (between variables: genotype; within variables: current step), main effects of genotype: $F_{1,16} = 16.14$, $p < 0.001$; followed by Holm-Sidak's test, difference significant between genotypes for all 6 current steps. **(B)** Average CV for Dcdc2$^{wt/wt}$ (black) and Dcdc2$^{del2/del2}$ (red) neurons. Repeated measures ANOVA (between variables: genotype; within variables: current step), main effects of genotype: $F_{1,16} = 9.62$, $p < 0.01$; followed by Holm-Sidak's test, difference significant between genotypes for all 6 current steps. Average jitter was not correlated with RMP in **(C)** Dcdc2$^{wt/wt}$ or **(D)** Dcdc2$^{del2/del2}$ neurons at 300 pA and 500 pA current step (linear regression, R^2 values of best fitted lines indicated on graphs). Error bars indicate SEM. Dcdc2$^{wt/wt}$, n = 9; Dcdc2$^{del2/del2}$, n = 9.

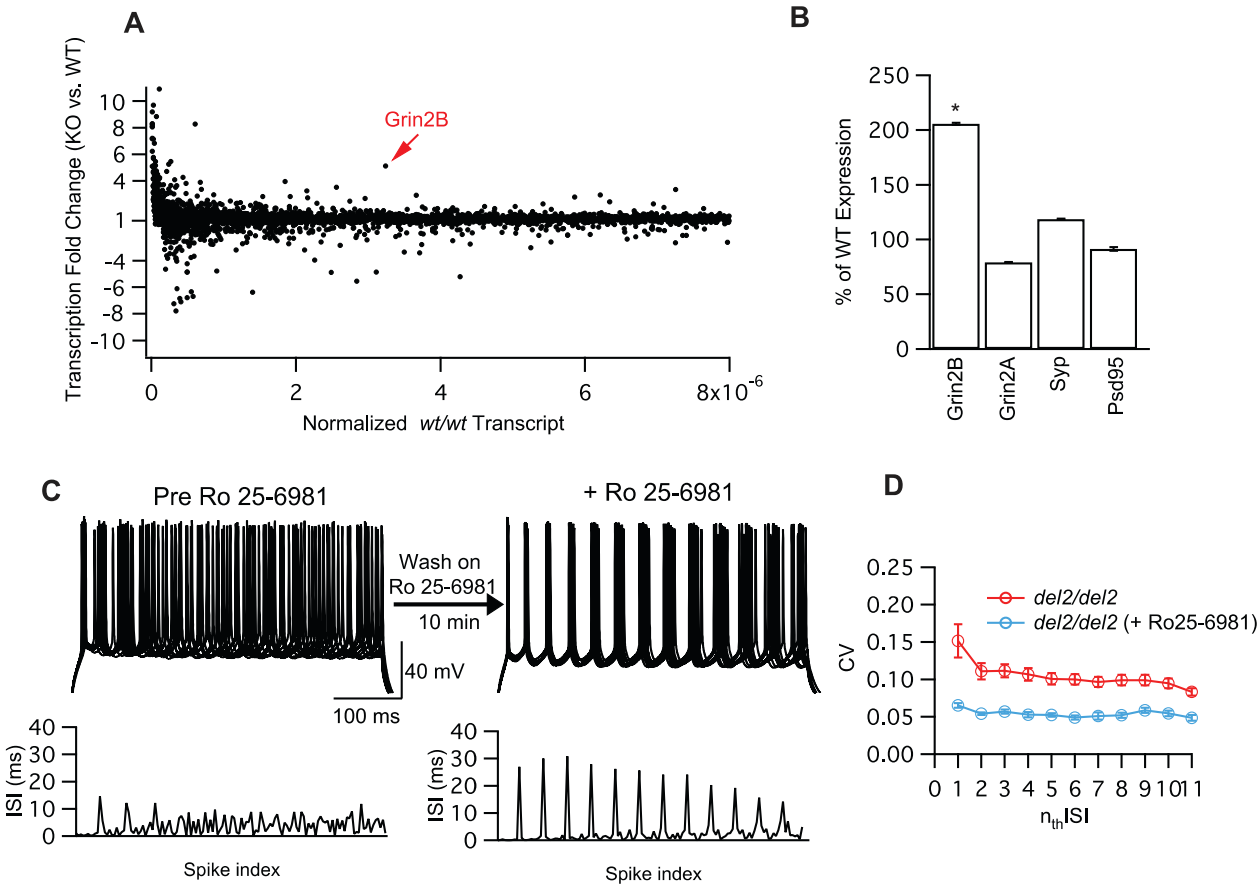

Figure 2-3. Dcdc2 mutants show elevated Grin2B expression and improved spike-time precision by NMDAR2B-specific antagonist Ro 25-6981. **(A)** RNA-seq profile of transcribed genes in P22 mouse forebrain. Transcription fold change (number of normalized reads in Dcdc2$^{del2/del2}$ relative to reads in Dcdc2$^{wt/wt}$ for each gene) was plotted against normalized Dcdc2$^{wt/wt}$ transcript reads. Grin2B is indicated by red arrow. **(B)** Expression levels of Grin2B, Grin2A, Synaptophysin (Syp) and Psd95 determined by qRT-PCR. Grin2B Dcdc2$^{wt/wt}$ vs. Dcdc2$^{del2/del2}$: Student's t-test, $p < 0.0005$. Dcdc2$^{wt/wt}$ and Dcdc2$^{del2/del2}$: n = 6. Grin2A, Syp and Psd95 were not differentially regulated in RNA-seq, and also not significantly different from Dcdc2$^{wt/wt}$ expression levels by qRT-PCR. **(C)** Representative spike trains and ISI histograms of a Dcdc2$^{del2/del2}$ neuron pre (left) and post (right) washing on Ro 25-6981 (0.5 M). Spike trains were evoked by 500 ms dc current input and voltage traces from 15 trials were overlaid. Twelve-spike AP trains for both conditions was achieved by adjusting the amplitude of current step. **(D)** Mean effect of Ro 25-6981 on CV of ISIs of 12-spike trains in Dcdc2$^{del2/del2}$ neurons. Repeated measures ANOVA, matching: event (1st to 11th ISI) and treatment (pre Ro 25-6981 and in Ro 25-6981), main effect of treatment: $F_{1,6} = 9.40$, $p < 0.005$. Error bars indicate SEM. Dcdc2$^{del2/del2}$, n = 7.

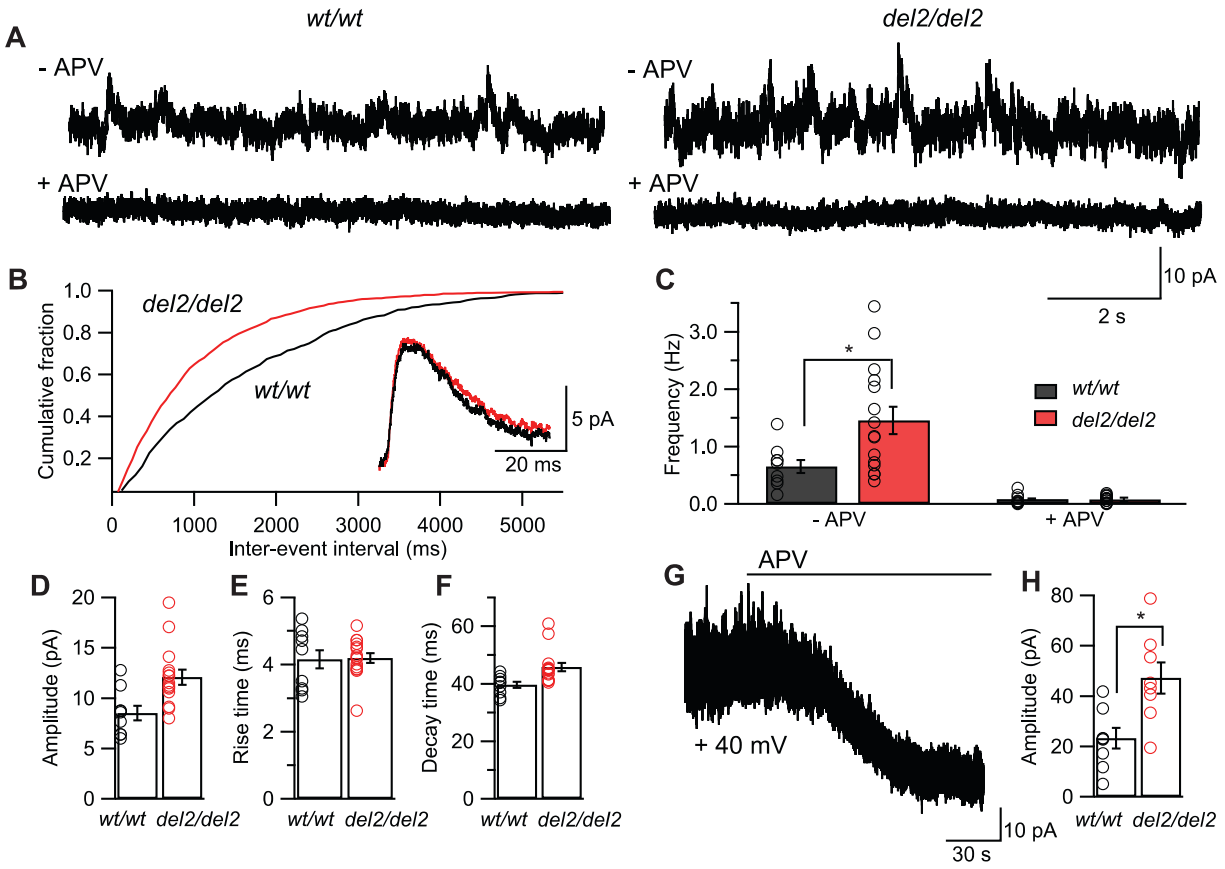

Figure 2-4. Dcdc2$^{del2/del2}$ neurons show more spontaneous NMDAR activity compared to Dcdc2$^{wt/wt}$ neurons. (A) Representative traces illustrate spontaneous NMDAR-mediated currents recorded at +40 mV in normal recording solution (top) and after washing on DL-APV (100 μM, bottom) for Dcdc2$^{wt/wt}$ (left) and Dcdc2$^{del2/del2}$ (right) neurons. **(B)** Cumulative probability histogram for inter-event interval of NMDAR-mediated events in normal recording solution for Dcdc2$^{wt/wt}$ and Dcdc2$^{del2/del2}$ neurons. The histogram is a mean of individual histograms from all cells recorded in both conditions. Inset, average waveform across the population (Dcdc2$^{wt/wt}$: black, Dcdc2$^{del2/del2}$: red) **(C)** Comparison of phasic NMDAR-mediated event frequencies in Dcdc2$^{wt/wt}$ versus Dcdc2$^{del2/del2}$ neurons. Student's *t*-Test, $t_{22} = 2.46$, $p < 0.05$; Dcdc2$^{wt/wt}$, n = 9; Dcdc2$^{del2/del2}$, n =15. Bath application of APV abolished NMDAR-mediated spontaneous events in the same Dcdc2$^{wt/wt}$ or Dcdc2$^{del2/del2}$ neurons. **(D)** Mean amplitude ($t_{22} = 1.54$, NS), **(E)** rise time ($t_{22} = 0.13$, NS], and **(F)** decay time ($t_{22} = 0.38$, NS) of Dcdc2$^{wt/wt}$ and Dcdc2$^{del2/del2}$ neurons were not significantly different. **(G)** Representative trace of the change in NMDAR-mediated tonic current and current variance during the application of APV at holding potential of +40 mV in a Dcdc2$^{del2/del2}$ neuron. Dotted lines indicate baseline averages. **(H)** Comparison of the change in mean tonic current pre and post

APV in Dcdc2$^{wt/wt}$ and Dcdc2$^{del2/del2}$ neurons. Student's t-test, t (14) = 3.23, $p < 0.01$. Dcdc2$^{wt/wt}$: n=8, Dcdc2$^{del2/del2}$: n=8. Circles indicate measurements from individual neurons. Error bars indicate SEM.

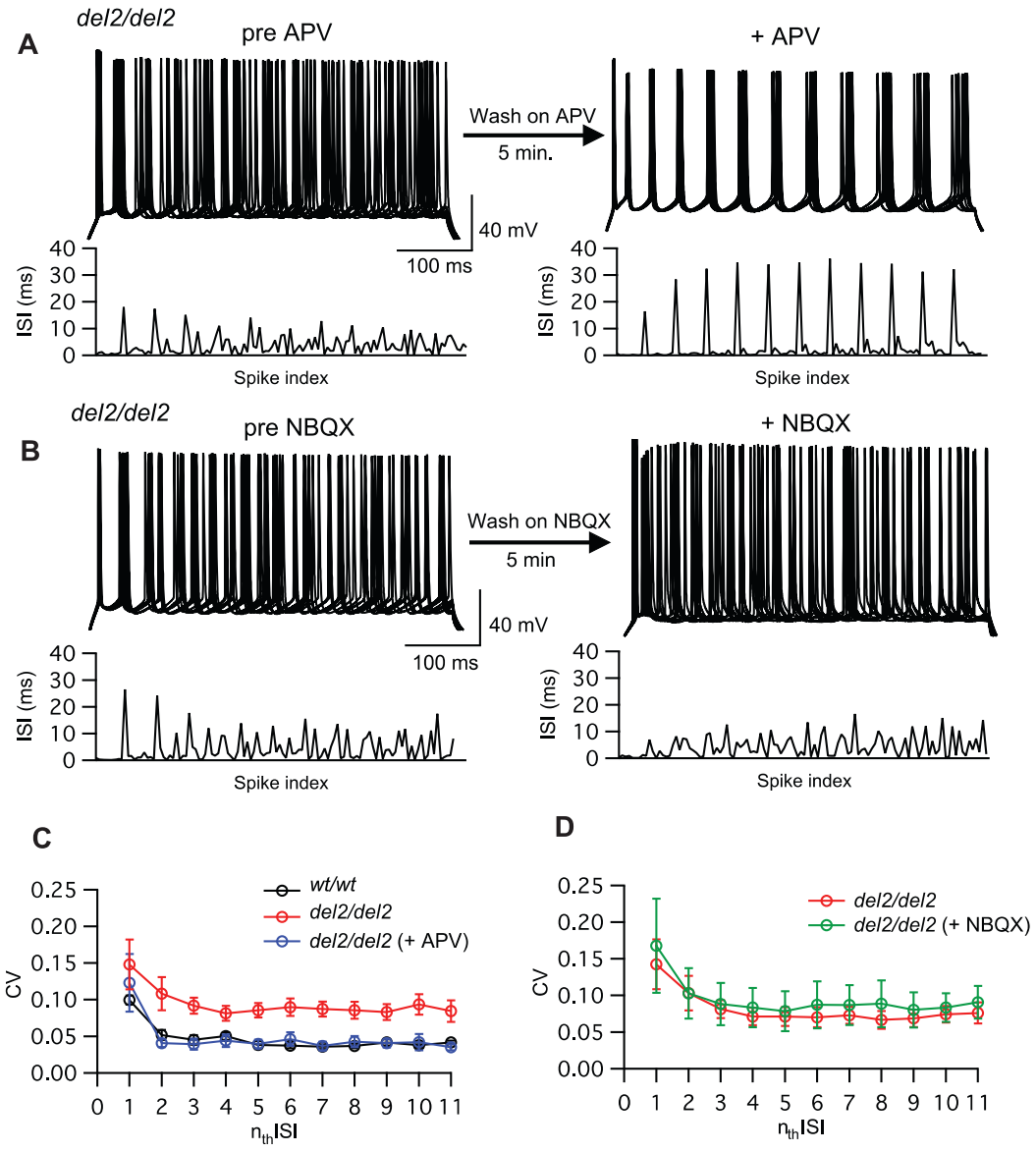

Figure 2-5. Blockade of NMDAR but not AMPAR restores spike timing variability in Dcdc2$^{del2/del2}$ neurons. Representative spike trains and ISI histograms of a Dcdc2$^{del2/del2}$ neuron pre (left) and after (right) washing on **(A)** DL-APV (100 M) and **(B)** NBQX (1 M). Spike trains were evoked by 500 ms dc current input and voltage traces from 15 trials were overlaid. Twelve-spike AP trains for both conditions was achieved by adjusting the amplitude of current step. **(C)** Mean effect of APV on CV of ISIs of 12-spike trains in Dcdc2$^{del2/del2}$ neurons. Dcdc2$^{del2/del2}$ pre vs. in APV: repeated measures ANOVA, matching: event (1st to 11th ISI) and treatment (pre APV and in APV); main effect of treatment: $F_{1,9} = 40.26$, $p < 0.005$. Dcdc2$^{del2/del2}$ in APV vs. Dcdc2$^{wt/wt}$: repeated measures ANOVA, between variables: genotype (Dcdc2$^{wt/wt}$ and Dcdc2$^{del2/del2}$); within variables: event (1st to 11th ISI); main effects of genotype: $F_{1,18} = 0.67$, NS. Dcdc2$^{wt/wt}$, n

= 10; Dcdc2$^{del2/del2}$, n = 10. **(D)** Mean effect of NBQX on CV of ISIs a 12-spike train in Dcdc2$^{del2/del2}$ neurons. Repeated measures ANOVA, matching: event (1st to 11th ISI) and treatment (pre NBQX and in NBQX); main effect of treatment: $F_{1,9}$ = 0.16, NS. Dcdc2$^{wt/wt}$: n=10, Dcdc2$^{del2/del2}$: n=10. Error bars indicate SEM.

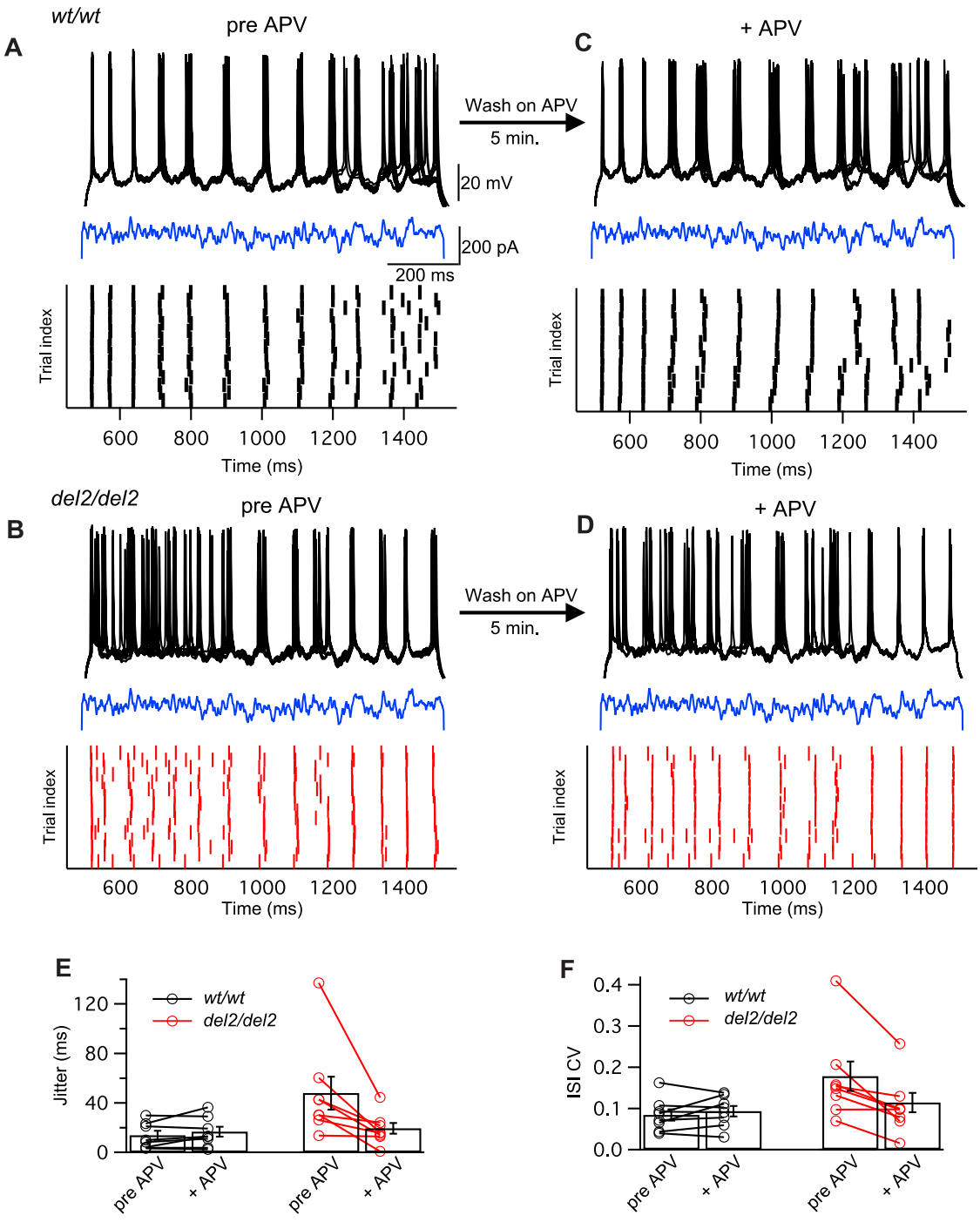

Figure 2-6. Blockade of NMDAR restores spike-time precision of Dcdc2$^{del2/del2}$ spike trains elicited by fluctuating current. A frozen noise stimulus (shown in blue; Gaussian white noise, mu = 200 pA, sigma = 100 pA, and tau = 3 ms) was applied repeatedly to evoke action potential trains. Overlaid voltage traces and rastergrams in a representative **(A)** Dcdc2$^{wt/wt}$ and a **(B)** Dcdc2$^{del2/del2}$ neuron. Spike trains and

rastergrams of the same **(C)** Dcdc2$^{wt/wt}$ and **(D)** Dcdc2$^{del2/del2}$ neurons after washing on DL-APV (100 M). **(E)** Effect of washing on APV on average Dcdc2$^{wt/wt}$ jitter (black) versus Dcdc2$^{del2/del2}$ jitter (red). Circles connected with lines indicate jitter measurement of the same cell before and after APV. Repeated measures ANOVA, between variables: genotype (Dcdc2$^{wt/wt}$ and Dcdc2$^{del2/del2}$), within variables: treatment (pre APV and in APV); genotype x treatment interaction: $F_{1,14} = 9.40$, $p < 0.01$; followed by Sidak's test, difference significant between genotypes pre APV, no significance in APV **(F)** Effect of washing on APV on average ISI CV in Dcdc2$^{wt/wt}$ (black) versus ISI CV in Dcdc2$^{del2/del2}$ (red). Circles connected with lines indicate CV calculated for the same cell before and after APV. Repeated measures ANOVA, between variables: genotype, within variables: treatment, genotype x treatment interaction: $F_{1,14} = 13.34$, $p < 0.005$; followed by Sidak's test, difference significant between genotypes pre APV, no significance in APV. Bars indicate averages and error bars indicate SEM. Dcdc2$^{wt/wt}$, n = 8; Dcdc2$^{del2/del2}$, n = 8.

III. *Dcdc2* Regulates Presynaptic Glutamate Release between Layer 4 Neurons of Neocortex

Abstract

We have shown previously that increased NMDAR-mediated activity is the cause for degraded spike-time precision in Dcdc2 mutant mice. In the present study, we showed increased synaptic release, but not increased postsynaptic NMDAR number or ambient glutamate concentration, is responsible for elevated NMDAR activation on the postsynaptic cell. When postsynaptic NMDAR are blocked, NMDAR antagonists restore both the elevated spontaneous and evoked release in mutant layer 4 somatosensory cortex back to wildtype levels, demonstrating that glutamate release in the mutants is tonically augmented by presynaptic NMDAR (preNMDAR) activation. Further, the locus of preNMDAR activation in the mutants is at the layer 4-layer 4 synaptic connections rather than the thalamocortical inputs. These results demonstrate the first synaptic role of a dyslexia-associated gene, and reveal that *Dcdc2* plays a role in restricting preNMDAR function within neocortical circuits.

Introduction

RD is a phenotypically and genetically complex disorder that is poorly understood at the level of neocortical microcircuits (Peterson and Pennington 2012; Rosenberg et al. 2012). One possible path towards eventually understanding how dyslexia may arise from changes at the level of synaptic microcircuits is to determine the synaptic function or functions of genes associated with dyslexia. While variants or mutations in any single gene do not

invariably cause dyslexia, genetic variants in *DCDC2* have been linked to an increased risk of dyslexia in multiple gene association studies in several populations (Meng et al. 2005; Schumacher et al. 2006; Couto et al. 2009; Marino et al. 2011; 2012). Furthermore, a recent fMRI study has made a connection between *DCDC2*, dyslexia and neocortical function by showing that a complex tandem repeat that can occur in the *DCDC2* gene associates with changes in neural activation in multiple neocortical areas, including regions of the inferior parietal lobe complex involved in reading (Eicher and Gruen 2013).

Requirements of Dcdc2 for normal electrophysiological patterns are beginning to be revealed by analyzing electrophysiological responses in Dcdc2 mutant mice (see chapter 2 and Che et al. 2013). Specifically, neocortical pyramidal neurons in layers 2/3 and 4 in Dcdc2 mutants display degraded spike-time precision caused by elevation in spontaneous NMDAR activation (Che et al. 2013). The possible causes of elevation in NMDAR activation in *Dcdc2* mutants include, but are not limited to, an increase in postsynaptic NMDARs, increase in the probability of vesicular transmitter release from glutamatergic terminals, and/or elevated levels of background glutamate levels. We report in this present study that the probability of excitatory transmitter release onto layer 4 neurons is elevated in somatosensory neocortex of Dcdc2 mutants, that release elevation is regulated by preNMDAR function, and that *Dcdc2* mutant mice show decreased somatosensory discrimination. The link between Dcdc2 gene function and elevated transmitter release mediated by preNMDAR function discovered here

may indicate novel therapeutic targets for forms of RD that are non-responsive to present interventions.

Materials and Methods

Immunohistochemistry and microscopy

All experiments involving animals were performed under the approval of the University of Connecticut Animal Care and Use Committee. For histology, P25 Tg(Dcdc2a-EGFP)JC 158 Gsat mice were transcardially perfused under deep anesthesia with 4% paraformaldehyde in 1X PBS. Brains were post-fixed for 24 hours prior to being sectioned with a vibratome (Leica) at 60 µm, and processed for immuno-staining as floating sections. Primary antibody used was goat anti-GFP (1:1000, Molecular Probes) and secondary antibody was rabbit anti-goat conjugated with Alexa 488 (1:400, Molecular Probes). Photomicrographs were acquired with Zeiss Axio Imager 2 with a Zeiss ApoTome module.

Acute brain slice preparation

P20-P28 wildtype and Dcdc2 mutant mice were deeply anesthetized with isoflurane and then decapitated. Brains were rapidly removed and immersed in ice-cold oxygenated (95% O_2 and 5% CO_2) dissection buffer containing (in mM): 83 NaCl, 2.5 KCl, 1 NaH_2PO_4, 26.2 $NaHCO_3$, 22 glucose, 72 sucrose, 0.5 $CaCl_2$, and 3.3 $MgCl_2$. Coronal slices (400 µm) were cut using a vibratome (VT1200S, Leica), incubated in dissection buffer for 40 min at 34°C, and then stored at room temperature for reminder of the recording day. All slice recordings were

performed at 34°C unless otherwise specified. Slices were visualized using IR differential interference microscopy (DIC) (E600FN, Nikon) and a CCD camera (QICAM, QImaging). Individual cells were visualized with a 40x Nikon Fluor water immersion (0.8 NA) objective.

Whole-cell recording

For all experiments, external recording buffer was oxygenated (95% O_2 and 5% CO_2) and contained (in mM): 125 NaCl, 25 $NaHCO_3$, 1.25 NaH_2PO_4, 3 KCl, 25 dextrose, 1 $MgCl_2$, and 2 $CaCl_2$. Patch pipettes were fabricated from borosilicate glass (N51A, King Precision Glass, Inc.) to a measured tip resistance of 2-5 MΩ when pipettes were filled with an internal solution containing (in mM): 125 potassium gluconate, 10 HEPES, 4 Mg-ATP, 0.3 Na-GTP, 0.1 EGTA, 10 phosphocreatine, 0.05% biocytin, adjusted to pH 7.3 with KOH and to 278 mOsm with double-distilled H_2O. Signals were amplified with a Multiclamp 700A amplifier (Molecular Devices), digitized with an ITC-18 digitizer (HEKA Instruments Inc.) and filtered at 2 KHz. Data were monitored, acquired and in some cases analyzed using Axograph X software. Series resistance was monitored throughout the experiments by applying a small test voltage step and measuring the capacitive current. Series resistance was 5~25 MΩ and only cells with <20% change in series resistance and holding current were included for analysis. Liquid junction potential was not corrected.

All excitatory miniature EPSCs (mEPSCs) were measured in the presence of the $GABA_A$ receptor blocker SR-95531 (Gabazine, 5μM, Ascent Scientific) and in tetrodotoxin (TTX, 1μM, Ascent Scientific) to isolate AMPAR-mediated events.

AMPAR-mediated mEPSC were recorded at -80 mV and MK-801 (1 mM) was added in recording pipette additionally to block the postsynaptic NMDAR-mediated currents in experiments where the effect of preNMAR blockade was examined. Frequency, amplitude, rise and decay time of mEPSCs were measured before and after the application of the NMDAR blocker DL-2-amino-5-phosphopentanoic acid (DL-APV, also abbreviated as APV, 100 μM, Ascent Scientific). 100μM DL-APV washes were 8-10 min in duration and 180 s chart recordings before and after (while APV application continued) the drug wash were acquired and used for analysis. In specified experiments, Ro25-6981 (0.5 μM, Ascent Scientific) was used to block NR2B subunits; N-Methyl-D-aspartic acid (NMDA, 20 μM, Tocris) or threo-β-Benzyloxyaspartic acid (TBOA, 30 μM, Tocris) was used to increase glutamate receptor activation. To detect mEPSC events, a variable amplitude template was slid through the 180 s chart recordings (Clements 1997). The parameters of the template, including amplitude, 10-90% rise time, and decay time, were determined based on an average of real events as well as previously reported values. The detection threshold was 5 to 7 times of the noise standard deviation, and events with large baseline error were rejected additionally.

EPSCs were evoked using an isolated pulse stimulator unit (A-M system, model 2100, Sequim WA) with a glass electrode filled with the same external recording solution, placed 100-150 μm lateral to the recording pipette for extracellular stimulation of horizontal layer 4 connections. For paired-pulse experiments pairs of stimuli (30 Hz) were delivered every 20 s and EPSCs were

recorded at -80 mV to isolate AMPAR-mediated excitatory responses. In experiments where the effect of APV was accessed, MK-801 (1 mM) was added in recording pipette to ensure blockade of postsynaptic NMDAR-mediated currents. Small adjustments were made to the placement of the stimulating electrode so that single-peak EPSC responses were elicited. In cases where consistent single-peak EPSCs were unachievable, only the first, well-defined peak of the multicomponent EPSCs were used for analysis. Amplitude of the EPSCs were measured relative to a 2 ms baseline period 1 ms before the onset of the stimulation. For thalamocortical stimulation, slices were prepared following methods described by Agmon and Connors (Agmon and Connors 1991) with modifications (Porter et al. 2001). The stimulating electrode was placed in the ventrobasal nucleus of the thalamus, and recordings were made at room temperature in excitatory cells in the barrel cortex. To compare the effect of APV on first-spike amplitude and variance, baclofen (5 μM), a $GABA_B$ receptor agonist, was used to reduce presynaptic release, and NBQX (0.3 μM) was used to partially block postsynaptic AMPARs. For every cell recorded, 20-50 sweeps were collected after each drug wash.

For recording synaptically connected pairs of layer IV neurons, simultaneous whole cell recordings were performed on two cells located in close proximity. Synaptic connections were established by eliciting action potentials in one neuron by injecting 3 nA current for 1 ms, and recording EPSCs from another. Resting membrane potential of the presynaptic neuron was adjusted to -75 mV with holding current, and ESPCs were recorded in the postsynaptic cell

at -80 mV. Of 64 pairs attempted in wildtypes, 14 pairs were synaptically coupled (connectivity rate: 21.9%), similar to previous reports (Feldmeyer et al. 1999; Brasier and Feldman 2008). Four of the 14 pairs were not used for analysis due to cell dying or large change in input resistance. In Dcdc2 mutants, 69 pairs were attempted and 16 pairs were found synaptically coupled (connectivity rate: 23.2%). 3 of the 16 pairs were excluded from data analysis. Pairs found to be synaptically coupled were tested for bi-direction connections, of which none of the 14 wildtype pairs were connected bi-directionally, and 3 of the 6 mutant pairs were. In these two mutant pairs, the stronger synaptic connection was used for analysis. Once a synaptic connection was identified, pairs of action potentials were generated in the presynaptic cell at 30 Hz every 20 seconds, and unitary EPSCs were recorded in the postsynaptic cell. For every cell recorded, 50 sweeps were collected after each drug wash condition. Paired-pulse ratios and response amplitudes were determined for each pair then averaged, excluding failures.

For NMDA-to-AMPA ratio experiments, the internal solution contained (in mM): 110 $CsMeSO_4$, 10 CsCl, 10 HEPES, 10 Cs_4-BAPTA, 5 QX-314•Br, 0.1 spermine, 4 Mg-ATP, 0.4 Na-ATP, 10 phosphocreatine, 0.05% biocytin, adjusted to pH 7.3 with CsOH and to 278 mOsm with double-distilled H_2O. Recordings began at least 10 min after initial whole-cell recording was achieved to allow dialysis of Cs^+ internal solution. A single extracellular stimulation was delivered every 10 seconds, while the cell was held at either -90 mV (AMPAR-mediated responses), 0 mV, or +50 mV (mixed AMPAR-mediated and NMDAR-mediated

responses). Amplitudes of AMPAR-mediated current were measured as the average amplitude of a 1 ms window at the response peak relative to the baseline when the cell was clamped at -90 mV. The NMDAR-mediated current was measured at + 50 mV as the average of a 10 ms window beginning 25 ms after the stimulus artifact, when AMPAR-mediated current has decayed to baseline [modified from (Myme et al. 2003)]. For measuring spontaneous NMDAR-mediated events, cells were voltage clamped at +40 mV, and the AMPAR antagonist NBQX (10 μM) was included in addition to SR-95531 and TTX in the external recording buffer. Evident detection methods, similar to those described for mEPSC measurement but with different parameters, were used to obtain the average waveforms, amplitude, rise and decay time.

PSD preparation and western blotting

Postsynaptic density (PSD) fractions were prepared from mouse forebrains adapted from a previously described protocol for rat (Cho et al. 1992). Briefly, synaptosome fractions (SNS) for pools of 3 forebrains (P21-P30) were isolated from homogenates (WCL) (n=4 pools; 12 mutant brains, n=4 pools; 12 wildtype brains) by differential and density gradient centrifugation and then extracted with 0.5% Triton X-100 for 15 min. The resulting PSD fraction was pelleted by centrifugation at 36,800×*g* for 45 min. For western blot analysis 20 ug of protein for wildtypes and mutants were run for WCL, SNS, and PSD fractions. Western blots were performed with an NR2B rabbit polyclonal antibody (Gift of Dr. Randall Walikonis) and mouse anti beta-actin (sigma). Quantification of

NR2B was determined with a LICOR IR imager, and levels normalized to beta-actin.

Tactile discrimination task

Eleven wildtype and 9 Dcdc2 mutant mice were tested on a tactile discrimination task adapted from Wu et al.(Wu et al. 2013), based on general principles of novel object recognition task (using vibrissal rather than visual input). The test apparatus was a (40 cm × 24 cm × 20 cm) plexiglass tub with opaque walls. The target "objects" were 5 cm × 7.5 cm sheets of aluminum oxide sandpaper (3M, St. Paul, MN) affixed to the lateral walls of the test chamber (right and left sides), approximately 3 cm from back corner and 2 cm above the floor of the chamber. Two different grades of sandpaper were used for the texture discrimination task; 80- and 180-grit (average particle width of 190 μm and 82 μm, respectively).

For the tactile discrimination task, the following experimental protocol was used (Figure. 3-10A). One day prior to testing, subjects were habituated to the testing chamber for 10 minutes. On testing day, subjects were given one additional habituation period for 5 minutes, immediately followed by a 5-minute “familiarization” period where they were exposed to two identical sheets of 80-grit sandpaper, each located opposite from one another on the lateral walls. During the familiarization phase, subjects were placed in the center of the testing chamber, equidistant and facing away from the identical textured sandpaper. Following the familiarization phase, subjects were returned to their home cage for a 5-minute resting period. During the resting period, the textured sheets used

during the familiarization phase was removed and replaced with one identical 80-grit sheet and one novel 180-grit sheet. The side with the novel and familiar object was counterbalanced throughout testing. Following the resting period, subjects were placed back into the testing chamber for a final 3-minute testing period. A Sony video camera was used to record the testing period and the amount of time each subject actively interacted with each of the textured sheets was used for analysis.

Four weeks following the texture discrimination task, a visual control task was employed to insure that any differences in texture discrimination behavior could be attributed to differences in tactile processing and not visual information. Clear transparent film (Computer Grafix, Maple Heights, OH) was used to cover the textured faces of the sandpaper (making the objects textureless), and the experimental protocol was repeated (Figure. 3-10A). This allowed for evaluation of the possible use of visual information by the subjects in order to discriminate between the two different grades of sandpaper.

Data analysis and statistics

Data analysis was performed using Axograph X built-in analysis and IGOR Pro software (Wavemetrics) on a Macintosh computer. Statistics were performed using Prism 5 software (Graphpad), and graphs were generated in IGOR Pro software. Statistical significance was determined using either Student's t-Tests (indicated on graphs with asterisks, *$p < 0.05$; **$p < 0.01$; ***$p < 0.001$; ns, $p > 0.05$) or ANOVA (indicated by p values in legends as well as results). For multiple comparisons tests following ANOVA, multiplicity adjusted p values were

reported (indicated on graphs with asterisks, *$p < 0.05$; **$p < 0.01$; ***$p < 0.001$; ns, $P > 0.05$). Significance was based on p values < 0.05. Means and standard errors were reported for all results unless otherwise specified.

Results

Glutamatergic synaptic activity in layer 4 is elevated following loss of *Dcdc2*

We directed whole-cell patch-clamp recordings to layer 4 pyramidal and stellate RS neurons of somatosensory cortex in *Dcdc2* mutant mice and wildtype mice. As previously described, the mutant mice used in this study were engineered to carry a deletion in exon 2 of *Dcdc2* – a deletion which causes a premature stop codon and loss of *Dcdc2* mRNA by nonsense-mediated decay(Wang et al. 2011). We focused our cellular recordings on layer 4 neurons because Dcdc2 promoter activity is strongest in these neurons as indicated by dense eGFP labeling in *Dcdc2*-BAC transgenic mice (Figure 3-1A,B; GENSAT BAC transgene, Tg(Dcdc2a-EGFP)JC158Gsat); however, it should be noted that *in situ* hybridization and RT-PCR results indicate that *Dcdc2*, while potentially expressed more highly in layer 4, is expressed at some level throughout the brain(Meng et al. 2005; Magdaleno et al. 2006; Burbridge et al. 2008). To test for changes in synaptic properties in layer 4, we compared the frequency and amplitude of miniature spontaneous excitatory postsynaptic currents (mEPSCs) in wildtype (Dcdc2$^{wt/wt}$, or *wt/wt* in figures) and Dcdc2 mutant mice (Dcdc2$^{del2/del2}$, or *del2/del2* in figures). Spontaneous glutamatergic synaptic currents were significantly elevated in frequency in the mutants (1.93 ± 0.31 Hz in Dcdc2$^{wt/wt}$ vs.

7.66 ± 0.87 Hz in Dcdc2$^{wt/wt}$, t_{21} = 6.39, p < 0.0001), but were unchanged in amplitude (12.46 ± 1.04 pA in Dcdc2$^{wt/wt}$ vs. 12.19 ± 0.56 pA in Dcdc2$^{del2/del2}$, t_{21} = 0.22, p = 0.83) or decay (5.40 ± 0.38 pA in Dcdc2$^{wt/wt}$ vs. 5.06 ± 0.60 pA in Dcdc2$^{del2/del2}$, t_{21} = 0.48, p = 0.63) (Figure 3-1C-E) relative to Dcdc2$^{wt/wt}$ controls. An increase in the frequency of glutamatergic mEPSCs without a change in amplitude or decay can result from either an increase in the presynaptic probability of neurotransmitter release or an increase in the number of synapses. To test whether there was an increase in the probability of evoked transmitter release, we performed paired-pulse analysis on electrically evoked postsynaptic currents (EPSCs) by stimulation within layer 4, 50-100 mm lateral to the recorded layer 4 neurons (Figure 3-1F,G). All evoked responses were measured in the presence of SR-95531 (gabazine, 5 μM) to isolate excitatory synaptic circuitry from inhibitory circuits. In paired-pulse analysis, a decrease in the second synaptic response amplitude relative to the first, or paired-pulse depression at the 30 Hz stimulation frequency indicates higher probability of transmitter release as apposed to paired-pulse facilitation (Del Castillo and Katz 1954; Zucker and Regehr 2002). The amplitude of the second excitatory synaptic response in wildtype neurons was either the same or slightly elevated relative to the first response amplitude (Figure 3-1G,H). In contrast, the mutants consistently showed paired-pulse depression, suggesting increased probability of transmitter release during the first synaptic response. The paired-pulse ratio was significantly lower in the mutants relative to wildtypes (1.08 ± 0.06 in Dcdc2$^{wt/wt}$ vs. 0.86 ± 0.02 pA in Dcdc2$^{del2/del2}$, t_{40} = 3.55, p = 0.001, Figure 3-1H), and this

observation, along with the increase in spontaneous synaptic frequency without a change in spontaneous event amplitude or decay, is most consistent with elevation in the presynaptic probability of transmitter release in Dcdc2 mutants.

Paired recordings indicate increased reliability of transmission between layer 4 neurons in Dcdc2 mutants

Changes in paired pulse ratios and release probabilities assessed by electrical field stimulation as described above could be explained by several differences between mutant and wildtype circuits, including an increase in release probability from the same population of presynaptic fibers, elevation of the membrane potential in presynaptic neurons, and/or a change in the population of stimulated presynaptic fibers such that extracellular stimulation activates axons with higher release probabilities. For example, we previously reported that the resting membrane potential in Dcdc2 mutant neurons was more depolarized compared to wildtype neurons in somatosensory cortex (Che et al. 2013). In order to distinguish some of these possibilities we isolated synaptic connections between pairs of identified layer IV neurons by paired cell whole-cell recordings (Figure 3-2A). Responses between connected layer 4 pairs were elicited by single action potentials in one neuron with membrane potential adjusted to -75 mV, and recording EPSCs in the connected neuron at -80 mV (Figure 3-2A,B). Similar to results from field stimulation, results from connected pair recordings with controlled, consistent membrane potentials showed paired-pulse depression in Dcdc2$^{del2/del2}$ layer 4 pairs but paired pulse facilitation in pairs

recorded from Dcdc2$^{wt/wt}$ (1.33 ± 0.16 in Dcdc2$^{wt/wt}$ vs. 0.83 ± 0.05 in Dcdc2$^{del2/del2}$, $t_{21} = 3.21$, $p = 0.0042$, Figure 3-2C).

In order to further characterize the physiological difference in lateral excitatory connections between layer 4 neurons, we quantified coefficient of variation (CV) and failure rates in paired layer 4 recordings. From principles of quantal transmitter release, unitary synaptic connections with a higher probability of transmitter release should show both a decrease in CV from response to response, and a decrease in the rate that a given presynaptic activation will result in a failure of synaptic response in the postsynaptic neuron (Korn and Faber 1991). Consistent with this prediction, we found a significant decrease both in the CV of EPSC amplitudes (0.47 ± 0.05 in Dcdc2$^{wt/wt}$ vs. 0.29 ± 0.03 in Dcdc2$^{del2/del2}$, $t_{21} = 3.18$, $p = 0.0045$, Figure 3-2D) and significant decrease in failure rate in mutant layer 4 relative to wildtype neurons (0.17 ± 0.04 in Dcdc2$^{wt/wt}$ vs. 0.06 ± 0.03 in Dcdc2$^{del2/del2}$, $t_{21} = 2.23$, $p = 0.037$, Figure 3-2E). In addition, we found no significant difference in the average amplitude of unitary responses when failures were excluded (16.24 ± 3.38 in Dcdc2$^{wt/wt}$ vs. 22.66 ± 3.42 in Dcdc2$^{del2/del2}$, $t_{21} = 1.31$, $p = 0.21$, data not shown), suggesting, similar to the mEPSC results, no change in postsynaptic properties. We further confirmed this by measuring the NMDAR/AMPAR ratio (Myme et al. 2003, Figure 3A) and analyzing the waveform of spontaneous postsynaptic NMDAR-mediated events (Figure 3-3C). We found no significant differences relative to wildtype in NMDAR/AMPAR ratios of EPSCs (1.11 ± 0.24 in Dcdc2$^{wt/wt}$ vs. 1.18 ± 0.32 in Dcdc2$^{del2/del2}$, $t_{14} = 0.18$, $p = 0.86$, Figure 3-3B) or in amplitudes of spontaneous

miniature NMDAR-mediated synaptic events recorded at +40 mV (8.76 ± 0.75 in Dcdc2$^{wt/wt}$ vs. 10.69 ± 0.86 in Dcdc2$^{del2/del2}$, t_{22} = 0.14, p = 0.14, Figure 3-3D), despite the increase in their frequency reported previously (see chapter 2). This set of negative results confirms that postsynaptic NMDAR number and function are unaltered in Dcdc2 mutants.

Elevated frequency of spontaneous glutamatergic synaptic events in Dcdc2 mutants is decreased by NMDAR antagonists

Presynaptic transmitter release can be influenced by a large number of mechanisms, including several types of metabotropic (Takahashi and Kajikawa 1998; Cartmell and Schoepp 2000; Karim et al. 2001; Kreitzer and Regehr 2002; Freund et al. 2003) and ionotropic receptors (Berretta and Jones 1996; Chittajallu et al. 1996; Turecek and Trussell 2001). Although NMDARs are classically thought to be involved in postsynaptic depolarization and calcium influx, there have been a large number of studies showing non-postsynaptic NMDARs regulating release probability in various brain regions including the neocortex (Corlew et al. 2008; McGuinness et al. 2010; Larsen et al. 2011; Kunz et al. 2013). While the NR2B protein levels at the PSDs remained unaltered in the mutants by Western blot analysis (0.59 ± 0.15 in Dcdc2$^{wt/wt}$ vs. 0.66 ± 0.20 in Dcdc2$^{del2/del2}$, relative to beta-actin, t_6 = 0.25, p = 0.81, Figure 3-3F), we have previously reported an up-regulation in NR2B subunit (Che et al. 2013), which preNMDARs are known to contain (Woodhall et al. 2001; Sjöström and Turrigiano 2003; Corlew et al. 2007; Brasier and Feldman 2008; Larsen et al. 2011). We therefore tested the possibility that the increased probability of

release in Dcdc2$^{del2/del2}$ mice may be due to increased activation of preNMDARs. The effects of NMDA antagonists on spontaneous and evoked synaptic responses were examined in wildtypes and mutants while postsynaptic NMDARs were blocked. Miniature EPSCs were recorded at -80 mV in TTX (1 μM) and SR-95531 (5 μM), and MK-801 (1 mM) was added to the intracellular solution in recording pipettes to further block postsynaptic NMDARs in the recorded cells. Consistent with the hypothesis of elevated preNMDAR influence, we found that APV (DL-APV, 100 μM) had a significantly greater effect on decreasing the frequency of spontaneous mEPSCs in the mutant than in wildtype L4 neurons (repeated-measures ANOVA, $F_{1,21} = 27.21$, $p < 0.0001$, Bonferroni's multiple comparisons tests see figure legend, Figure 3-4A-C). We also tested the NR2B subunit-specific blocker Ro 25-6981 (0.5 μM), and found that blocking NR2B subunit-containing NMDARs also reduced mEPSC frequency in the mutants (repeated-measures ANOVA, $F_{1,18} = 4.68$, $p = 0.042$, Figure 3-4D).

Increased synaptic release measured is not caused by changes in ambient glutamate level or depolarized RMP

Elevations in extracellular glutamate concentrations without changes in receptor number or function could lead to NMDAR-dependent increases in mEPSC frequencies. To test whether or not this was the case, we measured mEPSC frequencies in high concentrations of the NMDAR agonist NMDA (20 μM) or the excitatory amino acid transporters blocker TBOA (30 μM), followed by bath application of APV in both Dcdc2 mutants and wildtypes. If the elevated mEPSC frequency in the mutants was a result of high concentrations of ambient

glutamate alone, we would predict an increase in mEPSC frequency in wildtypes in the presence of NMDA (through presynaptic mechanisms) and/or TBOA that would reach mutant levels. We found that mEPSC frequencies in wildtypes did not increase to mutant levels in the presence of NMDA or TBOA, and furthermore the addition of APV did not affect wildtype mEPSC frequencies (repeated-measures ANOVA, NMDA: $F_{2,30} = 2.60$; TOBA: $F_{2,22} = 2.41$, Tukey's pair-wise multiple comparisons tests see legend, Figure 3-5A,B).

We also considered the possibility that depolarized RMP in the mutants (Che et al. 2013) could lead to increased synaptic spontaneous glutamate release without changes in synaptic functions. We did not, however, observe an increase in mEPSC frequencies in wildtype recordings that approached mutant levels when extracellular K^+ concentrations were elevated from 3 mM to 6 mM (2.55 ± 0.58 Hz vs. 2.75 ± 0.60 Hz, $t_5 = 0.97$, $p = 0.37$) to depolarize wildtype neurons (-73.80 ± 1.00 mV to -62.90 ± 2.40 mV), and APV did not have additional effect on mEPSC frequencies in wildtype at depolarized membrane potentials (One-way ANOVA with Tukey's multiple comparisons tests, $F_{1.42,7.08} = 0.34$, $p = 0.65$, Figure 3-5C). These results indicate that the increased frequency of spontaneous glutamatergic synaptic events in Dcdc2 mutants is not due to elevated ambient glutamate or increased depolarization.

PreNMDARs affect evoked synaptic currents in Dcdc2 mutants

We next tested whether the difference in the probability of evoked release between the wildtype and Dcdc2 mutant mice, revealed by extracellular stimulation within layer 4, was differentially affected by NMDAR block. APV in

wildtype slices had no significant effect on paired-pulse ratios (1.14 ± 0.05 before APV vs. 1.12 ± 0.08 in APV, t_7 = 0.22, p = 0.83, Figure 3-6A-C) of synaptic responses from 30 Hz stimulus pairs. In contrast, APV in mutants significantly increased paired-pulse ratios (0.85 ± 0.04 before APV vs. 1.02 ± 0.05 in APV, t_9 = 4.76, p = 0.001, Figure 3-6B), reverting the paired-pulse ratios to levels observed at wildtype synapses (repeated-measures ANOVA, $F_{1,16}$ = 5.05, p = 0.039, Bonferroni's multiple comparisons tests see legend, Figure 3-6C). In addition, APV decreased the amplitude of the first synaptic response in mutants (normalized, 1.06 ± 0.02 before APV and 0.71 ± 0.05 in APV, t_7 = 7.08, p = 0.0002) but had no significant effect in wildtype responses (0.96 ± 0.02 before APV and 0.98 ± 0.03 in APV, t_6 = 1.11, p = 0.31, Figure 3-6E) indicating that there is an enhancement in single responses in Dcdc2 mutants dependent upon preNMDAR activation that is not apparent in wildtypes. Taken together, these results suggest that elevated preNMDAR activity may be responsible for both increased spontaneous and evoked transmitter release in Dcdc2 mutants.

In order to further confirm that the effect of NMDAR block on Dcdc2 mutants was due to a presynaptic effect, we plotted normalized $1/CV^2$ versus amplitude before and after the application of APV (Malinow and Tsien 1990; Faber and Korn 1991). In mutant neurons, APV decreased the amplitude of response and this was paralleled by a reduction in $1/CV^2$. A similar reduction was observed with baclofen (5 μM), a $GABA_B$ receptor agonist known to act presynaptically (Manabe et al. 1993; Tzounopoulos et al. 2007) (Figure 3-6F). By contrast, sub-saturating concentration of NBQX (0.3 μM), which reduces

response amplitude by blocking postsynaptic glutamate receptors, left CV unaffected (Figure 6F).

Presynaptic NMDAR effects in Dcdc2 mutants are present at layer 4 intracortical connections but not thalamocortical connections

To test whether preNMDAR activity was responsible for the difference in synapses between layer 4 neurons, we measured the effect of APV on presynaptic release probability in paired recordings. Consistent with extracellular stimulation experiments, APV had no significant effect on paired-pulse ratio (1.32 ± 0.16 before APV and 1.14 ± 0.13 in APV, $t_9 = 1.12$, $p = 0.29$, Figure 3-7C) or response amplitude (16.24 ± 3.38 before APV and 14.58 ± 2.83 in APV, $t_9 = 1.36$, $p = 0.21$, Figure 3-7F) in the wildtypes. In Dcdc2 mutants, APV significantly increased paired-pulse ratio (0.83 ± 0.05 before APV and 1.04 ± 0.09 in APV, $t_{12} = 2.93$, $p = 0.01$, Figure 3-7C), accompanied by a decrease in first response amplitude (22.66 ± 3.43 before APV and 17.60 ± 2.94 in APV, $t_{12} = 3.81$, $p = 0.003$, Figure 3-7F). Paired-pulse ratio was reverted back to wildtype-level in APV (repeated-measures ANOVA, $F_{1,21} = 5.45$, $p = 0.030$, Bonferroni's multiple comparisons tests see legend, Figure 3-7D), and CV analysis indicates that the effect of APV has a presynaptic locus in the mutants (Figure 3-7E).

Layer 4 excitatory neurons in somatosensory barrel cortex mostly receive synaptic inputs from intracortical connections and inputs from the thalamus (Benshalom and White 1986; Agmon and O'Dowd 1992; Feldmeyer et al. 1999; Petersen and Sakmann 2000; Schubert et al. 2003). Results with paired recordings show that changes in NMDAR-mediated presynaptic release

probability is present at the synapses between two connected layer 4 excitatory neurons. Although horizontal extracellular stimulation within layer 4 used in our experiments should mostly recruit intracortical connections (Feldman et al. 1998; Che et al. 2013), given the high efficacy of thalamocortical synapses (Gil et al. 1999), we tested whether APV had a differential effect on release probability of the thalamic inputs to layer 4 in the mutants. We found similar paired-pulse ratios with values consistent with previous reports (Hull et al. 2009) in both wildtypes and mutants (0.71 ± 0.05 in Dcdc2$^{wt/wt}$ vs. 0.68 ± 0.08 in Dcdc2$^{del2/del2}$), and APV had no apparent effect on either paired pulse (repeated-measures ANOVA, $F_{1,12} = 3.97$, $p = 0.070$, Bonferroni's multiple comparisons tests see figure legend, Figure 3-7G) or response amplitude (first response amplitude, normalized, 1.02 ± 0.07 in Dcdc2$^{wt/wt}$ vs. 0.95 ± 0.07 in Dcdc2$^{del2/del2}$, $t_{12} = 0.72$, $p = 0.48$, Figure 3-7H). In summary, these data suggest increased synaptically evoked release probability in Dcdc2 mutants is mediated by enhanced activation within layer 4, specifically between L4-L4 connections.

Presynaptic NMDAR effects on evoked response are enhanced by higher amount of glutamate release

During paired recording experiments between layer 4 neurons, we observed greater increase in paired-pulse ratios in Dcdc2 mutant neurons with larger response amplitudes. Interestingly, when average response size and the change in paired-pulse ratio for each cell were compared, we found while amplitudes did not correlate with changes in paired-pulse ratio after applying APV in wildtypes, larger amplitudes correlated with larger changes in Dcdc2

mutant neurons (Pearson correlation, Dcdc2$^{wt/wt}$: p = 0.89; Dcdc2$^{del2/del2}$: p = 0.029, Figure 3-8). This suggests that preNMDAR activation by evoked release in the mutants is even more pronounced when glutamate release amplitude is larger, with average preNMDAR effect already significant compared to the wildtypes. Further, preNMDARs in the mutants are likely autoreceptors at the synapse given the increased activation and the effect on the first EPSC (Berretta and Jones 1996; Casado et al. 2002; Brasier and Feldman 2008). We hypothesize that additional preNMDAR autoreceptors can be activated with higher glutamate concentration, revealing larger change in paired-pulse ratio after preNMDARs are blocked by APV.

Stimulus intensity-dependent NMDARs activation has been previously reported at excitatory synapses in cerebellar molecular layer interneurons (Clark and Cull-Candy 2002). Therefore to test this hypothesis, we tuned extracellular stimulation intensity to evoke minimal responses, with amplitudes comparable to ones observed in paired-recording experiments on average. In the same postsynaptic neuron, we then increased stimulation intensity to levels previously used to evoke large responses. Small and large responses evoked by set intensities were assessed again after washing in APV (Figure 3-9A,B). Interestingly, while paired-pulse ratios of small and large responses in the mutants were comparable pre APV, small response paired-pulse ratios were not affected by NMDAR block (2-way ANOVA, $F_{1,9}$ = 8.04, p < 0.05, Bonferroni's multiple comparisons test see legend, Figure 3-9D). We argue that the discrepancy between the absence of preNMDAR effect in minimum extracellular

stimulation and presence in paired recordings could be due to that a different population of fibers were tested, and that connections with larger release probabilities were under-represented in extracellular stimulation experiments. Under these assumptions, to further test if additional glutamate released accounts for enhanced APV effect, we performed paired-pulse analysis on synaptic responses evoked with minimum stimulation in the presence of low concentration of TBOA (3 μM) to partially limit glutamate uptake by neuronal excitatory amino acid transporters (EAATs) (Tzingounis and Nicoll 2004). In the presence of TBOA, APV increased paired-pulse ratios of mutant neurons, returning them back to wildtype levels (repeated-measures ANOVA, $F_{1,14} = 6.70$, $p < 0.05$, Figure 3-9E,F). These results indicate that during evoked synaptic release, activation of preNMDAR is enhanced in higher concentration of glutamate in addition to the requirement for depolarization of presynaptic terminals.

Tactile discrimination is impaired in Dcdc2 mutants

We next tested whether there was a measurable behavioral change in tactile discrimination that might be predicted by changes in synaptic responses in layer 4 of somatosensory cortex. We adapted a novel object recognition task, a behavior that takes advantage of the tendency of mice to explore novel stimuli, as a tactile discrimination test (Wu et al. 2013). In this test, mice were first familiarized to two identical sandpapers (80-grit) attached to opposite walls in a testing chamber (learning phase). Next, one sheet was replaced with a novel, 180-grit sandpaper, and subjects were then tested to determine whether they

would spend more time with the novel tactile stimulus (Figure 3-10A). The discrimination index (DI) indicates levels of preference towards one texture versus another, with DI = 0 being no discrimination, or chance level exploration with the novel and familiar stimulus. Wildtype mice showed significant discrimination between textures (DI = 0.49 ± 0.17, t_{10} =2.92, $p < 0.05$), and more than 70% of subjects tested had DI > 0.5 (Figure 3-10C). The mutants, in contrast, showed no significant preference for the novel, 180-grit texture relative to the 80-grit texture (DI = 0.08 ± 0.21, t_8 =0.37, $p = 0.72$, Figure 3-10C). The difference in discrimination between wildtype and mutant mice was not due to levels of general exploratory activity, since the total time animals in each genotype spent investigating both objects during both learning and testing phases was not significantly different (2-way ANOVA, $F_{1,18} = 0.03$, $p = 0.86$, Figure 3-10B). To confirm that the difference in tactile discrimination was independent of visual cues that may differ in the sand papers, a visual control task was performed in which the sandpaper was covered by clear transparent film. In this condition where only minimal visual differences between the sandpapers could be used by the mice, neither wildtype nor mutant mice showed preference for the novel versus familiar stimulus (Dcdc2$^{wt/wt}$: $t_{10} = 0.12$, $p = 0.91$; Dcdc2$^{del2/del2}$: $t_8 = 1.01$, $p = 0.34$; Figure 3-10D).

Discussion

Several possible changes in mechanisms underlying glutamatergic transmitter release could account for the elevated synaptic transmission in Dcdc2 mutant L4 neurons. In this study, we show that in Dcdc2 mutant mice,

glutamatergic synaptic transmission is elevated at least in part through a preNMDAR-mediated mechanism at unitary L4 synaptic connections, while postsynaptic properties remain unaffected. Our results not only demonstrate that deletion of a dyslexia-associated gene leads to changes in excitatory cortical connections, but also strengthen the role of preNMDAR function and regulation in maintaining normal cognitive abilities.

We showed that the NMDARs responsible for increased synaptic transmission at L4-L4 connections in Dcdc2 mutants are not located postsynaptically, since their function was not blocked by hyperpolarizing the postsynaptic cell and including MK-801 internally. Moreover, MK-801 also rule out changes in extrasynaptic NMDAR functions on the postsynaptic cell, which are also comprised of NR2B subunits (Tovar and Westbrook 1999). As changes in NMDARs do not occur on postsynaptic sites, they could only take place on the presynaptic terminal and/or on the somatodendritic compartment of the presynaptic cell, or a third cell such as a synaptically connected astrocyte (Conti et al. 1996; 1997; Lalo et al. 2006). Given that preNMDAR blockade decreases the probability of evoked release evident at the first AMPA-mediated EPSC, and that in the mutants APV effect is enhanced with higher evoked glutamate concentration, increased preNMDAR activation is likely present on the L4-L4 axonal terminal via the action of autoreceptors, where release probability can be directly modulated. We cannot, however, exclude the possibility that additional preNMDARs are activated on extrasynaptic locations other than the terminals on the presynaptic cell.

In the mutants, APV was able to reduce spontaneous release measured by decreased mEPSC frequencies, suggesting that preNMDARs are activated in basal, ambient glutamate concentration. Previous studies have shown that in wildtype mice or rats, preNMDARs are not fully-activated in ambient glutamate, and they can modulate spontaneous, non-action potential-mediated release as well as evoked release at low and high frequencies (Woodhall et al. 2001; Sjöström and Turrigiano 2003; Corlew et al. 2007; Brasier and Feldman 2008), perhaps through independent mechanisms (Kunz et al. 2013). However, whether tonic activation is sufficient in affecting release probability under evoked condition in a mutant model like ours is unclear, although our results that APV has larger effect on release probability between paired L4 neurons, and that TBOA enhances the APV effect on response evoked by minimal stimulation suggests that additional EPSC-mediated synaptic release at least further increase preNMDAR activation.

It has been reported that in juvenile rat somatosensory cortex, preNMDARs are not broadly expressed, only evident at L4-L2/3 synapses but not at L4-L4 synapses (Brasier and Feldman 2008). In mouse visual cortex, however, preNMDAR activities were found to be developmentally regulated at L4-L4 synapses and present only in young mice less than 3 weeks old (Corlew et al. 2007). These different findings suggest that preNMDARs may be tightly regulated spatially and temporally based on cellular specialization and developmental processes. In wildtype layer 4 neurons at the ages we tested, we did not detect any changes in spontaneous or evoked events as a result of

preNMDAR, consistent with previous report in rat somatosensory cortex (Brasier and Feldman 2008). Dcdc2 mutants, on the other hand, showed increased preNMDAR activities in layer 4. Thus, the target-specific control of preNMDAR expression might be compromised due to Dcdc2 deletion. Alternatively, Dcdc2 might be involved in the developmental regulation of preNMDARs in L4 neurons, for example change in preNMDAR densities, altered subunit composition or redistribution of existing subunits. In addition, although Dcdc2 promoter activity is strongest in layer 4, we cannot rule out changes in preNMDAR activity in other cortical layers and regions, either as a direct result of Dcdc2 deletion in those cell populations, or as a consequence of altered excitatory synaptic transmission in layer 4. It is also worth noting that due to the lack of a reliable Dcdc2 antibody that produces both good immunofluorescence signals in wildtype brain slices and low background signals in the mutants in our hands, we utilized the Tg(Dcdc2a-EGFP)JC158Gsat mouse to visualize regions with strong promoter activity. Our immunostaining of eGFP expression pattern of Dcdc2 in the cortex (Figure 3-1A,B) was similar to DAB and immunofluorescence images published on GENSAT. Thus, although expression pattern of promoter activities cannot be equated to Dcdc2 protein levels, GENSAT BAC transgenic mouse provided a reasonable target region for us to investigate functional changes.

Despite the fact that specific molecular link between increased transmitter release and Dcdc2 cannot yet be establish, we provide a basis for connecting cognitive changes associated with dyslexia to functional cellular neurophysiology. The enhanced level of glutamate release is attributable to increased background

excitation, resulting in elevated network excitability and synaptic noise fluctuations, both of which could lead to less precise neural encoding of stimuli and sensory processing (Harsch and Robinson 2000; Chance et al. 2002; Ermentrout et al. 2008; Mozzachiodi and Byrne 2010; Centanni et al. 2013; Che et al. 2013). Elevated glutamate levels have been previously found in neurodevelopmental disorders including ADHD (Carrey et al. 2007) and autism (Brown et al. 2013), and most recently associated with individual differences in reading ability in emergent readers (Pugh et al. 2014). Our study provides a potential cellular basis, i.e. increased presynaptic transmitter release, for previously reported neurofunctional and neurochemical changes associated with RD.

In neocortex, preNMDARs have been found to regulate release, and their activation is necessary for the induction of cortical tLTD at least in younger rodents (Sjöström and Turrigiano 2003; Bender et al. 2006; Corlew et al. 2007; Rodríguez-Moreno and Paulsen 2008), which may underlie important aspects of development, plasticity and circuitry map refinement (Sjöström and Turrigiano 2003; Feldman and Brecht 2005; Bender et al. 2006). In recent years, evidence suggests that NMDARs at locations other than the postsynaptic density may play important roles in developing neuropathologies (Lipton 2006; Zhao 2006; Okamoto et al. 2009; Hardingham and Bading 2010; Talantova et al. 2013) which were previously attributed to postsynaptic NMDARs. In particular, preNMDAR dysfunction is found to be involved in epilepsy (Yang 2006), fetal alcohol spectrum disorder(Valenzuela et al. 2008), schizophrenia (Kristiansen et al.

2010), chronic pain (Zhao 2006), and spreading depression (Zhou et al. 2013). However, given the growing number of studies demonstrating that preNMDARs play an important role in synaptic transmission and maturation, relatively little is known about how they contribute to normal cognitive function, or through what mechanisms preNMDAR dysfunction impacts neural circuits. Our study provides evidence for a possible association between the gene Dcdc2 and preNMDAR function. Although the specific effects on stimulus processing caused by emergent preNMDAR activation in layer 4 connections in Dcdc2 mutants are not yet known, this mutant should provide an ideal model to address this issue, and to test whether NMDAR antagonism is sufficient to reverse effects of DCDC2 hypofunction.

References

Agmon A, Connors BW. Thalamocortical responses of mouse somatosensory (barrel) cortex in vitro. Neuroscience. 1991;41(2):365–79.

Agmon A, O'Dowd DK. NMDA receptor-mediated currents are prominent in the thalamocortical synaptic response before maturation of inhibition. Journal of Neurophysiology. J Neurophysiol. 1992 Jul;68(1):345-9.

Bender KJ, Allen CB, Bender VA, Feldman DE. Synaptic basis for whisker deprivation-induced synaptic depression in rat somatosensory cortex. J Neurosci. 2006 Apr 19;26(16):4155–65.

Benshalom G, White EL. Quantification of thalamocortical synapses with spiny stellate neurons in layer IV of mouse somatosensory cortex. J Comp Neurol. 1986;253(3):303–14.

Berretta N, Jones RS. Tonic facilitation of glutamate release by presynaptic N-methyl-D-aspartate autoreceptors in the entorhinal cortex. Neuroscience. 1996 Nov;75(2):339–44.

Brasier D, Feldman DE. Synapse-Specific Expression of Functional Presynaptic NMDA Receptors in Rat Somatosensory Cortex. J Neurosci. 2008 Feb 27;28(9):2199-211

Brown MS, Singel D, Hepburn S, Rojas DC. Increased Glutamate Concentration in the Auditory Cortex of Persons With Autism and First-Degree Relatives: A 1H-MRS Study. Autism Res. 2013 Feb;6(1):1-10.

Burbridge TJ, Wang Y, Volz AJ, Peschansky VJ, Lisann L, Galaburda AM, et al. Postnatal analysis of the effect of embryonic knockdown and overexpression of candidate dyslexia susceptibility gene homolog Dcdc2 in the rat. Neuroscience. 2008 Mar 27;152(3):723–33.

Carrey NJ, MacMaster FP, Gaudet L, Schmidt MH. Striatal creatine and glutamate/glutamine in attention-deficit/hyperactivity disorder. J Child Adolesc Psychopharmacol. 2007 Feb;17(1):11–7.

Cartmell J, Schoepp DD. Regulation of neurotransmitter release by metabotropic glutamate receptors. J Neurochem. 2000 Sep;75(3):889-907.

Casado M, Isope P, Ascher P. Involvement of presynaptic N-methyl-D-aspartate receptors in cerebellar long-term depression. Neuron. 2002 Jan 3;33(1):123–30.

Centanni TM, Booker AB, Sloan AM, Chen F, Maher BJ, Carraway RS, et al. Knockdown of the Dyslexia-Associated Gene Kiaa0319 Impairs Temporal

Responses to Speech Stimuli in Rat Primary Auditory Cortex. Cereb Cortex. 2014 Jul;24(7):1753-66.

Chance FS, Abbott LF, Reyes AD. Gain modulation from background synaptic input. Neuron. 2002 Aug 15;35(4):773–82.

Che A, Girgenti MJ, LoTurco J. The Dyslexia-Associated Gene Dcdc2 Is Required for Spike-Timing Precision in Mouse Neocortex. Biol Psychiatry. 2014 Sep 1;76(5):387-96

Chittajallu R, Vignes M, Dev KK, Barnes JM. Regulation of glutamate release by presynaptic kainate receptors in the hippocampus. Nature. 1996 Jan 4;379(6560):78-81.

Clark BA, Cull-Candy SG. Activity-dependent recruitment of extrasynaptic NMDA receptor activation at an AMPA receptor-only synapse. J Neurosci. 2002 Jun 1;22(11):4428–36.

Conti F, DeBiasi S, Minelli A, Melone M. Expression of NR1 and NR2A/B subunits of the NMDA receptor in cortical astrocytes. Glia. 1996 Jul;17(3):254–8.

Conti F, Minelli A, DeBiasi S, Melone M. Neuronal and glial localization of NMDA receptors in the cerebral cortex. Mol Neurobiol. 1997 Feb-Apr;14(1-2):1-18.

Corlew R, Brasier DJ, Feldman DE, Philpot BD. Presynaptic NMDA Receptors: Newly Appreciated Roles in Cortical Synaptic Function and Plasticity. The Neuroscientist. 2008 Dec 1;14(6):609–25.

Corlew R, Wang Y, Ghermazien H, Erisir A, Philpot BD. Developmental Switch in the Contribution of Presynaptic and Postsynaptic NMDA Receptors to Long-Term Depression. J Neurosci. 2007 Sep 12;27(37):9835–45.

Couto JM, Gomez L, Wigg K, Ickowicz A, Pathare T, Malone M, et al. Association of attention-deficit/hyperactivity disorder with a candidate region for reading disabilities on chromosome 6p. Biol Psychiatry. 2009 Aug 15;66(4):368-75.

Del Castillo J, Katz B. Statistical factors involved in neuromuscular facilitation and depression. J Physiol. 1954 Jun 28;124(3):574-85.

Eicher JD, Gruen JR. Imaging-genetics in dyslexia: Connecting risk genetic variants to brain neuroimaging and ultimately to reading impairments. Molecular Genetics and Metabolism. 2013 Nov 1;110(3):201–12.

Ermentrout GB, Galán RF, Urban NN. Reliability, synchrony and noise. Trends in Neurosci. 2008 Aug;31(8):428–34.

Faber D, Korn H. Applicability of the coefficient of variation method for analyzing

synaptic plasticity. Biophysical Journal. 1991;60(5):1288–94.

Feldman DE, Brecht M. Map plasticity in somatosensory cortex. Science. 2005;310(5749):810.

Feldman DE, Nicoll RA, Malenka RC, Isaac JT. Long-term depression at thalamocortical synapses in developing rat somatosensory cortex. Neuron. 1998;21(2):347–57.

Feldmeyer D, Egger V, Lübke J, Sakmann B. Reliable synaptic connections between pairs of excitatory layer 4 neurones within a single “barrel” of developing rat somatosensory cortex. J Physiol. 1999 Nov 15;521 Pt 1:169–90.

Freund TF, Katona I, Piomelli D. Role of endogenous cannabinoids in synaptic signaling. Physiol Rev. 2003 Jul;83(3):1017-66.

Gil Z, Connors BW, Amitai Y. Efficacy of thalamocortical and intracortical synaptic connections: quanta, innervation, and reliability. Neuron. 1999;23(2):385–97.

Hardingham GE, Bading H. Synaptic versus extrasynaptic NMDA receptor signalling: implications for neurodegenerative disorders. Nat Rev Neurosci. 2010 Sep 15;11(10):682–96.

Harsch A, Robinson H. Postsynaptic variability of firing in rat cortical neurons: the roles of input synchronization and synaptic NMDA receptor conductance. J Neurosci. 2000;20(16):6181–92.

Hull C, Isaacson JS, Scanziani M. Postsynaptic Mechanisms Govern the Differential Excitation of Cortical Neurons by Thalamic Inputs. Journal of Neuroscience. 2009 Jul 15;29(28):9127–36.

Karim F, Wang CC, Gereau RW. Metabotropic glutamate receptor subtypes 1 and 5 are activators of extracellular signal-regulated kinase signaling required for inflammatory pain in mice. J Neurosci. 2001 Jun 1;21(11):3771-9.

Korn H, Faber DS. Quantal analysis and synaptic efficacy in the CNS. Trends in Neurosciences. 1991 Oct;14(10):439–45.

Kreitzer AC, Regehr WG. Retrograde signaling by endocannabinoids. Curr Opin Neurobiol. 2002 Jun;12(3):324-30.

Kristiansen LV, Bakir B, Haroutunian V, Meador-Woodruff JH. Expression of the NR2B-NMDA receptor trafficking complex in prefrontal cortex from a group of elderly patients with schizophrenia. Schizophrenia Research. 2010 Jun 1;119(1-3):198–209.

Kunz PA, Roberts AC, Philpot BD. Presynaptic NMDA Receptor Mechanisms for Enhancing Spontaneous Neurotransmitter Release. J Neurosci. 2013 May 1;33(18):7762–9.

Lalo U, Pankratov Y, Kirchhoff F, North RA, Verkhratsky A. NMDA receptors mediate neuron-to-glia signaling in mouse cortical astrocytes. J Neurosci. 2006 Mar 8;26(10):2673–83.

Larsen RS, Corlew RJ, Henson MA, Roberts AC, Mishina M, Watanabe M, et al. NR3A-containing NMDARs promote neurotransmitter release and spike timing–dependent plasticity. Nat Neurosci. 2011 Feb 6;14(3):338–44.

Lipton SA. Paradigm shift in neuroprotection by NMDA receptor blockade: Memantine and beyond. Nat Rev Drug Discov. 2006 Jan 20;5(2):160–70.

Magdaleno S, Jensen P, Brumwell CL, Seal A, Lehman K, Asbury A, et al. BGEM: An In Situ Hybridization Database of Gene Expression in the Embryonic and Adult Mouse Nervous System. PLoS Biol. 2006;4(4):e86.

Malinow R, Tsien RW. Presynaptic enhancement shown by whole-cell recordings of long-term potentiation in hippocampal slices. Nature. 1990 Jul 12;346(6280):177–80.

Manabe T, Wyllie D, Perkel D. Modulation of synaptic transmission and long-term potentiation: effects on paired pulse facilitation and EPSC variance in the CA1 region of the hippocampus. J Neurophysiol. 1993 Oct;70(4):1451-9.

Marino C, Mascheretti S, Riva V, Cattaneo F. Pleiotropic effects of DCDC2 and DYX1C1 genes on language and mathematics traits in nuclear families of developmental dyslexia. Behav Genet. 2011 Jan;41(1):67-76.

Marino C, Meng H, Mascheretti S, Rusconi M, Cope N, Giorda R, et al. DCDC2 genetic variants and susceptibility to developmental dyslexia. Psychiatr Genet. 2012 Feb;22(1):25–30.

McGuinness L, Taylor C, Taylor RDT, Yau C, Langenhan T, Hart ML, et al. Presynaptic NMDARs in the Hippocampus Facilitate Transmitter Release at Theta Frequency. Neuron. 2010 Dec 22;68(6):1109–27.

Meng H, Smith SD, Hager K, Held M, Liu J, Olson RK, et al. DCDC2 is associated with reading disability and modulates neuronal development in the brain. Proc Natl Acad Sci USA. 2005 Nov 22;102(47):17053–8.

Mozzachiodi R, Byrne JH. More than synaptic plasticity: role of nonsynaptic plasticity in learning and memory. Trends in Neurosciences. 2010 Jan;33(1):17–26.

Myme CIO, Sugino K, Turrigiano GG, Nelson SB. The NMDA-to-AMPA ratio at

synapses onto layer 2/3 pyramidal neurons is conserved across prefrontal and visual cortices. J Neurophysiol. 2003 Aug;90(2):771–9.

Okamoto S-I, Pouladi MA, Talantova M, Yao D, Xia P, Ehrnhoefer DE, et al. Balance between synaptic versus extrasynaptic NMDA receptor activity influences inclusions and neurotoxicity of mutant huntingtin. Nat Med. 2009 Nov 15;15(12):1407–13.

Petersen CCH, Sakmann B. The excitatory neuronal network of rat layer 4 barrel cortex. J Neurosci. 2000 Sep 28;20(20):7579–86.

Peterson RL, Pennington BF. Developmental dyslexia. The Lancet. 2012 May 26;379(9830):1997–2007.

Porter JT, Johnson CK, Agmon A. Diverse types of interneurons generate thalamus-evoked feedforward inhibition in the mouse barrel cortex. J Neurosci. 2001;21(8):2699–710.

Pugh KR, Frost SJ, Rothman DL, Hoeft F, Del Tufo SN, Mason GF, et al. Glutamate and Choline Levels Predict Individual Differences in Reading Ability in Emergent Readers. J Neurosci. 2014 Mar 12;34(11):4082–9.

Rodríguez-Moreno A, Paulsen O. Spike timing–dependent long-term depression requires presynaptic NMDA receptors. Nat Neurosci. 2008 May 30;11(7):744–5.

Rosenberg J, Pennington BF, Willcutt EG, Olson RK. Gene by environment interactions influencing reading disability and the inattentive symptom dimension of attention deficit/hyperactivity disorder. J Child Psychol Psychiatry. 2012 Mar;53(3):243-51.

Schubert D, Kötter R, Zilles K, Luhmann HJ, Staiger JF. Cell type-specific circuits of cortical layer IV spiny neurons. J Neurosci. 2003;23(7):2961–70.

Schumacher J, Anthoni H, Dahdouh F, König IR, Hillmer AM, Kluck N, et al. Strong Genetic Evidence of DCDC2 as a Susceptibility Gene for Dyslexia. Am J Hum Genet. 2006 Jan;78(1):52-62.

Sjöström P, Turrigiano G. Neocortical LTD via coincident activation of presynaptic NMDA and cannabinoid receptors. Neuron. 2003 Aug 14;39(4):641-54.

Takahashi T, Kajikawa Y. G-Protein-coupled modulation of presynaptic calcium currents and transmitter release by a GABAB receptor. J Neurosci. 1998 May 1;18(9):3138-46.

Talantova M, Sanz-Blasco S, Zhang X, Xia P, Akhtar MW, Okamoto S-I, et al. Aβ induces astrocytic glutamate release, extrasynaptic NMDA receptor

activation, and synaptic loss. Proc Natl Acad Sci U S A. 2013 Jul 2;110(27):E2518-27.

Tovar KR, Westbrook GL. The incorporation of NMDA receptors with a distinct subunit composition at nascent hippocampal synapses in vitro. J Neurosci. 1999 May 15;19(10):4180–8.

Turecek R, Trussell LO. Presynaptic glycine receptors enhance transmitter release at a mammalian central synapse. Nature. 2001 May 31;411(6837):587-90.

Tzingounis AV, Nicoll RA. Presynaptic NMDA receptors get into the act. Nat Neurosci. 2004 May;7(5):419–20.

Tzounopoulos T, Rubio ME, Keen JE, Trussell LO. Coactivation of Pre- and Postsynaptic Signaling Mechanisms Determines Cell-Specific Spike-Timing-Dependent Plasticity. Neuron. 2007 Apr;54(2):291–301.

Valenzuela CF, Partridge LD, Mameli M, Meyer DA. Modulation of glutamatergic transmission by sulfated steroids: role in fetal alcohol spectrum disorder. Brain Research Reviews. 2008;57(2):506–19.

Wang Y, Yin X, Rosen G, Gabel L, Guadiana SM, Sarkisian MR, et al. Dcdc2 knockout mice display exacerbated developmental disruptions following knockdown of doublecortin. Neuroscience. 2011 Sep 8;190:398–408.

Woodhall G, Evans DI, Cunningham MO, Jones RSG. NR2B-Containing NMDA Autoreceptors at Synapses on Entorhinal Cortical Neurons. J Neurophysiol. 2001 Oct;86(4):1644-51.

Wu H-PP, Ioffe JC, Iverson MM, Boon JM, Dyck RH. Novel, whisker-dependent texture discrimination task for mice. Behavioural Brain Research. 2013 Jan 15;237:238–42.

Yang J. Tonic Facilitation of Glutamate Release by Presynaptic NR2B-Containing NMDA Receptors Is Increased in the Entorhinal Cortex of Chronically Epileptic Rats. J Neurosci. 2006 Jan 11;26(2):406–10.

Zhao MG. Enhanced Presynaptic Neurotransmitter Release in the Anterior Cingulate Cortex of Mice with Chronic Pain. J Neurosci. 2006 Aug 30;26(35):8923–30.

Zhou N, Rungta RL, Malik A, Han H, Wu DC, MacVicar BA. Regenerative glutamate release by presynaptic NMDA receptors contributes to spreading depression. J Cereb Blood Flow Metab. 2013 Jul 3;33(10):1582–94.

Zucker RS, Regehr WG. Short-term synaptic plasticity. Annu Rev Physiol. 2002;64:355–405.

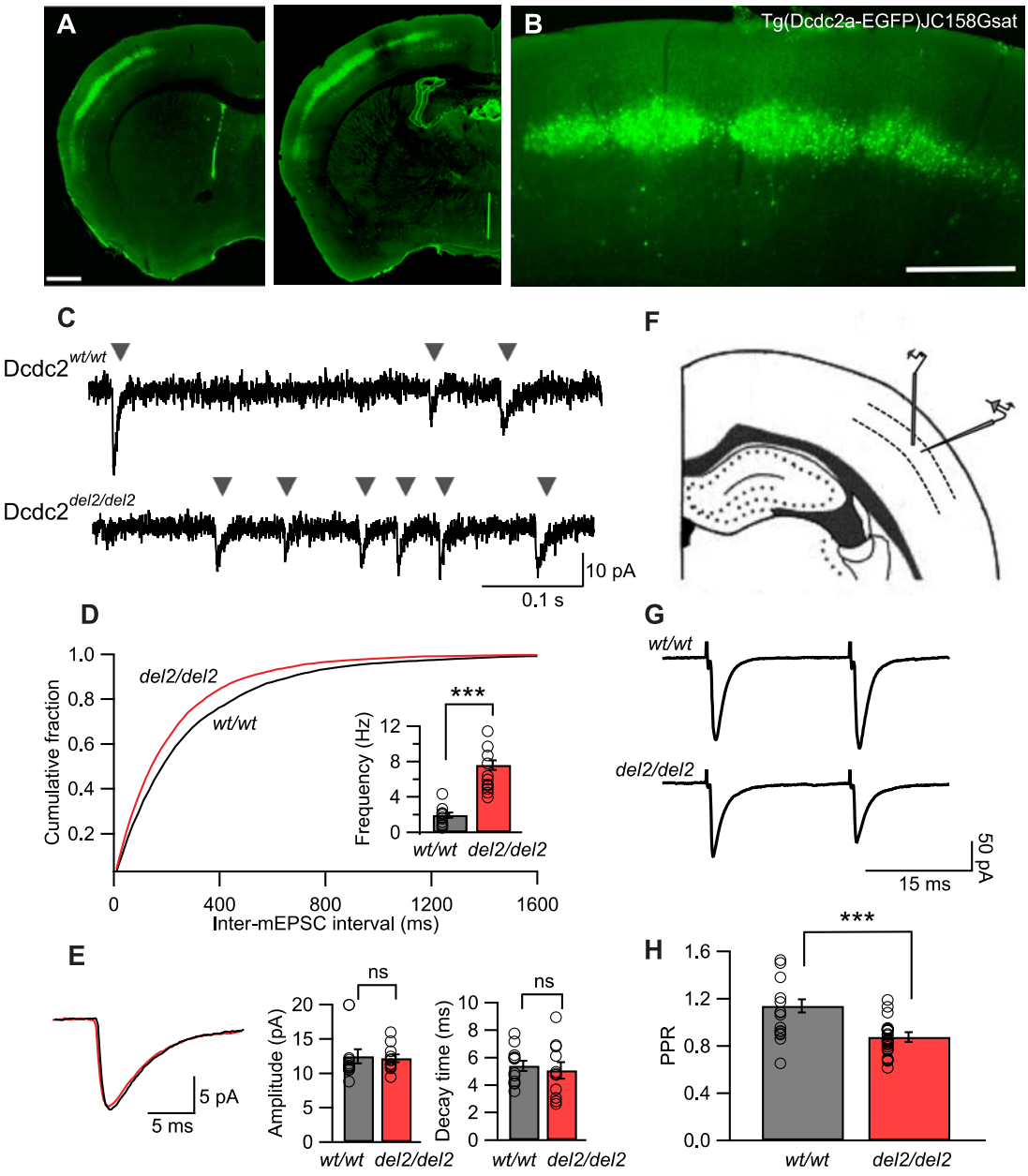

Figure 3-1. Somatosensory layer 4 neurons in Dcdc2$^{del2/del2}$ mice show increased glutamatergic synaptic activity. (A) Cells labeled by a BAC GFP transgene in the Dcdc2-EGFP GENSAT mouse [Tg(Dcdc2a-EGFP)JC158Gsat] are primarily within layer 4 of neocortex. **(B)** Somatosensory neocortex contains the highest density of GFP-positive neurons. Scale bars: ***a***: 500 µm, ***b***: 100 µm. **(C)** Sample traces of AMPAR-mediated mEPSCs from a Dcdc2$^{wt/wt}$ (top) and a Dcdc2$^{del2/del2}$ (bottom). Gray arrowheads indicate individual events. **(D)** Cumulative probability histogram for inter-mEPSC interval for Dcdc2$^{wt/wt}$ and Dcdc2$^{del2/del2}$ neurons. The histogram is from all recorded cells in Dcdc2$^{del2/del2}$ (red) and Dcdc2$^{wt/wt}$ (black) layer 4 somatosensory cortex.

Inset, mean mEPSC frequency for Dcdc2$^{wt/wt}$ and Dcdc2$^{del2/del2}$ neurons (p < 0.0001). **(E)** Average mEPSC waveforms (Dcdc2$^{wt/wt}$: black, Dcdc2$^{del2/del2}$: red), mean amplitude (p = 0.83) and decay time (p = 0.63) for Dcdc2$^{del2/del2}$ and Dcdc2$^{wt/wt}$. Student's t-test, Dcdc2$^{wt/wt}$: n = 12, Dcdc2$^{del2/del2}$: n = 11. **(F)** Schematic of the somatosensory cortical slice and approximate placements of recording and stimulating electrodes. **(G)** Representative synaptic responses in paired-pulse stimulation experiments in a Dcdc2$^{wt/wt}$ and a Dcdc2$^{del2/del2}$ layer 4 neuron. Red dotted line indicates the level of the first synaptic response in each pair. **(H)** Bar graph showing paired-pulse ratios (PPR, second response amplitude/first response amplitude) for recordings within layer 4 of Dcdc2$^{del2/del2}$ and Dcdc2$^{wt/wt}$ neocortex (p = 0.001). Student's t-test; Dcdc2$^{wt/wt}$: n=15, Dcdc2$^{del2/del2}$: n=27. Open circles indicating individual neurons. ***p < 0.001; ns, p > 0.05.

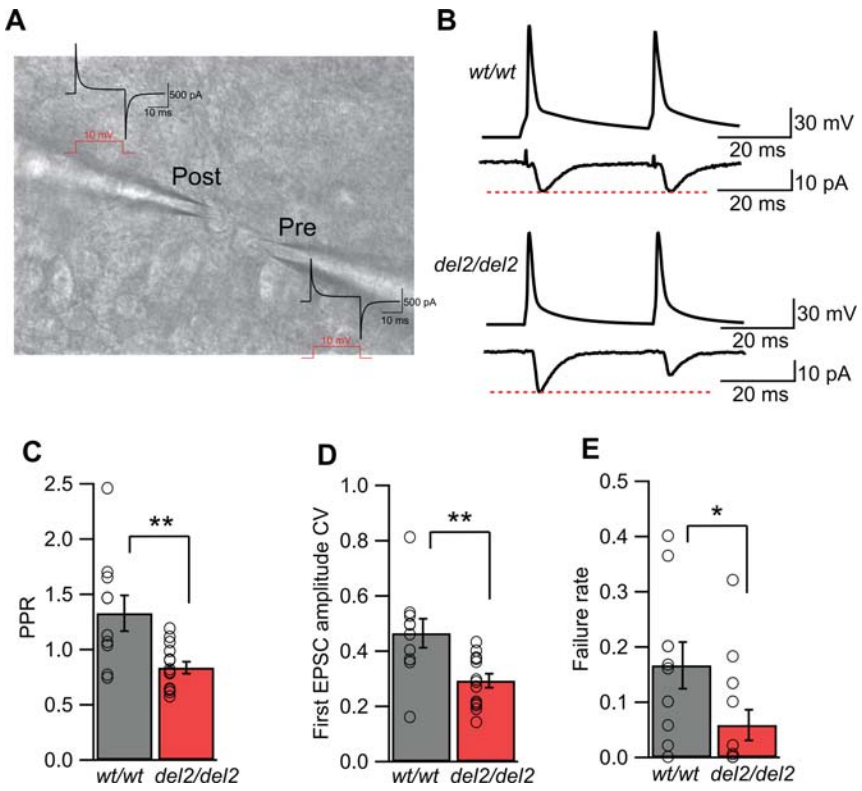

Figure 3-2. Probability of release is elevated at Dcdc2$^{del2/del2}$ layer 4-layer 4 unitary synapses. (A) Differential interference contrast image of example synaptically connected Dcdc2$^{wt/wt}$ layer 4 excitatory neurons. Current transients (black) responding to 10 mV test pulse (red) for these cells are displayed to demonstrate whole-cell configuration achieved. **(B)** Sample traces of a pair of action potentials elicited in the presynaptic neuron and corresponding EPSCs in the postsynaptic neuron for a pair of Dcdc2$^{wt/wt}$ (top) and Dcdc2$^{del2/del2}$ (bottom) synaptically coupled neurons. Dcdc2$^{wt/wt}$ traces correspond to pre and postsynaptic neurons labeled in **A**. **(C)** Average PPRs ($p < 0.05$), **(D)** coefficient of variance (CV) of first response amplitudes ($p < 0.01$), and **(E)** failure rates ($p < 0.01$) of Dcdc2$^{wt/wt}$ and Dcdc2$^{del2/del2}$ responses. Student's *t*-test; Dcdc2$^{wt/wt}$: n = 10 pairs, Dcdc2$^{del2/del2}$: n = 13 pairs. Open circles indicate averages from individual neurons. *$p < 0.05$, **$p < 0.01$.

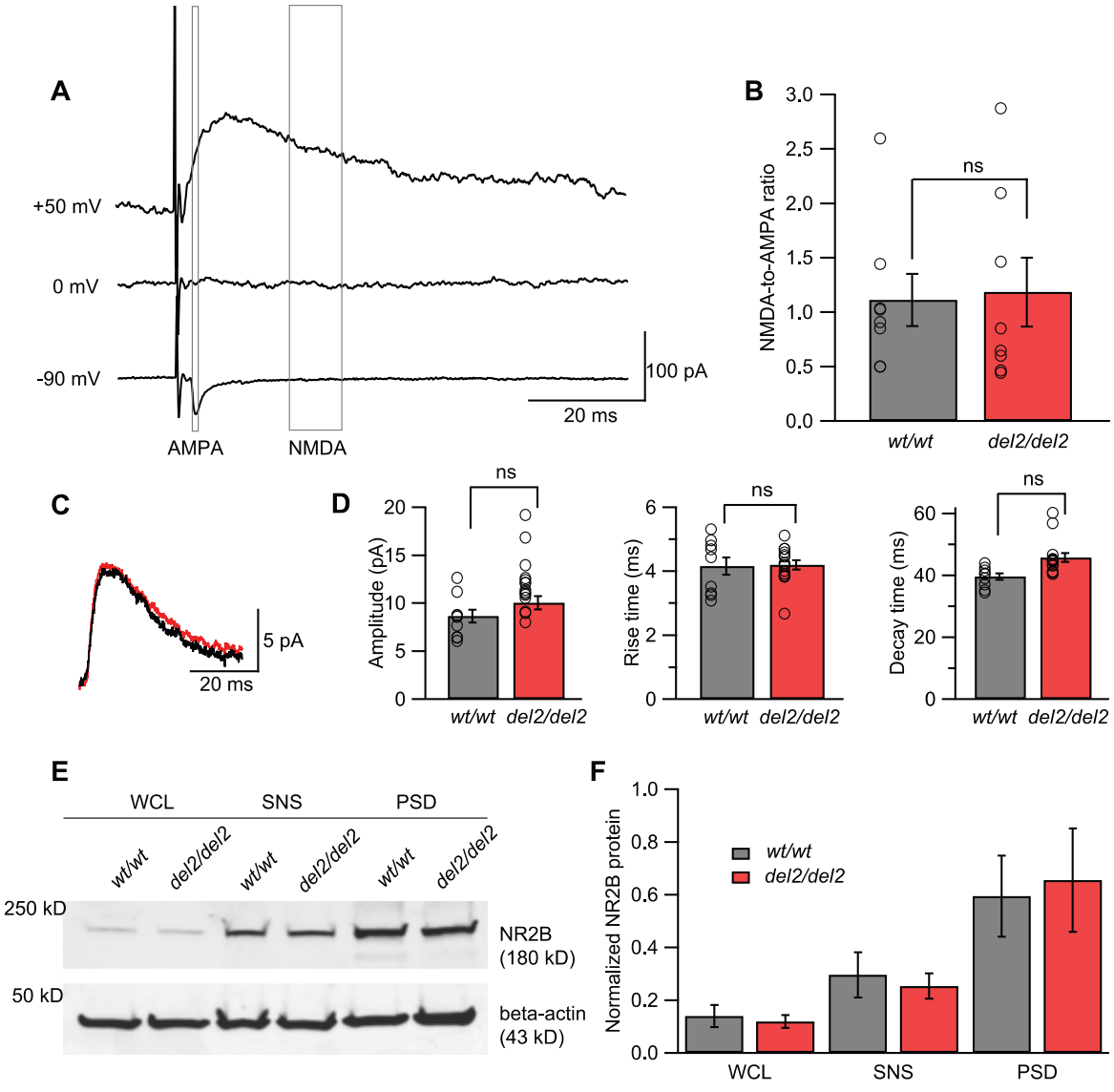

Figure 3-3. Postsynaptic NMDARs remain unaffected in Dcdc2$^{del2/del2}$ mice. **(A)** Averages of EPSCs evoked when a Dcdc2$^{wt/wt}$ layer 4 excitatory cell was held at –90, 0, and + 50 mV. Gray boxes indicate windows used to measure AMPAR-mediated component (1 ms at -90 mV) and NMDAR-mediated component (10 ms at +50 mV). (**B**) NMDA-to-AMPA ratios for Dcdc2$^{wt/wt}$ and Dcdc2$^{del2/del2}$ neurons (t_{14} = 0.18, p = 0.85). Open circles indicate individual neurons. Student's *t*-test. Dcdc2$^{wt/wt}$: n = 8, Dcdc2$^{del2/del2}$: n = 8. **(C)** Representative average waveforms of spontaneous miniature NMDAR-mediated synaptic events for a Dcdc2$^{wt/wt}$ (black) and a Dcdc2$^{del2/del2}$ (red) neuron. Membrane potential was held at +40 mV. Extracellular recording buffer included 10 µM NBQX, 5 µM SR-95531, and 1 µM TTX to isolate NMDAR-mediated events. **(D)** Mean amplitude (t_{22} = 1.54, p = 0.14), rise (t_{22} = 0.13, p = 0.90) and decay time (t_{22} = 0.38, p =

0.71) of average NMDA event waveforms. Open circles indicate individual neurons. Student's *t*-test. Dcdc2$^{wt/wt}$: n = 9, Dcdc2$^{del2/del2}$: n = 15. **(E)** Western blot for NMDAR2B subunit in whole cell lysate (WCL), synaptoneurosome (SNS), and postsynaptic density (PSD) in Dcdc2$^{wt/wt}$ (grey bars) and Dcdc2$^{del2/del2}$ (red bars) somatosensory cortex (P30). (**F**) Average NMDAR subunit expression relative to beta-actin in WCL (t_6 = 0.41, p = 0.69), SNS (t_6 = 0.43, p = 0.68) and PSD (t_6 = 0.25, p = 0.81) fractions. Dcdc2$^{wt/wt}$: n = 4, Dcdc2$^{del2/del2}$: n = 4; ns, $p > 0.05$.

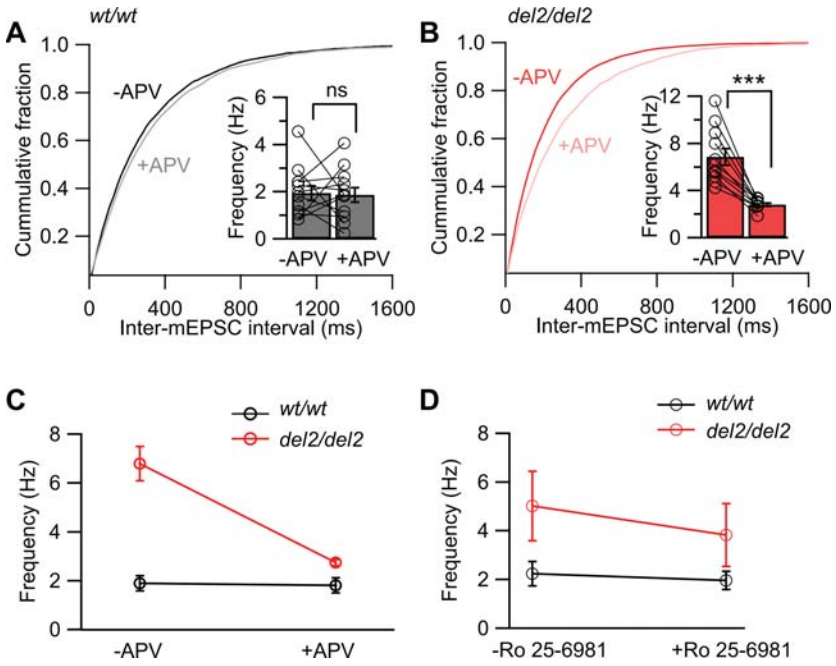

Figure 3-4. Blockade of NMDARs decreases elevated spontaneous vesicle release in Dcdc2$^{del2/del2}$ mice. Cumulative probability histograms showing intervals between mEPSCs in **(A)** Dcdc2$^{wt/wt}$ (black) and **(B)** Dcdc2$^{del2/del2}$ (red) layer 4 excitatory neurons before and after the application of DL-APV (100 μM). Inset, mean mEPSC frequencies for Dcdc2$^{wt/wt}$ and Dcdc2$^{del2/del2}$ neurons. Open circles indicate individual neurons. **(C)** Interaction graph showing the differential effect of APV on mEPSC frequencies in Dcdc2$^{del2/del2}$ and Dcdc2$^{wt/wt}$ neurons. Repeated-measures ANOVA, genotype x APV application interaction: $F_{1,21} = 27.21$, $p < 0.0001$. Followed by Bonferroni's multiple comparisons test within genotype (significance indicated on insets in **A** and **B**): Dcdc2$^{wt/wt}$: $p > 0.05$; Dcdc2$^{del2/del2}$: $p < 0.0001$. Dcdc2$^{wt/wt}$: n = 12, Dcdc2$^{del2/del2}$: n = 11. TTX (1 μM) and SR-95531 (5 μM) were included in the extracellular recording buffer, and MK-801 (1 mM) internally to block postsynaptic NMDARs. **(D)** Interaction graph showing the differential effect of Ro 25-6981 (0.5 μM) on mEPSC frequencies in Dcdc2$^{del2/del2}$ versus Dcdc2$^{wt/wt}$ cells. Repeated-measures ANOVA, genotype x Ro 25-6981 application interaction: $F_{1,18} = 4.68$, $p < 0.05$. Dcdc2$^{wt/wt}$: n = 10, Dcdc2$^{del2/del2}$: n = 10. ***$p < 0.001$; ns, $p > 0.05$.

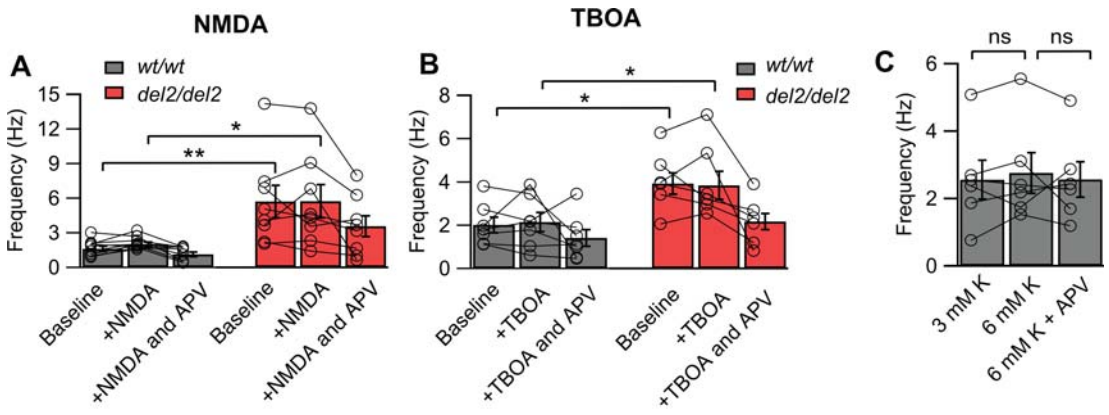

Figure 3-5. Elevated mEPSC frequency in Dcdc2$^{del2/del2}$ is not caused by changes in ambient glutamate level or difference in RMP. **(A)** Average mEPSC frequencies during baseline, NMDA (20 μM), NMDA (20 μM) plus DL-APV (100 μM) application for Dcdc2$^{wt/wt}$ (gray bars) and Dcdc2$^{del2/del2}$ (red bars) layer 4 neurons. Repeated-measures ANOVA (between variables: genotype, within variables: drug application), main effect of genotype on frequency: $F_{1,15}$ = 9.14, p < 0.01. Followed by Tukey's multiple comparisons tests, difference significant between Dcdc2$^{wt/wt}$ vs. Dcdc2$^{del2/del2}$: baseline (p < 0.01), +NMDA (p < 0.05); no significance: +NMDA and APV (p = 0.14). Dcdc2$^{wt/wt}$: n = 9, Dcdc2$^{del2/del2}$: n = 8. **(B)** Average mEPSC frequencies during baseline, TBOA (30 μM), TBOA (30 μM) plus DL-APV (100 μM) application for Dcdc2$^{wt/wt}$ (gray bars) and Dcdc2$^{del2/del2}$ (red bars) layer 4 neurons. Repeated-measures ANOVA, main effect of genotype on frequency: $F_{1,11}$ = 7.27, p < 0.05. Followed by Tukey's multiple comparisons tests, difference significant between Dcdc2$^{wt/wt}$ vs. Dcdc2$^{del2/del2}$: baseline (p < 0.05), +TBOA (p < 0.05); no significance: +TBOA and APV (p = 0.64). Dcdc2$^{wt/wt}$: n = 7, Dcdc2$^{del2/del2}$: n = 6. Average mEPSC frequencies for Dcdc2$^{wt/wt}$ neurons in 3 mM K^+ (normal), 6 mM K^+ and 6 mM K^+ plus APV. One-way ANOVA with Tukey's multiple comparisons tests, $F_{1.42,7.08}$ = 0.34, p = 0.65, n = 6. Open circles connected with lines indicate individual neurons. *p < 0.05; **p < 0.01; ns, p > 0.05.

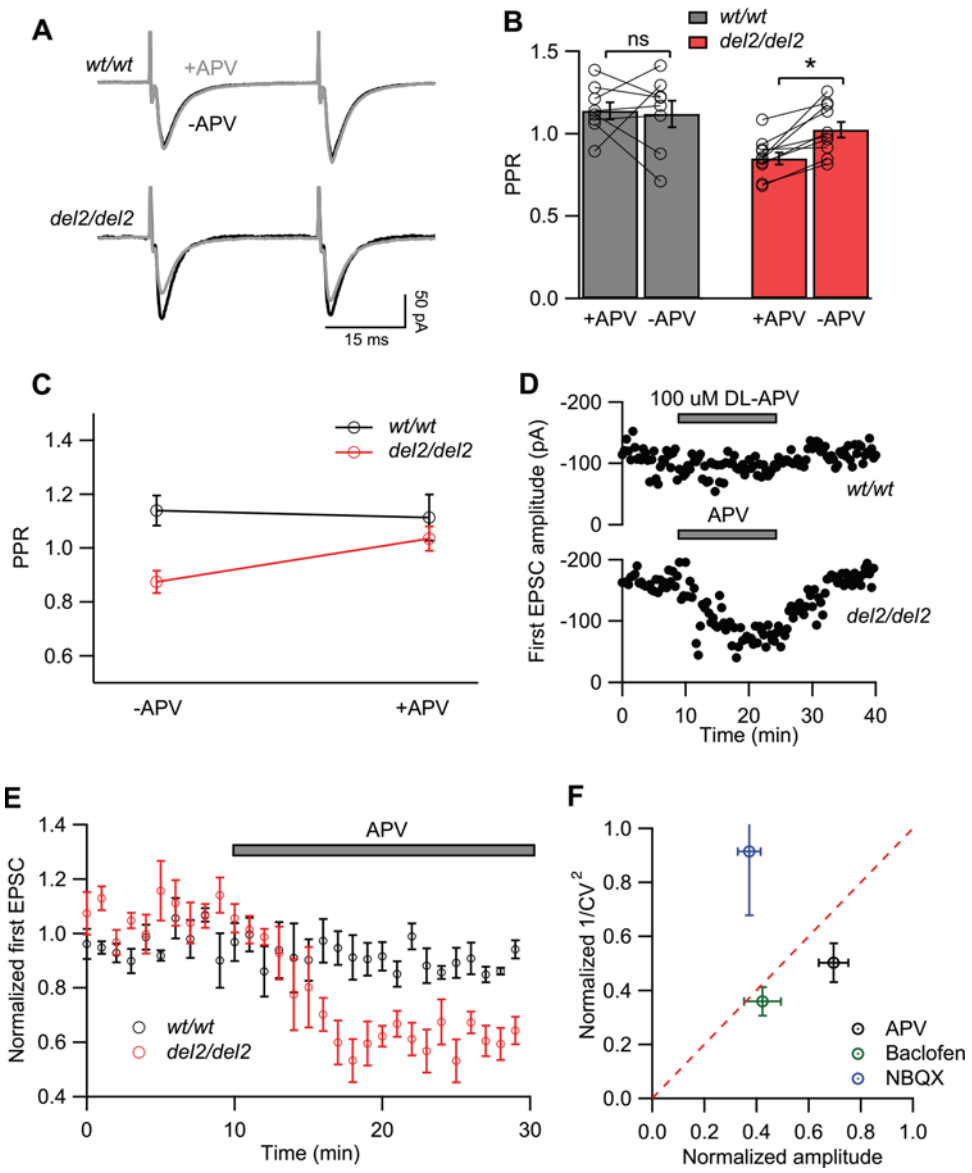

Figure 3-6. Blockade of NMDARs reduces probability of evoked release in Dcdc2$^{del2/del2}$ but not Dcdc2$^{wt/wt}$ mice. **(A)** Representative paired-pulse responses elicited by exrtasynaptic electrical stimulation in a Dcdc2$^{wt/wt}$ (top) and Dcdc2$^{del2/del2}$ (bottom) layer 4 excitatory cell before (black) and after (gray) APV application. **(B)** Effects of APV application on PPR in Dcdc2$^{wt/wt}$ (gray bars) and Dcdc2$^{del2/del2}$ (red bars) neurons. Open circles connected with lines indicate individual neurons. **(C)** Interaction graph showing the mean paired-pulse ratios for Dcdc2$^{wt/wt}$ and Dcdc2$^{del2/del2}$ neurons before and after APV. Repeated-measures ANOVA, genotype x APV application interaction: $F_{1,16} = 5.05$, $p < 0.05$. Followed by Bonferroni's multiple comparisons test within genotype (significance indicated in **B**): Dcdc2$^{wt/wt}$: adjusted $p > 0.05$; Dcdc2$^{del2/del2}$: $p < 0.05$). Dcdc2$^{wt/wt}$: n = 8, Dcdc2$^{del2/del2}$: n = 10. **(D)** Representative plot of peak

amplitudes of the first AMPA-mediated EPSCs over time in a Dcdc2$^{wt/wt}$ (upper) and Dcdc2$^{del2/del2}$ (lower) layer IV neuron before, during, and after APV application. Pairs of stimulations were delivered every 20 s. **(E)** Averages of normalized first EPSC amplitudes in Dcdc2$^{wt/wt}$ (n = 5; black circles) and Dcdc2$^{del2/del2}$ (n = 6; red circles) neurons showing the absence of APV effect in Dcdc2$^{wt/wt}$ and decrease in amplitudes in Dcdc2$^{del2/del2}$ mice. Every 3 EPSCs were averaged (covering 1-minute period), and normalized to the mean of the first minute. **(F)** CV analysis of Dcdc2$^{del2/del2}$ neurons by plotting EPSC amplitude ratio versus $1/CV^2$ ratio (post-drug/pre-drug) after and before NBQX (0.3 μM; blue circle, n = 6), baclofen (5 μM; green circle, n = 4), and DL-APV (100 μM; black circle, n = 12). Data points falling above the red dotted line indicate a postsynaptic site of action, and those below a presynaptic site of action. *$p < 0.05$; ns, $p > 0.05$.

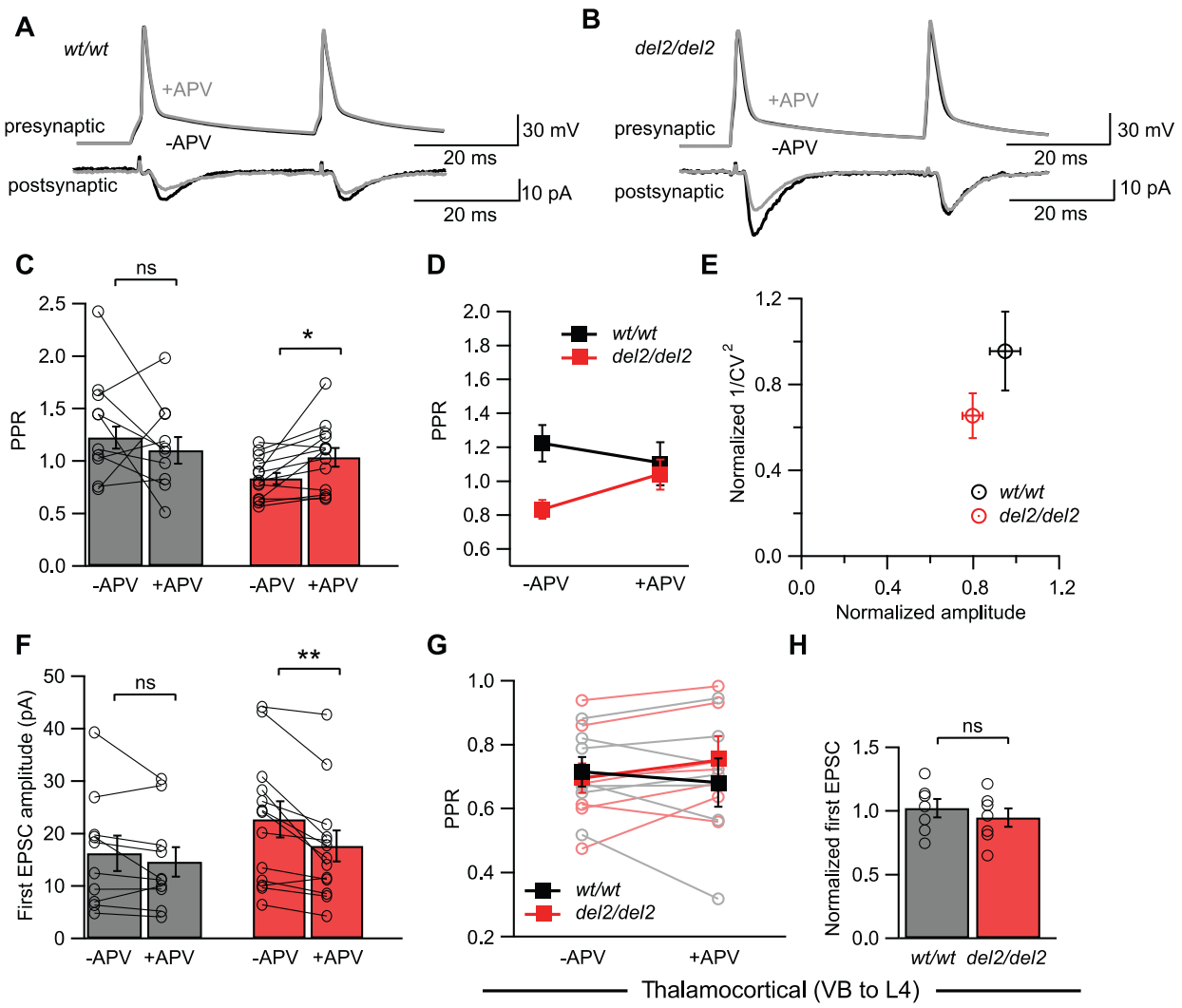

Figure 3-7. APV reduces release probability of Dcdc2$^{del2/del2}$ layer 4-layer 4 excitatory synapses to Dcdc2$^{wt/wt}$ levels. Postsynaptic unitary EPSCs elicited by a pair of presynaptic action potentials in a **(A)** Dcdc2$^{wt/wt}$ and a **(B)** Dcdc2$^{del2/del2}$ layer 4 excitatory cell pair before (black) and after (gray) APV application. **(C)** Effects of APV application on PPR in Dcdc2$^{wt/wt}$ (gray bars) and Dcdc2$^{del2/del2}$ (red bars) neurons. Student's *t*-test, Dcdc2$^{wt/wt}$: $t_9 = 1.12$, $p = 0.29$; Dcdc2$^{del2/del2}$: $t_{12} = 2.93$, $p = 0.01$. Open circles connected with lines indicate individual neurons. **(D)** Interaction graph showing the mean PPR for Dcdc2$^{wt/wt}$ (black filled square) and Dcdc2$^{del2/del2}$ (red filled square) cells before and after APV. Repeated-measures ANOVA, genotype x APV application interaction: $F_{1,21} = 5.45$, $p < 0.05$. Followed by Bonferroni's multiple comparisons test, difference significant between Dcdc2$^{wt/wt}$ vs. Dcdc2$^{del2/del2}$ before APV ($p < 0.01$), and no significance after APV application ($p > 0.99$). **(E)** Normalized plot of $1/CV^2$ versus amplitude of Dcdc2$^{wt/wt}$ (black circle) versus Dcdc2$^{del2/del2}$ (red circle) cells. Dcdc2$^{del2/del2}$

neurons on average show presynaptic APV effect, falling below the red-dotted diagonal line. **(F)** Effects of APV application on 1st response amplitude in Dcdc2$^{wt/wt}$ (gray bars) and Dcdc2$^{del2/del2}$ (red bars) neurons. Student's *t*-test, Dcdc2$^{wt/wt}$: $t_9 = 1.36$, $p = 0.21$; Dcdc2$^{del2/del2}$: $t_{12} = 3.81$, $p < 0.05$. Open circles connected with lines indicate individual neurons. Dcdc2$^{wt/wt}$: n = 10 pairs, Dcdc2$^{del2/del2}$: n = 13 pairs. **(G)** Interaction graph showing the effect of APV on mean paired-pulse ratios measured in layer 4 excitatory neurons while stimulating the VB for Dcdc2$^{wt/wt}$ (black filled square) and Dcdc2$^{del2/del2}$ (red filled square). Repeated-measures ANOVA, genotype x APV application interaction: $F_{1,12} = 3.97$, $p = 0.07$. Followed by Bonferroni's multiple comparisons test, difference significant between Dcdc2$^{wt/wt}$ vs. Dcdc2$^{del2/del2}$ before APV ($p = 0.62$), and no significance after APV application ($p = 0.21$). Open circles connected with lines indicate individual neurons (Dcdc2$^{wt/wt}$: gray, Dcdc2$^{del2/del2}$: light red). **(H)** Averages of normalized 1st EPSC amplitudes (EPSC after APV / EPSC before APV) in Dcdc2$^{wt/wt}$ (gray bar) and Dcdc2$^{del2/del2}$ (red bar) neurons. Student's *t*-test, $t_{12} = 0.72$, $p = 0.48$. Open circles indicate individual neurons. Dcdc2$^{wt/wt}$: n = 7, Dcdc2$^{del2/del2}$: n = 7.

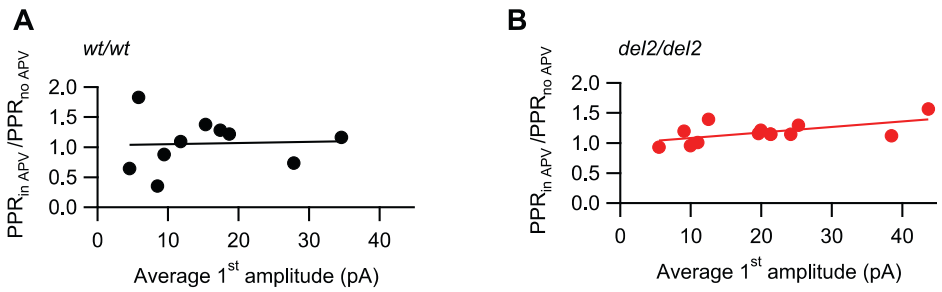

Figure 3-8. PPR change and average 1st response amplitude are positively correlated in Dcdc2$^{del2/del2}$. Correlation between Effects of APV on PPR (PPR after APV / PPR before APV application) and average EPSC amplitude of each postsynaptic cell recorded for **(A)** Dcdc2$^{wt/wt}$ and **(B)** Dcdc2$^{del2/del2}$ mice. Mean EPSC amplitude for each pair of responses was used in analysis. Pearson's correlation, Dcdc2$^{wt/wt}$: r = 0.05, p = 0.89; Dcdc2$^{del2/del2}$: r = 0.60, $p < 0.05$. Dcdc2$^{wt/wt}$: n = 9 pairs, Dcdc2$^{del2/del2}$: n = 13 pairs.

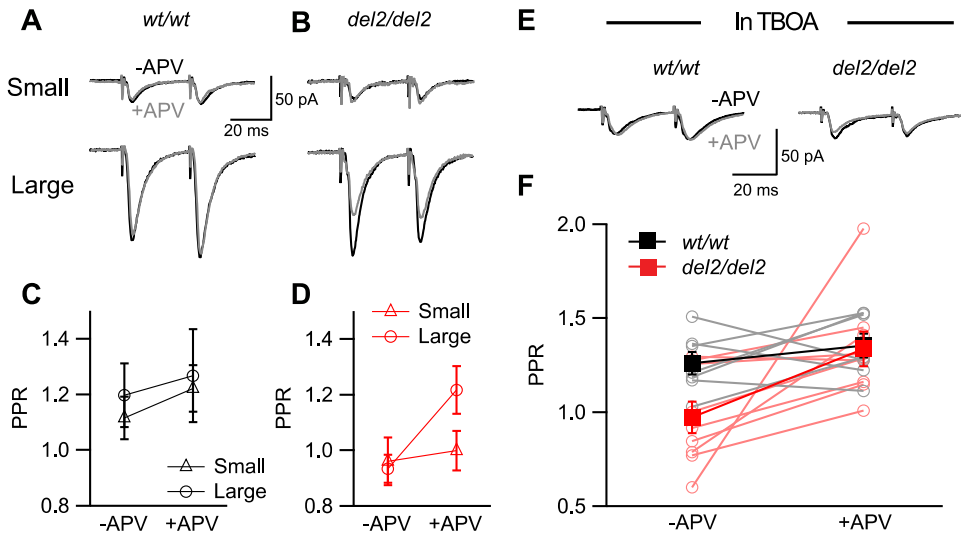

Figure 3-9. Effect of preNMDAR blockade on release probability is enhanced when extracellular glutamate concentration is elevated by larger synaptic release or TBOA. Representative EPSC pairs evoked by exrtasynaptic electrical stimulation at minimal (top) versus high (bottom) intensities in a **(A)** Dcdc2$^{wt/wt}$ and a **(B)** Dcdc2$^{del2/del2}$ layer IV excitatory cell before (black) and after (gray) APV application. **(C)** Interaction graph showing mean PPR for small amplitude response (open triangle) and large amplitude response (open circle) before and after APV for Dcdc2$^{wt/wt}$ (black) cells. Two-way ANOVA, response amplitude x APV application interaction: $F_{1,9} = 3.14$, $p = 0.11$. Followed by Bonferroni's multiple comparisons test before versus after APV application, no significance for large ($p = 0.60$) or small amplitude ($p = 0.27$). **(D)** Interaction graph showing mean PPR for small amplitude response (open triangle) and large amplitude response (open circle) before and after APV for Dcdc2$^{del2/del2}$ (red) cells. Two-way ANOVA, response amplitude x APV application interaction: $F_{1,9} = 8.04$, $p < 0.05$. Followed by Bonferroni's multiple comparisons test before versus after APV application, difference significant for large amplitude response $p < 0.05$), no significance for small amplitude ($p = 0.99$). Dcdc2$^{wt/wt}$: n = 10; Dcdc2$^{del2/del2}$: n = 10. **(E)** Representative EPSCs of a Dcdc2$^{wt/wt}$ (left) and a Dcdc2$^{del2/del2}$ (right) layer IV neuron evoked by minimal stimulus intensity before (black) and after (gray) APV application, measured in 3 μM TBOA at room temperature. **(F)** Interaction graph showing mean PPRs for Dcdc2$^{wt/wt}$ (filled black square) and Dcdc2$^{del2/del2}$ (filled red square) cells before and after APV. Open circles connected with lines indicate individual neurons (Dcdc2$^{wt/wt}$: gray, Dcdc2$^{del2/del2}$: light red). Repeated-measures ANOVA, main effect of APV: $F_{1,14} = 6.70$, $p < 0.05$. Followed by Bonferroni's multiple comparisons test, difference significant

between Dcdc2$^{wt/wt}$ and Dcdc2$^{del2/del2}$ before APV ($p < 0.05$); no significance after APV ($p > 0.05$). Dcdc2$^{wt/wt}$: n = 7, Dcdc2$^{del2/del2}$ n = 9.

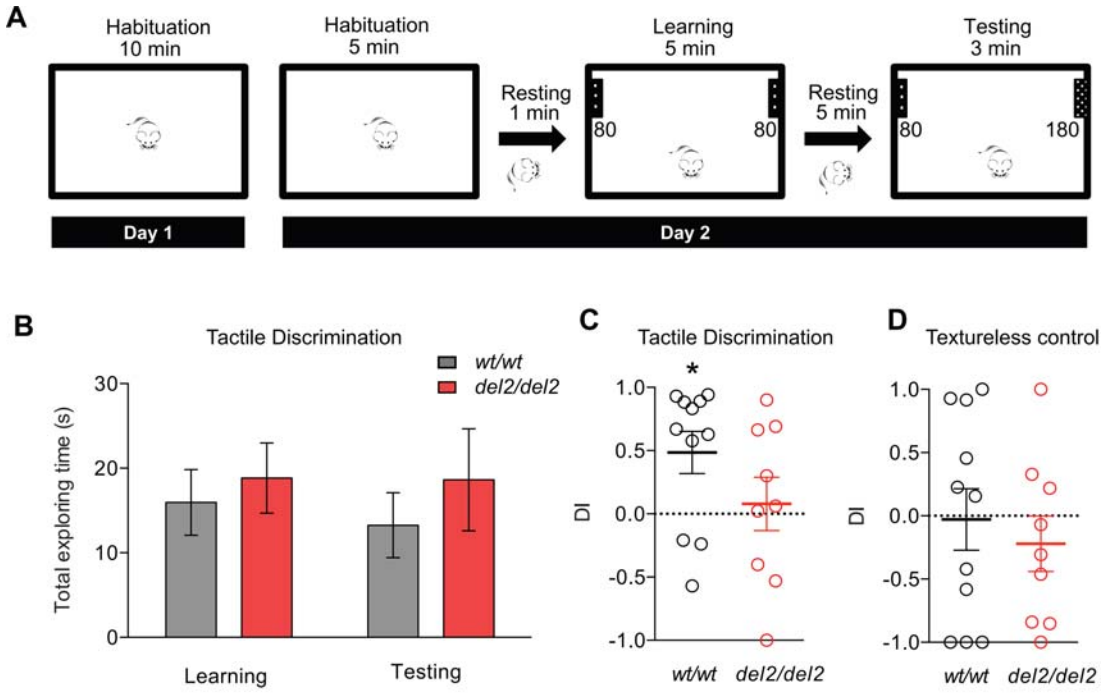

Figure 3-10. Dcdc2 Dcdc2$^{del2/del2}$ mice show impaired tactile discrimination compared to Dcdc2$^{wt/wt}$ mice. (A) Schematic diagrams depicting experimental protocol used for tactile discrimination test. On day 2, the testing chamber contained two identical sheets of 80-grit sandpaper affixed on opposing lateral walls during the 5-minute learning period. The testing period, which took place after a 5-minute interval during which the animal was returned to home cage to rest, contained one 80-grit sheet and one novel 180-grit sheet. The side with the novel and familiar sheet was counterbalanced throughout testing. The amount of time each subject actively interacted with each sheet was quantified for both learning and testing periods. **(B)** Total time spent exploring both sheets during learning (two 80-grit sheets) and testing (80 and 180-grit) was not significantly different for Dcdc2$^{wt/wt}$ (grey bars) and Dcdc2$^{del2/del2}$ (red bars) mice. Two-way ANOVA, $F_{1,18} = 0.03$, $p = 0.86$. **(C)** The discrimination index (DI = time spent with 180-grit / total time spent exploring) compared to chance level (DI = 0.5, back dotted line) for Dcdc2$^{wt/wt}$ (back) versus Dcdc2$^{del2/del2}$ (red) mice for discrimination task. Discrimination was determined when DI was significantly different from chance level. One-sample *t*-test, Dcdc2$^{wt/wt}$: $p < 0.05$, Dcdc2$^{del2/del2}$: $p = 0.72$. **(D)** DI compared to chance level for textureless control task. Same experimental protocol was used on the same animals only with sandpaper covered by clear transparent film. One-sample *t*-test, Dcdc2$^{wt/wt}$: $p = 0.91$, Dcdc2$^{del2/del2}$: $p = 0.34$. Open circles indicate individual animals. Dcdc2$^{wt/wt}$: n = 11, Dcdc2$^{del2/del2}$: n = 9. *$p < 0.05$.

IV. Concluding remarks and future directions

In summary, we have demonstrated a link between the dyslexia candidate gene *Dcdc2* and neurophysiological changes in a *Dcdc2* mutant mouse model using electrophysiological approaches. We showed that L4 somatosensory excitatory neurons in mutant brain have higher glutamatergic synaptic release, mediated at least in part by altered presynaptic NMDAR function, which in turn leads to elevated noise in local circuitry and degraded spike-time precision when action potential trains are produced. Our results compliment several reports in different aspects of RD research on a basic, cellular level.

First, variants in *GRIN2B*, a gene coding for NR2B subunit, has been linked to weak performances in tasks involving short-term memory in individuals with RD (Brkanac et al. 2008; Ludwig et al. 2009). Dcdc2 mice were shown to perform worse in short-term memory-based tactile discrimination tasks in our study as well as spatial working memory tasks in a previous study (Gabel et al. 2011). These findings encourage speculation that the short-term memory deficits in Dcdc2 mutants are caused by similar changes in NR2B-associated pathways as in RD individuals. The Dcdc2 mutant should provide an ideal model to test this hypothesis.

Second, our results are compatible with the elevated glutamate levels found in emergent readers with lower reading scores using magnetic resonance spectroscopy (Pugh et al. 2014). In addition, we provided a mechanism through which elevated glutamate levels could occur during synaptic transmission – increased presynaptic release, and the change in release is mediated by

elevated preNMDAR function. Interestingly, both SNPs in *GRIN2B* (Tannock et al. 2007) and abnormal glutamate levels (Carrey et al. 2007) have been shown in families and clinical samples of ADHD, which shares 25%-40% comorbidity with RD (Pennington 2006; Shanahan et al. 2006). Affected *GRIN2B* expression and glutamatergic transmission could be the common cause for changes in certain aspect of cognitive process involved in both of these complex developmental disorders.

Lastly, our results link physiological dysfunction in spike-time precision to temporal processing problems found in dyslexics as shown by multiple studies (for example McAnally and Stein 1996; Ramus 2003; Lehongre et al. 2011; Centanni et al. 2013). It has been reported that individuals with RD appear to process information with heightened neural "noise" and instability, as well as greater variability in reaction time and accuracy of related behavioral measures (Sperling et al. 2006; Centanni et al. 2013; Hornickel and Kraus 2013; Pugh et al. 2013). Increased variability can result in reduced stimulus-evoked response and inconsistent response to different stimuli, as demonstrated in human imaging studies (McAnally and Stein 1996; Ziegler et al. 2009). We demonstrated that altered cell-autonomous, intrinsic firing properties alone could lead to changes in spike-time precision and increased variability observed on the network level in animal models, and perhaps even in human subjects.

We have demonstrated changes in excitatory synaptic transmission in layer 4 somatosensory cortex, and attributed them to altered preNMDAR function as measured by electrophysiological methods. Although the expression locus

and function of NMDARs located presynaptically are still debated in this field of research (review see Duguid 2013), we argue that changes in preNMDAR function in Dcdc2 mutants may be the most parsimonious explanation. This is supported by two main lines of evidence. First, we were unable to find evidence supporting any changes in postsynaptic NMDAR and AMPAR expression or function. Second, although electrotonic spread of somatodendritic NMDAR activation could also contribute to increased glutamate release in the mutant particularly given the depolarized resting membrane potential, we did not observe changes in mEPSC frequencies when RMPs were significantly depolarized in wildtype L4 neurons, suggesting that depolarized membrane potential alone without changes in NMDAR function could not account for the altered synaptic release measured. Our physiological assessment of altered, preNMDAR-mediated glutamate release probability does not provide the exact locus of preNMDAR that are affected in Dcdc2 mutants, but the effectiveness of non-postsynaptic NMDAR blockade in reverting the effects back to wildtype levels could potentially provide an effect therapeutic target.

Although the focus of this study has been functional changes in cellular neurophysiology associated with loss of *Dcdc2*, the molecular pathways through which *Dcdc2* regulates preNMDAR function still remain to be elucidated. Biochemical approaches should be used to determine whether *Dcdc2* acts through 1) regulating *Grin2B* gene expression spatially and/or developmentally; 2) mediating NMDAR trafficking/sorting to axonal versus dendritic locations; 3) affecting other cellular processes (for example migration and neuritic growth)

which then influencing preNMDAR function downstream. These possibilities are not exclusive and DCDC2 may function through other mechanisms, but findings from these experiments should provide directions for future studies on processes underlying RD and other developmental cognitive disorders.

Considerable progress has been made in the past two decades in understanding dyslexia's manifestation, neuropsychology, genetics and neurobiology. Research on RD has helped to promote scientific knowledge and public awareness of the complexity of this developmental disorder. Although increasing number of studies link genetics, structural and functional data to RD, our study is among the first to address neurophysiological changes taking place on a cellular level as a direct association of the manipulation of a dyslexia candidate gene. Results from this study, and future studies using similar physiological approaches, should provide basis for understanding neuronal circuitry changes underlying functional anomalies revealed by imaging studies, which have been much more extensively characterized since late 1980s. Through these studies, cellular pathways and novel therapeutic targets should be identified to benefit clinical neuroscience in understanding and treating RD. In particular, our study identified NMDAR, more specifically preNMDAR antagonism, as a possible approach to reverse DCDC2 hypofunction. It is interesting to note that two FDA approved medications, atomoxetine for ADHD and memantine for Alzheimer's desease, are both found to work through NMDAR, and preferentially extrasynaptic NMDAR blockade (Johnson and Kotermanski 2006; Lipton 2006; Ludolph et al. 2010; Xia et al. 2010). It would be

fruitful to test in the future the effects of these medications on the neurophysiology and behaviors of this Dcdc2 mouse model, as well as testing their effectiveness on ameliorating RD associated deficits.

References

Brkanac Z, Chapman NH, Igo RP, Matsushita MM, Nielsen K, Berninger VW, et al. Genome scan of a nonword repetition phenotype in families with dyslexia: evidence for multiple loci. Behav Genet. 2008 Sep;38(5):462–75.

Carrey NJ, MacMaster FP, Gaudet L, Schmidt MH. Striatal creatine and glutamate/glutamine in attention-deficit/hyperactivity disorder. J Child Adolesc Psychopharmacol. 2007 Feb;17(1):11–7.

Centanni TM, Booker AB, Sloan AM, Chen F, Maher BJ, Carraway RS, et al. Knockdown of the Dyslexia-Associated Gene Kiaa0319 Impairs Temporal Responses to Speech Stimuli in Rat Primary Auditory Cortex. Cereb Cortex. 2014 Jul;24(7):1753-66.

Duguid IC. Presynaptic NMDA receptors: are they dendritic receptors in disguise? Brain Res Bul. 2013;93:4-9.

Gabel LA, Marin I, Loturco JJ, Che A, Murphy C, Manglani M, et al. Mutation of the dyslexia-associated gene Dcdc2 impairs LTM and visuo-spatial performance in mice. Genes, Brain and Behavior. 2011 Oct 19;10(8):868–75.

Hornickel J, Kraus N. Unstable representation of sound: a biological marker of dyslexia. J Neurosci. 2013 Feb 20;33(8):3500–4.

Johnson J, Kotermanski S. Mechanism of action of memantine. Current Opinion in Pharmacology. 2006 Feb;6(1):61–7.

Lehongre K, Ramus F, Villiermet N, Schwartz D, Giraud A-L. Altered low-γ sampling in auditory cortex accounts for the three main facets of dyslexia. Neuron. 2011 Dec 22;72(6):1080–90.

Lipton SA. Paradigm shift in neuroprotection by NMDA receptor blockade: Memantine and beyond. Nat Rev Drug Discov. 2006 Jan 20;5(2):160–70.

Ludolph AG, Udvardi PT, Schaz U. Atomoxetine acts as an NMDA receptor blocker in clinically relevant concentrations. Br J Pharmacol. 2010 May;160(2):283-91.

Ludwig KU, Roeske D, Herms S, Schumacher J, Warnke A, Plume E, et al. Variation in GRIN2Bcontributes to weak performance in verbal short-term memory in children with dyslexia. Am J Med Genet B Neuropsychiatr Genet. 2010 Mar 5;153B(2):503-11.

McAnally KI, Stein JF. Auditory temporal coding in dyslexia. Proc Biol Sci. 1996 Aug 22;263(1373):961–5.

Pennington BF. From single to multiple deficit models of developmental

disorders. Cognition. 2006 Sep;101(2):385-413.

Pugh KR, Frost SJ, Rothman DL, Hoeft F, Del Tufo SN, Mason GF, et al. Glutamate and Choline Levels Predict Individual Differences in Reading Ability in Emergent Readers. J Neurosci. 2014 Mar 12;34(11):4082–9.

Pugh KR, Landi N, Preston JL, Mencl WE, Austin AC, Sibley D, et al. The relationship between phonological and auditory processing and brain organization in beginning readers. Brain Lang. 2013 May;125(2):173–83.

Ramus F. Developmental dyslexia: specific phonological deficit or general sensorimotor dysfunction? Curr Opin Neurobiol. 2003 Apr;13(2):212-8.

Shanahan MA, Pennington BF, Yerys BE, Scott A, Boada R, Willcutt EG, et al. Processing speed deficits in attention deficit/hyperactivity disorder and reading disability. J Abnorm Child Psychol. 2006 Oct;34(5):585–602.

Sperling AJ, Lu ZL, Manis FR. Motion-Perception Deficits and Reading Impairment It's the Noise, Not the Motion. Psychol Sci. 2006 Dec;17(12):1047-53.

Tannock R, Kennedy JL, Ickowicz A. Association of the glutamate receptor subunit gene GRIN2B with attention-deficit/hyperactivity disorder. Genes Brain Behav. 2007 Jul;6(5):444-52.

Xia P, Chen HSV, Zhang D, Lipton SA. Memantine Preferentially Blocks Extrasynaptic over Synaptic NMDA Receptor Currents in Hippocampal Autapses. J Neurosci. 2010 Aug 18;30(33):11246–50.

Ziegler JC, Georgel CP, George F. Speech-perception-in-noise deficits in dyslexia. Dev Sci. 2009 Sep;12(5):732-45.

APPENDIX I

List of Abbreviations

AMPAR	α-amino-3-hydroxy-5-methyl-4-isoxazolepropionic acid receptor
AP	action potential
CV	coefficient variation
DCDC2	doublecortin domain-containing 2
DCX	doublecortin
DL-APV	DL-2-amino-5-phosphonopentanoic acid
DYX	dyslexia susceptibility
DYX1C1	dyslexia susceptibility 1 candidate 1 (also known as EKN1)
EAAT	neuronal excitatory amino acid transporter
EM	electron microscopy
fMRI	functional magnetic resonance imaging
ISI	inter-spike interval
JNK	cJun-N-terminal kinase
MEG	magnetoencephalography
mEPSC	miniature excitatory postsynaptic current
mIPSC	miniature inhibitory postsynaptic current
NBQX	2,3-dioxo-6-nitro-1,2,3,4-tetrahydrobenzo[f]quinoxaline-7-sulfonamide
NMDAR	N-methyl-D-aspartate receptor
PET	positron emission tomography
PP1	protein phosphates 1
PPR	paired-pulse ratio

RD	reading disability
RMP	resting membrane potential
RNAi	RNA interference
ROBO1	roundabout drosophila homolog 1
RS	regular spiking
SNP	single nucleotide polymorphism
STR	short tandem repeat
TBOA	DL-*threo*-β-Benzyloxyaspartic acid
tLTD	timing-dependent long-term synaptic depression
VB	ventrobasal nucleus of the thalamus